UNIVERSITY OF CALIFORNIA
RIVERSIDE

Sustainable Brackish Desalination Management: Oxidative Removal of Antiscalants and Scale-Forming Constituents From Desalination Concentrate

A Dissertation submitted in partial satisfaction
of the requirements for the degree of

Doctor of Philosophy

in

Chemical and Environmental Engineering

by

Tushar Jain

September 2019

Dissertation Committee:
Dr. Haizhou Liu, Chairperson
Dr. Jinyong Liu
Dr. Yujie Men

The Dissertation of Tushar Jain is approved:

Committee Chairperson

University of California, Riverside

Acknowledgements

I would like to express my greatest appreciation to Dr. Haizhou Liu for his meticulous reviews of my drafts, and for his rigorous and kind supervision of my research work. His encouraging words have been decisive for finishing the work. He is one of the smartest and most hard working people I know. I hope that I could be as enthusiastic and energetic as Dr. Liu. He has always been very supportive, and his thoughtful guidance allowed me to solve my initial hurdles at the beginning of the program, and has always given me his generous support during my studies at Riverside. I also would like to thank my committee members Dr. Jinyong Liu and Dr. Yujie Men. Dr. Jinyong Liu's research group extended a great hand in the analytical work to complete chapter 3.

A good support system is important to surviving and staying sane in grad school. I would like to thank all the members of Dr. Haizhou's group: Wei Li, Michelle Chebeir, Mathew Chen, John Orta, Cheng Tan, Liang Wu, Zhiwen Chen, Ananta Azad, Andrew Sanchez, Sumant Avasarala, JiaJie Qian and Soyoon Kum. I would also like to thank Kiranmayi Mangalgiri and Samuel Patton for patiently teaching me radical chemistry. I am particularly grateful to Gongde Chen for giving me company on our long late-night experimental days and discussing different hypotheses while developing our projects.
I would also like to specially thank Changxu Ren for running umpteen number of samples for me.

I would like to thank my undergraduate students Yu Shen, Edgar Sanchez, Osvaldo Mireles, Jesus Trujillo, Nadia Estrada, Weiyu Yao and Sheila Cervantes, who helped me on my research projects.

Lastly, a big thank you to my wider support system. To my housemates, Rameswar Panda, Abhishek Aich, Aakash Parikh and Siddharth Agarwal and friends, thanks for tolerating my stress throughout the year, and to Anguluri Rajasekhar, for keeping me inspired in research, science and beyond. My special thanks to Apoorva Rudra, Apoorva Sarode and Shardul Wadekar for being a positive sounding board and supporting me in times of need. I would like to thank my friends from undergraduate days Mayuri Ukidwe, Abhilasha Dehankar and Dhanshri Tijare for their support during this journey.

Parts of this doctoral work have been published in or submitted to the following journal, Chapter 2 (published in Environmental Science: Water Research and Technology, 2019). Chapter 3 and chapter 4 are in preparation for submission.

This research has been funded by UC Riverside Faculty Initiation Fund, U.S. National Science Foundation CAREER Program, Early-concept Grants for Exploratory Research Program, U.S. National Science Foundation GOALI Program, U.S. Department of Interior Bureau of Reclamations, National Water Research Institute, and The Metropolitan Water District of Southern California, Metropolitan Water District of Southern California and the Southern California World Water Forum College Grant. Any opinion, findings, and conclusions or recommendations in this material are the authors(s) and do not necessarily reflect the views of any these organizations listed above.

Dedication

I would like to dedicate this thesis to my parents, Alka and Ashok. Thank you for providing me with the opportunity to engage in this project. Without their support I may not have found myself at University of California, nor had the courage to engage in this task and see it through. They are well-aware how this project and my studies throughout my five years have formulated my outlook, determination, motivation and perspective that will sculpt my future. Through my sister and my twin brother's emotional support, intellectual stimulation and many hours of identity-forming conversation, I am inspired to pursue an unconventional dream in which I truly believe. So, thank you, to Mom, Dad, Bhumika and Tejas for being the most supportive family one could hope for.

ABSTRACT OF THE DISSERTATION

Sustainable Brackish Desalination Management: Oxidative Removal of Antiscalants and Scale-Forming Constituents From Desalination Concentrate

by

Tushar Jain

Doctor of Philosophy, Graduate Program in Chemical and Environmental Engineering
University of California, Riverside, September 2019
Dr. Haizhou Liu, Chairperson

Brackish water desalination has become increasingly important in arid inland regions for sustainable water supplies, but the management of desalination brine waste is costly. In particular, the presence of oversaturated calcium as scale-forming compounds in the brine is the most important factor limiting the recovery of water. Removal of these antiscalants from the brine can induce the precipitation of oversaturated scale-forming substances, enable additional water recovery from RO concentrate, and reduce the risk of eutrophication after brine disposal.

In this dissertation, we aimed to investigate the the impact of photochemical degradation of three widely used antiscalants, *i.e.*, nitrilotri-methylenephosphonic acid (NTMP), ethylenediaminetetra-methylenephosphonic acid (EDTMP) and diethylenetriaminepentakis-methylphosphonic acid (DTPMP) with hydrogen peroxide and persulfate as the photo-oxidants on inducing the precipitation of scale-forming constituents. Firstly, the three antiscalants have the active phosphonate functional groups, they affect the precipitation kinetics of calcium solids differently. Antiscalants are only effective in temporarily stabilizing the oversaturated desalination brine and delay the scale-

forming substances (in this case, calcium solids) from precipitation. Results from this study established a quantitative relationship between the nucleation rate of three most commonly observed calcium-scaling solids and three most widely used antiscalants. Results showed that the antiscalants could be effectively degraded at the optimized conditions. DTPMP degrades much slower compared to NTMP and EDTMP with all the oxidants in this study. DTPMP also has much higher inhibition capacity in delaying the precipitation of gypsum. Among the oxidants tested, persulfate shows the highest degradation rate of all the antiscalants tested. It was also observed that induction time depends on the extent of UV exposure. A synergistic effect of nucleation and antiscalant degradation was observed for the demineralization of gypsum in presence of UV oxidant. Furthermore, a systematic approach that included radical steady state distribution measurement for different radicals such as hydroxyl radical ($HO^{\cdot}$), sulfate radical ($SO_4^{\cdot -}$), reactive chlorine species using various organic probe compounds at different water quality parameters such as pH, chloride and presence of NOM was tested. pH did not have any significant effect on the antiscalant degradation. However, the presence of NOM and chloride significantly affected the antiscalant degradation rate due to scavenging and shielding effects respectively. This study shows an effective way to increase the water recovery in desalination concentrate with the help of a UV/oxidant-assisted removal of TDS and thereby employing a secondary reverse osmosis.

Table of Contents

List of Figures

Chapter 1

Introduction

1.1 Depleting freshwater reserves

Clean and accessible water is a scarce and stressed resource because only 1% of all the water on earth is available for human use and consumption purpose.[1,2] There are presently around 2 billion people live in areas of water scarcity and 844 million people lack access to safe water.[3] The scarcity of water not just affects social and economic sectors but also threatens the health of ecosystems. The situation is further worsening due to expansion in agricultural sector, increased differences between water supply and demand, improper management and degradation of natural water resources. Furthermore, the increasing domestic and international conflicts are aggravating the water crisis.[4,5]

Future forecasts demonstrate that 3.6 billion people will live in regions with water stress or shortage in 2035 due to increase in population causing more water scarcity.[6] Water supply in particularly parched and semi-parched regions (High Plains[7] and Central Valley[8]), are insufficient to meet demand and a major portion of the United States, especially the western region is severely affected with drought.[9] The demand of water in future in expected to increase the stress on groundwater resources. If the per capita usage of water and power generation remains the same in the United States, then by 2050 the demand for water could rise by 12.3 percent.[10]; Moreover, this enhanced water demand combined with anticipated environmental change could create moderate to outrageous hazard to water-supply sustainability for the greater part of the United States.[11] Climate models foresee that the increasing global water shortage will increase as atmospheric changes become more extreme. Due to these changes, the behavior of water changes and its precipitation pattern becomes irregular, evaporation and transpiration rates are also

affected with increased air temperature thus making the water scarcer and less safe.[12] The regions with maximum risk would be in the southwestern and central parts of the United States, Texas, parts of the Mississippi River Valley, and Florida. Without the impacts of environmental change, less zones in the United States would be at outrageous hazard, however moderate-to high-chance territories could reach out over the Southwest, the Northwest, portions of the Mississippi River Valley, and Florida (Figure 1.1).[13] Along these lines, a stronger water supply is required inside the water area to help alleviate environmental change.

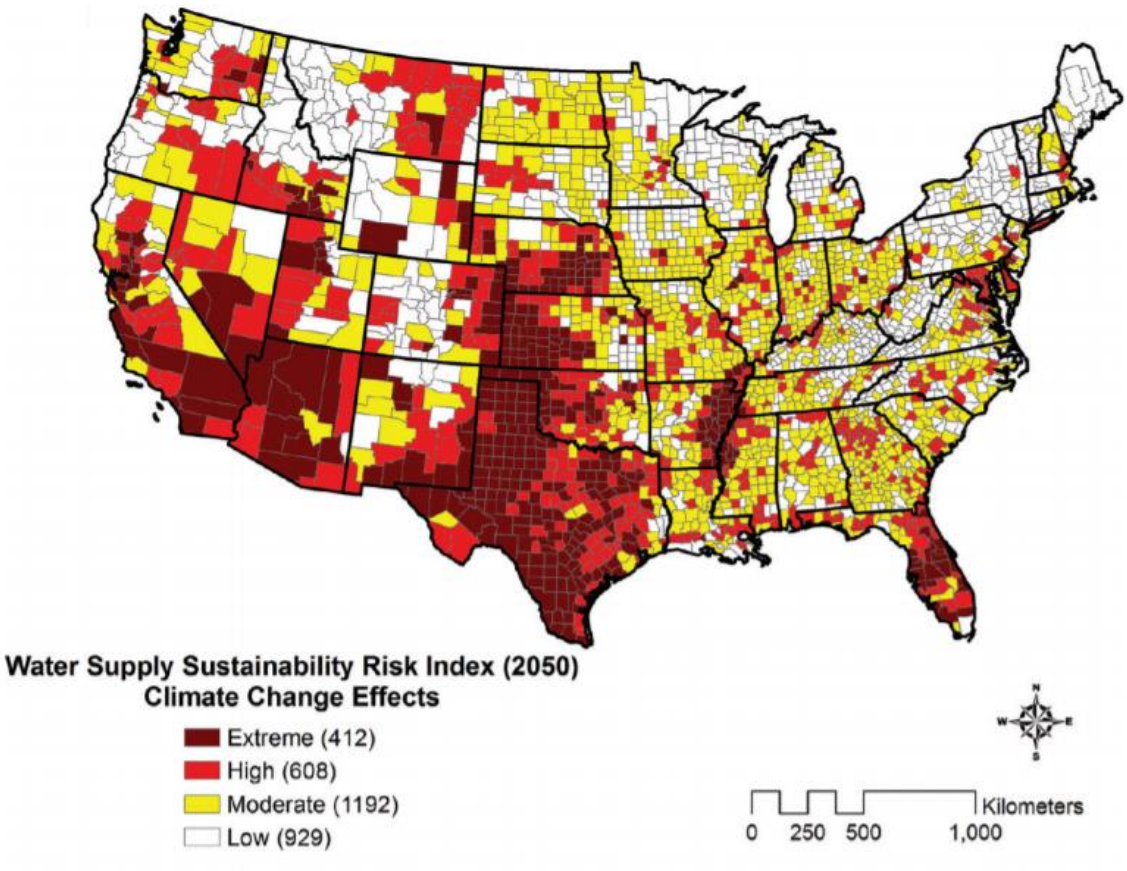

Figure 1. 1 Water-supply sustainability risk index for United States in 2050 linking water demand to population growth, increases in power generation, and climate change.[13]

Even though past examples of population, water usage and power generation do not indicate future demand, it will continue to grow. The combination of these factors has prompted worries about the accessibility of freshwater to meet residential, farming, industrial, mining, and natural needs. Efforts are taken to develop and further advance alternative water production technologies to address this challenge of water shortage.[14] As freshwater scarcity becomes more severe, alternative water sources - in particular, brackish groundwater - have become increasingly important for arid inland regions.[15,16]

1.2 Alternative water resource

For more than a century, infrastructure-intensive, centralized water supply systems have controlled the supply of water in cities. Satisfying the consistently expanding need for healthy freshwater through traditional concentrated frameworks for both consumable and non-consumable applications has just turned into an unrealistic desire. This is because there is competing demands on limited financial resources and limited flexibility of existing water infrastructure for adaptation and expansion. People have modified natural water systems often with the purpose of securing enough supply of water to meet the needs and necessities. However, in numerous regions, the arrangement of conventional water supply is not widespread, and when it exists, is frequently untrustworthy as far as quality and congruity of supply.[17] Hence, to balance the demand for freshwater, it has become increasingly important to develop sustainable alternative water sources.

Brackish water is increasingly observed as a resource for water supply[18,19,20] due to the energy requirements of reverse osmosis is minimized[21,22], and hence the expense of

desalination is diminishing. However, brackish groundwater is groundwater that has a dissolved mineral with concentrations higher than freshwater, and sometimes the term "brackish groundwater" is used interchangeably with "saline groundwater". However, multiple classification mechanisms have been used to quantitatively describe waters which have different dissolved-solids concentrations. Majority of the classification schemes consider saline groundwater to have a dissolved solids concentration between 1000 and 10000 milligrams per liter (mg/L)[23-25] Brackish groundwater is usually formed because of geological salt deposition or long-term agricultural activities.[26-28] Brackish groundwater desalination specifically has increased most extreme significance in parched inland districts.[29,30] Reverse Osmosis (RO) desalination is as of now the most dependable and generally utilized system for seawater and saline water desalination.[31,32,33] The use of RO for desalination has altogether expanded since the 1950s.[34] On the basis of the nature of the feed water, RO procedures can be grouped into brackish water RO plants where the salinity is in the scope of 500 mg/L to 10,000 mg/L and seawater RO plants where the salinity is around 30,000 mg/L. Brackish water reverse osmosis is further sub-sorted into low salinity brackish water RO that procedure feed water with saltiness somewhere in the range of 500 and 2500 mg/L and high salinity salty water RO plants that process water with salinity somewhere in the range of 2500 and 10,000 mg/L. Table 1.1 contains a summarized brine characteristics data of desalination plants. Globally, around half of the desalinated water accessible is created by utilizing RO.[33]

Table 1. 1 Composition of water sample of brine from different desalination plants.[35]

Component	Concentration	Units
Sodium (Na^+)	431-5250	mg/L
Calcium (Ca^{2+})	417-962	mg/L
Magnesium (Mg^{2+})	280-448	mg/L
Potassium (K^+)	43-145	mg/L
pH	7.1-8.1	
Bicarbonate (HCO_3^-)	37-464	mg/L
Chloride (Cl^-)	1964-8118	mg/L
Sulfate (SO_4^{2-})	1143-3881	mg/L
Nitrate (NO_3^-)	51-56	mg/L
TDS	8990-15960	mg/L

In recent years, membrane-based brackish water desalination has been increasingly implemented to supply drinking water in inland areas worldwide, including Australia, the Middle East and the United States.[36-40] For example, all the operational as well as planned

brackish groundwater desalination plants in California have a combined annual capacity of 260 million gallons per day as of 2013.[41]

1.3 Increasing use of groundwater and reverse osmosis

In many of the moderate to high risk locations in the states, surface water is almost fully utilized which makes the groundwater the only source of water which can meet the requirements. However, utilizing the groundwater has its own problems. In many areas in states, the amount of groundwater getting used is more than the amount of it getting recharged.[42] To add to the problem, as per the recent study done on the usage of groundwater and its projected implications on the climate changes by 21st century, there will be a total reduction of 10 to 20 percent in the recharge across the south western part of the United States.[43] To ensure the national water security, untapped water sources may need to be developed in some areas. A non-traditional water source – Brackish groundwater may act as one of the solutions to the current and the future water scarcity problem. Water supply in the semi-arid and arid area of the united states is inadequate and not able to meet the demands causing severe drought conditions. Because of this and predicted increase in the water utilization further mounts more tension on the groundwater resources.

A recent survey showcased that above 80 percent of the municipal desalination plants are inland groundwater facilities – mainly based in Florida, California, and Texas (Figure 1.2) – and most of this municipal desalination has been for treating the groundwater in brackish salinity range.[44] Brackish groundwater is surpassing as a supplement or

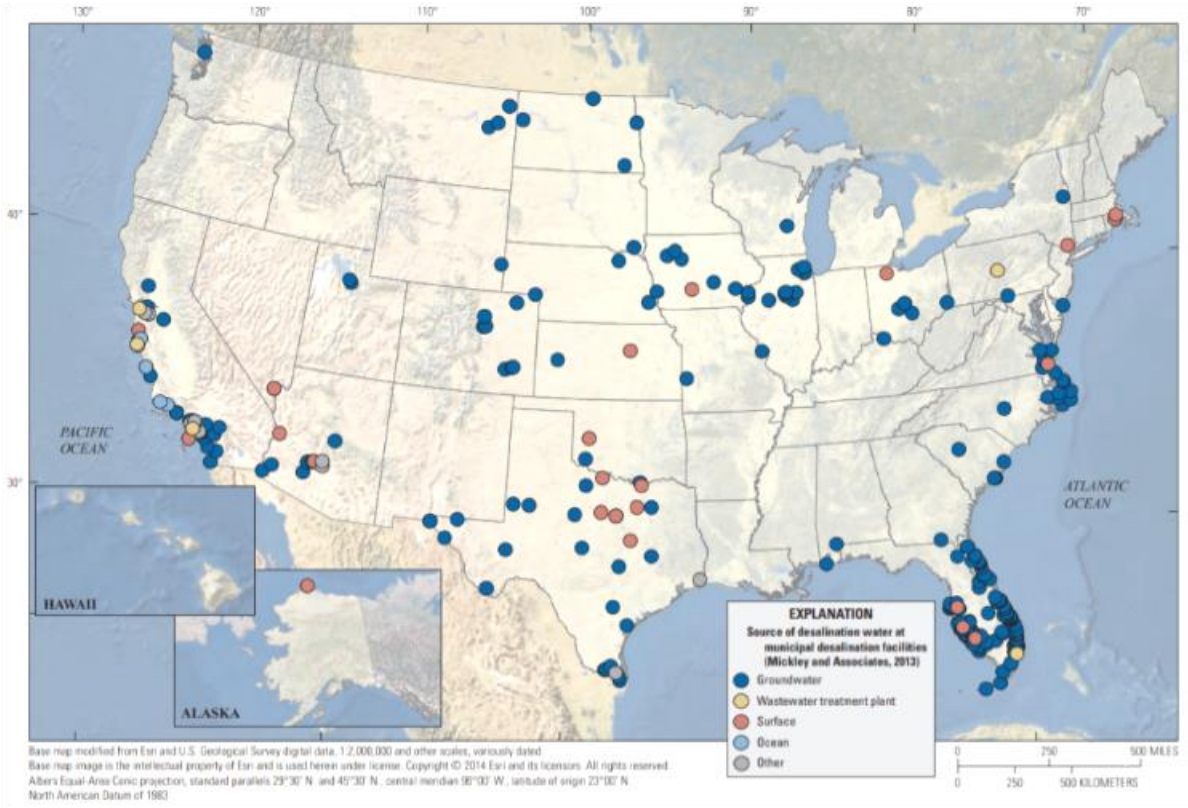

Figure 1. 2 Locations and sources of desalination water at municipal desalination facilities in the United States in 2010.[44]

substitution for freshwater. Implementing inland desalination in large proportion would mandate operation at high product water recovery in order to reduce the ecological and technical problems. It will also minimize disposal costs and water source loss, associated with the generated reverse osmosis concentrate.[45,46] Data from the USGS Water-Use Program indicate that an estimated 3,290 million gal/d of saline groundwater (dissolved-solids concentration of greater than or equal to [≥] 1,000 mg/L) was used in the United States in 2010, which is about 4 percent of the total groundwater use.[47] Most of the use was reported in Alaska, California, Florida, Oklahoma, Texas, Utah, and Wyoming.

1.4 Use of antiscalants in membrane processes

The problem of mineral salt scaling remains a serious impediment to achieving high recovery in brackish water desalination. Mineral salt scaling can occur when scale precursor ions (e.g., Ca^{2+}, Ba^{2+}, SO_4^{2-}, CO_3^{2-}, PO_4^{3-}, etc.) in the membrane retentate stream are concentrated above the solubility limits of various sparingly water soluble mineral antiscalants such as calcium sulfate dihydrate ($CaSO_{4(s)}$ gypsum), calcium carbonate ($CaCO_{3(s)}$ e.g., vaterite, calcite), calcium phosphate $Ca_5(PO_4)_3OH_{(s)}$ (hydroxylapatite) and barium sulfate ($BaSO_{4(s)}$ barite) at the membrane surface.[48,49] Mineral salt scaling leads to permeate flux decline and eventually the shortening of membrane useful life. To control membrane scaling, scale-inhibiting chemicals known as antiscalants are typically added into the feed water.[50-52] The use of these antiscalants can suppress mineral salt precipitation to some extent, thereby partially alleviating mineral scaling. However, even with the use of antiscalants, which can significantly increase the cost of reverse osmosis desalting, mineral salt scaling remains an impediment to achieving high product water recovery, partially due to the increased potential of fouling (including biofouling) when excessive dose of antiscalants is applied.[53]

These chemicals can interfere with the nucleation process of calcium solids and retards the crystal growth.[54] The continuous application of antiscalants in the feed water results in an oversaturated level of dissolved calcium that co-exists with antiscalants in the brackish desalination concentrate (also known as brine).[55,56] Meanwhile, the inhibiting effects of antiscalants on the precipitation of calcium solids is time sensitive. For example, in Inland Empire of Southern California, a 70-mile brine pipeline system carries inland

brackish water desalination concentrate to a coastal disposal facility.[57] The presence of antiscalants prevents calcium precipitation at the entry point to the brine line, but as the brine wastewater travels along the pipeline, a substantial amount of additional solids are subsequently generated, and creates problematic scaling issues in the pipeline.[58,59] Other studies similarly reported the delayed precipitation of solids in membrane concentrate.[60-62] This inadvertent solid formation and associated challenge in scale formation during brine disposal make it urgent to understand time-sensitive effects of antiscalants on solid formation in desalination brine.

Furthermore, conventional brine disposal approaches including evaporation pond are costly.[63] To reduce the cost, a reduction of TDS level in the brine is required.[64,65] Considering that a considerable contribution to TDS is the oversaturated calcium associated with the presence of antiscalants, a tunable control on antiscalants can potentially accelerate the precipitation of calcium solids and reduce TDS level. Therefore, it is critical to understand the nature and effects of antiscalants on the chemical stability of calcium solids in the brine, which can lead to the development of a sustainable concentrate management for inland desalination. Industrial antiscalants typically comprise of polycarboxylates, polyacrylates, polyphosphonates and polyphosphates. Prior desalination configurations used sodium hexametaphosphate (SHMP) as an antiscalant, but it is no longer used because SHMP was shown to be a food source for bacteria and resulted in biofouling.[66] Most antiscalants are organic phosphorus chemicals known as phosphonic acids. They contain multiple phosphonate functional groups ($-PO_3H_2$) within a tertiary amine structure.[67,68] The phosphorus-carbon bond in antiscalants exhibits a good thermal

stability,[69] and promotes their applications in desalination plants as well as cooling towers.[70,71]

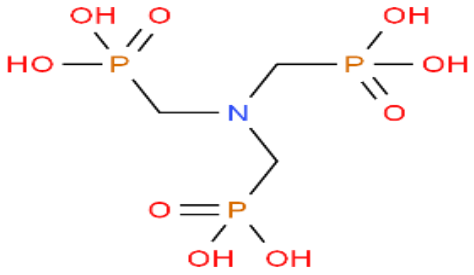

NTMP

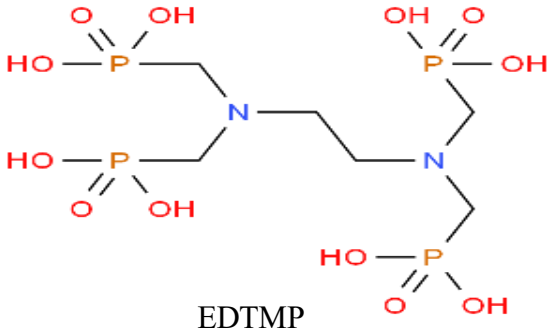

EDTMP

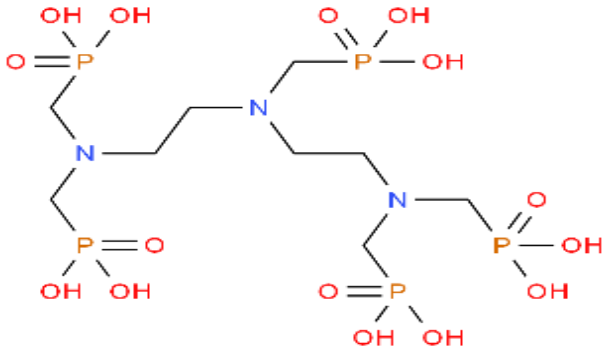

DTPMP

Figure 1. 4 Molecular structures of the three most widely used phosphonic antiscalants that are examined in this study.
NTMP: nitrilotris(methylenephosphonic acid);
EDTMP: ethylenediaminetetra(methylenephosphonic acid);
DTPMP: diethylenetriaminepenta(methylenephosphonic acid)

The typical concentration of phosphonic acids in desalination concentrate is in the sub- to several mg/L range.[72] In particular, nitrilotri-methylenephosphonic acid (NTMP), ethylenediaminetetra-methylenephosphonic acid (EDTMP) and diethylenetriaminepentakis-methylphosphonic acid (DTPMP) are among the most widely used antiscalants in water industry.[73-76] Their molecular structures are shown in Figure 1.3. Phosphonic antiscalants can form complexes with calcium and undergo multiple steps of deprotonation.[77-79]

These polyphosphonates are very strong complexing agents towards alkaline earth, transition, and heavy metal ions. The formation constants of the water soluble (1:1) complexes are similar to those of the commonly applied aminopolycarboxylates, such as popular ethylenedinitrilotetraacetic acid.[80] They are also able to form multinuclear complexes of varying stoichiometry, which make them even more efficient. The second, even more important property, is their ability to prevent the precipitation of hardly soluble salts of alkaline earth metals under substoichiometric conditions by interfering with early stages of the crystallization processes. It should be emphasized that in some cases only one molecule of a polyphosphonate is required to retain 5000–10,000 calcium ions in a solution. This is accompanied with a modification in the shape of the alkaline earth salt crystals and a change in their morphology that leads to amorphous solids that can be easily removed. Due to their high charge density, they are recognized as polyelectrolytes offering additionally superior dispersing functionalities for inorganic materials.[81,82]

1.5 Existing treatment technologies and challenges

High recovery operation helps in reduction of concentrate production and source water pumping. Effective pretreatment is a very common approach which is implemented in order to upscale the recovery of the reverse osmosis desalination. The easiest method here can be the recirculation of the concentrate back to an activated sludge process.[83] However, because of the high salt content of the membrane concentrates and low biodegradability, this is viable only for a short time period or, the recirculation could cause trouble in many plants for long term operation. Thus, it is a necessity to bring an intermediate step for concentrates. Various technologies could be applied in further treatment of the membrane concentrates like shear enhanced membrane filtration (nanofiltration or reverse osmosis), coagulation, advanced oxidation, activated carbon adsorption, electrodialysis and capacitive deionization.[84,85,86,87,88]

Most regular ways of disposing RO concentrate are surface water discharge, deep well injection, evaporation ponds and land application.[89] The mode of disposal of the concentrate depends on the site and the viability of the option mainly depends on the concentrate quantity and quality. Choosing the mode of option to be employed for disposal depends on the cost involved.[90,91,92,93] Various available options to surface waters include discharge to rivers, bays, tidal lakes, brackish canals, or oceans. [94] Many plants have been avoiding surface water discharge due to lengthy and costly permit reviews forcing them to go for other options.[95] The cost involved for well injection or sea discharge is estimated to be 0.05–0.06 US$/m^3 of product water and for the evaporation ponds is 0.56 US$/m^3. However, this is the only method which allows for recovery of the resource.[96] The other

possible option is blending of high ionic strength residuals with other wastewaters or Dilution. Also, concentrate mixed with industrial or municipal wastewaters can be treated further. An intermediate step can be employed to make sure that the feed stream is compatible with the RO membrane, so as to negate or minimize the potential of scale formation and of biofouling on the membrane and on flow channels and to reduce cleaning frequency requirements.

With the help of lime softeners, pellet softeners or fluidized bed crystallizers chemical softening of the primary RO concentrate can be achieved. A study used lime slurry (calcium hydroxide) for primary RO concentrate treatment.[97] While the other used flocculants that increased floc formation and assisted the removal of hardness ions.[98] The RO recovery has been enhanced marginally by using accelerated seeded precipitation and chemically enhanced seeded precipitation.[99,100,101] A research studied the three materials ($Ca_5(PO_4)_3OH_{(s)}$, $CaCO_3$ and $CaSO_4$) as seed crystals for reduction of calcium concentration in the RO concentrate during wastewater treatment.[102] Amongst these three materials, $(Ca_5(PO_4)_3OH_{(s)p}$ known as phosphate ion helped in reducing the calcium concentration by above 90%. While $CaCO_3$ and $CaSO_4$ as seed crystals did not prove to be very much effective. A substitute to lime addition is sodium hydroxide to increase the pH value. Selecting the chemical addition depends on the composition of the concentrate that requires treatment and the cost of the chemical involved.[103] The most challenging part of using these chemical softening processes is handling the sludge and efforts to be put in accurately maintaining the pH of the contactor.

Another way to remove divalent ions and metals from the RO concentrate is Electrocoagulation. In this method, an electrolytic reactor with electrodes (aluminum, iron, or stainless steel) and a separation tank in which RO concentrate is flown through a reactor and coagulation/flocculation occurs with the metal dissolved from the electrodes.[104,105] The benefit of implementing electrocoagulation for RO concentrate treatment is that it produces lesser waste sludge as compared with the regular chemical softening and high removal rates of scale-forming ions and metals. Hydrogen gas bubble forms at the cathode end along with the metal anode dissolution, this captures the flocs and causes flotation of the suspended solids, removing contaminants. However this process comes with a disadvantage of including high maintenance and operation costs due to timely electrode replacement and high energy usage and finite full-scale plant experience.[106] Recently, researchers have been focusing on membrane bioreactors to boost the process performance and to regain wastewater after removing some additional salt, i.e. reverse osmosis membrane.[107,108]

Several techniques have been proposed for separation of antiscalants. Different studies have reported that iron coated waste filtration sand and intermediate concentrate demineralization can eliminate antiscalant from the RO concentrate.[109,46] However, this method requires chemicals addition, generates sludge, low permeate quality, high operating costs, and the antiscalant in the RO concentrate is still not completely separated. Advanced oxidation is a promising treatment mode for the RO concentrate because of its great efficiency.[110] The amount of the antiscalants and organic pollutants in the RO concentrate can be reduced after the advanced oxidation together with the increase in the

following membrane performance.[111,112,113] Even though researches on the treatment of reverse osmosis concentrate with some oxidants have been performed,[105,114] there is a rift in the literature on the impact of degradation of antiscalants using advanced oxidation process on the precipitation kinetics of different scaling minerals as well as the induction time of nucleation. Further study is required to understand the growth in the recovery of secondary reverse osmosis process owing to a reduction in the concentrate volume.

Hence, the first step for RO is implemented until the concentrations of scale forming ions reach threshold membrane scaling. Before ingesting the concentrate to the secondary membrane process, the scale forming ions should be segregated from the water with an optimized way.

Ultraviolet-based advanced oxidation processes (UV/AOPs) have been increasingly required as part of the treatment train process to remove these contaminants. During UV treatment, an oxidant is photolyzed to generate short-lived radicals. Hydrogen peroxide (H_2O_2) is the most widely used oxidant to generate reactive hydroxyl radicals ($HO^{\cdot}$):

$$H_2O_2 \xrightarrow{h\nu} 2HO^{\bullet} \tag{3.5}$$

Recently, UV/persulfate ($S_2O_8^{2-}$) has been proposed and sulfate radicals ($SO4^{\cdot -}$) are generated as the radical initiation step:

$$S_2O_8^{2-} \xrightarrow{h\nu} 2SO_4^{\bullet -} \tag{3.6}$$

$SO_4^{\cdot -}$ has a similar oxidizing power compared to $HO^{\cdot}$ but possesses higher reaction rate constants with electron-rich contaminants.[115]

1.6 Motivation, aim and scope

The motivation of this doctoral research originates from the increasing challenges associated with the limited recovery of the reverse osmosis processes for desalination of saline water, particularly for brackish groundwater in inland areas. For the aforementioned reasons, scaling minerals decreases the recovery to an extent which leads to a huge amount of water wasted in the form of concentrate stream. Furthermore, conventional brine disposal techniques are costly and can negatively affect the ecosystems. To reduce the cost, a reduction of TDS level in the brine is required.[116,117] Considering that a considerable contribution to TDS is the oversaturated calcium associated with the presence of antiscalants, a tunable control on antiscalants can potentially accelerate the precipitation of calcium solids and reduce TDS level. Therefore, it is critical to understand the nature and effects of antiscalants on the chemical stability of calcium solids in the brine, which can lead to the development of a sustainable concentrate management for inland desalination.

The overarching goal of this research is to design a novel ultraviolet-based treatment process for the removal of scale-forming constituents and fundamentally understand the interaction of antiscalants with these scaling minerals.

Given the existing knowledge gap on the impact of degradation of antiscalants using advanced oxidation process on the precipitation kinetics of different scaling minerals as well as the onset of precipitation, We aim to utilize the advanced oxidation process and

fundamental nucleation principles and theories to investigate the precipitation chemistry of three commonly occurring scaling minerals calcium sulfate ($CaSO_{4(s)}$), calcium carbonate ($CaCO_{3(s)}$) and ($Ca_5(PO_4)_3OH_{(s)}$) in presence of three widely used antiscalants (*i.e.*, NTMP, EDTMP and DTPMP in brackish water concentrate. The acquired knowledge will help provide crucial information on the relationship among the rate of precipitation, the antiscalant dosage and the critical saturation index, which can help to determine the targeted amount of antiscalant that needs to be removed to achieve a high rate of demineralization.

Chapter 2

Impacts of Antiscalants on the Formation of Calcium Solids: Implication on Scaling Potential of Brackish Desalination Concentrate

Previously Published in ***Environmental Science: Water Research and Technology***

Jain, T.; Sanchez, E.; Owens-Bennett, E.; Trussell, R.; Walker, S. and Liu, H., Impacts of antiscalants on the formation of calcium solids: implication on scaling potential of desalination concentrate. *Environmental Science: Water Research & Technology* **2019**, 5, 1285-1294.

2.1 Abstract

Brackish water desalination has become increasingly important in arid inland regions for reliable water supplies, but the management of desalination brine waste is costly. In particular, the presence of oversaturated calcium as scale-forming compounds in the brine is challenging to dispose. This study investigated the effects of three widely used antiscalants, *i.e.*, nitrilotri-methylenephosphonic acid (NTMP), ethylenediaminetetra-methylenephosphonic acid (EDTMP) and diethylenetriaminepentakis-methylphosphonic acid (DTPMP) on the removal of calcium from solutions under chemical conditions relevant to brackish desalination brine, with an emphasis on the nucleation and precipitation of three calcium-containing solids including hydroxyapatite $Ca_5(PO_4)_3OH_{(s)}$, gypsum $CaSO_{4(s)}$ and vaterite $CaCO_{3(s)}$. Results showed that all three antiscalants exhibited uniquely time-dependent effects on the inhibition of calcium solid formation. The precipitation kinetics showed a three-phased behavior with an induction phase followed by a rapid reaction phase and a final equilibrium phase. The effectiveness of antiscalant in delaying calcium precipitation and in slowing down the rate of precipitation followed the order of DTPMP > EDTMP > NTMP. Antiscalants adsorb on the nuclei of calcium solids and inhibit the crystal growth process. Activation energy of nucleation increased linearly with antiscalant dosage, but it decreased as the regime changed from homogeneous to heterogeneous nucleation. This study generated vital information of the precipitation kinetics of calcium solids in the presence of phosphonate-containing antiscalants and advances the development of desalination brine management strategies.

2.2 Introduction

As freshwater scarcity becomes more severe with increasing population and climate change impact, alternative water sources - in particular, brackish groundwater - have become increasingly important for arid inland regions.[118,119] Brackish groundwater is usually formed as a result of geological salt deposition or long-term agricultural activities.[120-122] It typically contains total dissolved solid (TDS) levels between 1 and 10 g/L.[123-125] In recent years, membrane-based brackish water desalination has been increasingly implemented to supply drinking water in inland areas worldwide, including Australia, the Middle East and the United States.[126-130] For example, all the operational as well as planned brackish groundwater desalination plants in California have a combined annual capacity of 260 mgd as of 2013.[131]

A major challenge to desalination is membrane scaling, a phenomenon attributed to the inevitable precipitation of calcium-containing minerals including calcium sulfate $CaSO_{4(s)}$, calcium carbonate $CaCO_{3(s)}$ and calcium phosphate $Ca_5(PO_4)_3OH_{(s)}$ at the membrane surface.[132,133] To control membrane scaling, scale-inhibiting chemicals known as antiscalants are typically added into the feed water.[134-136] These chemicals can interfere with the nucleation process of calcium solids and retards the crystal growth.[137] The continuous application of antiscalants in the feed water results in an oversaturated level of dissolved calcium that co-exists with antiscalants in the brackish desalination concentrate (also known as brine).[138,139] Meanwhile, the inhibiting effects of antiscalants on the precipitation of calcium solids is time sensitive. For example, in Inland Empire of Southern California, a 70-mile brine pipeline system carries inland brackish water desalination

concentrate to a coastal disposal facility.[140] The presence of antiscalants prevents calcium precipitation at the entry point to the brine line, but as the brine wastewater travels along the pipeline, a substantial amount of additional solids are subsequently generated, and creates problematic scaling issues in the pipeline.[141,142] Other studies similarly reported the delayed precipitation of solids in membrane concentrate.[143-145] This inadvertent solid formation and associated challenge in scale formation during brine disposal make it urgent to understand time-sensitive effects of antiscalants on solid formation in desalination brine.

Furthermore, conventional brine disposal approaches including evaporation pond are costly.[146] To reduce the cost, a reduction of TDS level in the brine is required.[147,148] Considering that a considerable contribution to TDS is the oversaturated calcium associated with the presence of antiscalants, a tunable control on antiscalants can potentially accelerate the precipitation of calcium solids and reduce TDS level. Therefore, it is critical to understand the nature and effects of antiscalants on the chemical stability of calcium solids in the brine, which can lead to the development of a sustainable concentrate management for inland desalination.

Most antiscalants are organic phosphorus chemicals known as phosphonic acids. They contain multiple phosphonate functional groups ($-PO_3H_2$) within a tertiary amine structure.[149,150] The phosphorus-carbon bond in antiscalants exhibits a good thermal stability,[151] and promotes their applications in desalination plants as well as cooling towers.[152,153] The typical concentration of phosphonic acids in desalination concentrate is in the sub- to several mg/L range.[154] In particular, nitrilotri-methylenephosphonic acid

(NTMP), ethylenediaminetetra-methylenephosphonic acid (EDTMP) and diethylenetriaminepentakis-methylphosphonic acid (DTPMP) are among the most widely used antiscalants in water industry.[155-158] Their molecular structures are shown in Figure 1.3. Phosphonic antiscalants can form complexes with calcium and undergo multiple steps of deprotonation.[159-161]

Prior studies examined the impact of different antiscalants on the precipitation of calcite, gypsum, silica, *etc*.[29,162-164] Multiple studies have tried to quantify the dose response of antiscalants with respect to the extent of supersaturation.[52,165,166] However, the effect of antiscalants on the nucleation and crystal growth process of calcium solids remains unknown. Typically, the onset of solid precipitation is delayed in the presence of antiscalants. This delayed period, known as induction time, is controlled by the activation energy of the nucleation process.[167,168] A better and quantitative understanding on how antiscalants impacts the induction time is critical to predict the effectiveness of antiscalants. Furthermore, although the presence of antiscalants delays nucleation reaction, the nuclei formation eventually takes place. Therefore, it is important to quantify the kinetics of solid precipitation in the presence of antiscalants.

In addition, prior studies are mainly focused on $CaSO_{4(s)}$ and $CaCO_{3(s)}$ precipitation as the two calcium-containing solids.[164,169-172] In recent years, membrane-based advanced reuse of domestic wastewater in agricultural and industrial sectors are increasingly implemented. In these scenarios, the precipitation of calcium phosphate solid, especially hydroxyapatite $Ca_5(PO_4)_3OH_{(s)}$ in the brine becomes a major limiting factor.[173-175] However,

the nature of calcium phosphate formation and the associated antiscalant effect remains to be understood.

The objectives of this study were to examine the impacts of three widely used antiscalants (*i.e.*, NTMP, EDTMP and DTPMP in brackish water concentrate on the nucleation process of calcium-containing solids, *i.e.*, $Ca_5(PO_4)_3OH_{(s)}$, $CaSO_{4(s)}$, and $CaCO_{3(s)}$, quantify the precipitation kinetics of calcium solid formation, and examine the distinct crystal growth patterns of calcium minerals in the presence of different antiscalants.

2.3 Materials and methods

All solutions were prepared with analytical grade chemicals and deionized (DI) water (resistivity < 18.2 MΩ/cm). To start a precipitation experiment with $Ca_5(PO_4)_3OH_{(s)}$, stock solutions of 25-50 mM $CaCl_2$ and 1-3 mM Na_2HPO_4 were prepared and adjusted to pH 7.8 with droplets of 0.5 M NaOH and 0.5 M $HClO_4$. This pH level is typical of brackish water desalination brine.[176] Initial ionic strength of the mixing solution was fixed at 0.1 M by adding targeted amount of $NaClO_4$.

A 150-mL solution contains $CaCl_2$ and a 100-mL solution contains Na_2HPO_4 were adjusted to pH 7.8. Following that, 0-10 mM of NTMP, EDTMP or DTPMP prepared from its respective sodium-based salt was added into $CaCl_2$ and Na_2HPO_4 solutions with equal concentrations. Both solutions were then quickly mixed at a high stirring rate in a batch reactor. This approach of mixing avoided possible interference due to localized concentration spike. The final mixed solution created a targeted antiscalant concentration

ranging between 0 and 11 µM, and a saturation index between 14 and 15 with respect to $Ca_5(PO_4)_3OH_{(s)}$. The saturation index of $Ca_5(PO_4)_3OH_{(s)}$ is defined as:

$$SI_{Ca_5(PO_4)_3OH} = log\left(\frac{\alpha_{Ca^{2+}}^5 \times \alpha_{PO_4^{3-}}^3 \times \alpha_{OH^-}}{K_{sp,Ca_5(PO_4)_3OH_{(s)}}}\right) \quad (1.1)$$

where $\alpha_{PO_4^{3-}}$, , α_{OH^-} and, $\alpha_{Ca^{2+}}$ are activities of PO_4^{3-}, OH^- and Ca^{2+}, respectively. $K_{sp,Ca_5(PO_4)_3OH_{(s)}}$ is the solubility product of hydroxyapatite ($10^{-44.33}$). Equilibrium calculations and stability constants were from the Visual MINTEQ software database.[177]

The precipitation experiment with $CaSO_{4(s)}$ and $CaCO_{3(s)}$ were performed similarly to that of $Ca_5(PO_4)_3(OH)_{(s)}$, except that phosphate was replaced by sulfate and carbonate salt, respectively. The saturation index was controlled between 0.2 to 1.2 for $CaSO_{4(s)}$ and between 1.3 and 1.8 for $CaCO_{3(s)}$, respectively. The saturation index of each solid is defined as:

$$SI_{CaSO_4} = log\left(\frac{\alpha_{Ca^{2+}} \times \alpha_{SO_4{}^{2-}}}{K_{sp,CaSO_{4(s)}}}\right) \quad (1.2)$$

$$SI_{CaCO_3} = log\left(\frac{\alpha_{Ca^{2+}} \times \alpha_{CO_3{}^{2-}}}{K_{sp,CaCO_{3(s)}}}\right) \quad (1.3)$$

Where $\alpha_{SO_4^{2-}}, \alpha_{CO_3^{2-}}$ and $\alpha_{Ca^{2+}}$ are the activities of SO_4^{2-}, CO_3^{2-} and Ca^{2+}, respectively, while $K_{sp,CaSO_4}$ and $K_{sp,CaCO_3}$ are the solubility products of calcium sulfate and calcium carbonate, respectively. ($K_{sp,CaSO_4} = 10^{-4.61}$, $K_{sp,CaCO_3} = 10^{-8.48}$).[178]

After the mixing of respective solutions, precipitation experiments were conducted in a 250-mL batch reactor completely mixed at 400 rpm with a magnetic stir bar. The solid precipitation kinetics was monitored by measuring the change of turbidity at pre-determined time intervals using a HACH 2100N turbidimeter. The suspension pH was maintained at 7.8 ± 0.05 with a requisite amount of tris(hydroxymethyl)aminomethane (TRIS) buffer. The presence of TRIS buffer has a negligible impact on the calcium precipitation reaction (Figure S2.2). The rate of precipitation was calculated by fitting the turbidity-time profile to a Michaelis-Menten type model.[179] The rate model and the fitting are described in Text S2.1 and Figure S2.3. The concentration of antiscalants was confirmed by UV oxidation with H_2O_2 followed by analysis using the standard molybdate blue spectrophotometric method.[180] Zeta potential of precipitated calcium solids was measured using Zetasizer nano ZS90 analyzer (Malvern Panalytical, Inc.).

2.4 Results and discussions

2.4.1 Effect of antiscalant type on the precipitation of calcium solids

Figure 2.1A shows the kinetics of hydroxyapatite precipitation reaction in the presence of three antiscalants. The precipitation kinetics on the basis of the solution turbidity exhibited three distinct phases: an initial lag phase, a rapid precipitation phase and a final equilibrium phase. During the lag stage, hydroxyapatite nuclei underwent a constant formation and dissolution until a critical radius (denoted as $r_{critical}$) was achieved. This initial phase was followed by a rapid precipitation phase where crystals grew quickly until reaching equilibrium and becoming stationary in the end.

In the presence of 1 μM NTMP, EDTMP or DTPMP, the induction time for hydroxyapatite precipitation to occur ranged between 1 and 5 minutes (Figure 2.1A). Phosphonate antiscalants can adsorb onto the incipient nuclei generated during the induction period, resulting in a distortion of crystal growth pattern and a delay of nucleation.[181-183] Antiscalants can also act as an impurity on the surface of a growing crystal, which slows down its further growth. The presence of antiscalants can increase the surface energy of the growing crystals, which decreases the rate of nucleation and increases the induction time.[184]

The induction time of hydroxyapatite precipitation without an antiscalant was only a few seconds. It significantly increased in presence of an antiscalant compared to the control (Figure 2.1A). Calculations showed that a majority of calcium under the brine chemical condition exists as the free ion form rather than aqueous calcium-antiscalant complexes in the presence of antiscalants (Text S2.2 and Figure S2.4), indicating that the inhibitive effect by antiscalants likely results from the adsorption of antiscalants onto the incipient nuclei of hydroxyapatite.

In addition, the effectiveness of antiscalant in extending the induction time followed the order of DTPMP > EDTMP > NTMP (solid lines in Figure 2.1B). The longer induction time of hydroxyapatite nucleation in the presence of DTPMP compared to NTMP or EDTMP is likely contributed by two factors. First, antiscalants differ from each other in the number of amine functional groups in their backbone structure and the number of phosphonate groups (Figure 1.3). High-molecular-weight antiscalants with a larger number of amine groups (*e.g.*, DTPMP) have a bigger molecular structure compared to the

relatively low-molecular-weight antiscalants (*e.g.*, NTMP). When antiscalants adsorb on the incipient hydroxyapatite nuclei, the high-molecular-weight DTPMP molecules occupy a larger surface area of the nuclei structure, thus extending the induction time considerably.[69,185]

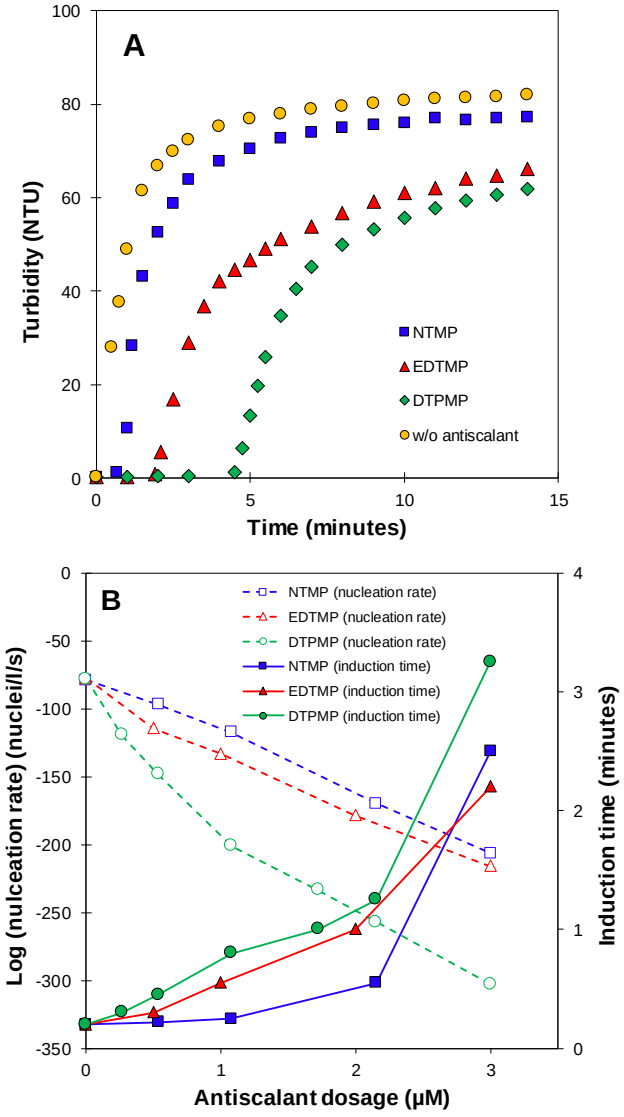

Figure 2. 1 (A) Comparison among three antiscalants on their effects on the kinetics of hydroxyapatite precipitation. [PO_4^{3-}] = 26 mg P/L; saturation index = 14.2; [antiscalant] = 1 μM. (B) Impact of different antiscalant dosage on the induction time (solid lines) and the nucleation rate (dash lines) of hydroxyapatite. [PO_4^{3-}] = 30 mg P/L; saturation index = 14.6. [Ca^{2+}] = 10 mM; pH = 7.8; ionic strength = 100 mM; [TRIS buffer] = 20 mM.

Furthermore, with the same saturation index of hydroxyapatite, the induction time increased with the antiscalant dosage (Figure 2.2A). For instance, an increase of EDTMP dosage from 0.5 to 3 µM increased the duration of induction time from 1.5 to 5 minutes, thus delaying the onset of homogeneous crystallization. A higher antiscalant concentration in the solution resulted in a higher surface adsorption of the nuclei and less surface areas were available for the nucleation to take place. In addition, the effects of antiscalant on the induction time also depends on the extent of calcium supersaturation. For example, a higher saturation index of hydroxyapatite reduced the induction time at the same dosage of EDTMP (Figure 2.2B).

Typically, as the dosage of antiscalant increased, it became more effective in delaying the onset of hydroxyapatite precipitation with more oversaturated solution, as shown by the extension of induction time with an increasing antiscalant dosage at a fixed saturation index (Figure 2.3). Furthermore, the three antiscalants exhibited different efficiencies in delaying hydroxyapatite precipitation. The duration of induction time was used to evaluate the antiscalant efficiency. A given antiscalant dosage was considered as efficient at and below the saturation index where a change in the initial saturation index showed a change in the average of the slope of the induction time more than 50% of its previous value. For example, at an antiscalant dosage of 0.5 µM, NTMP only became effective in delaying hydroxyapatite precipitation with a saturation index less than 14.40 (Figure 2.3A), whereas EDTMP became effective with a saturation index less than 14.55.

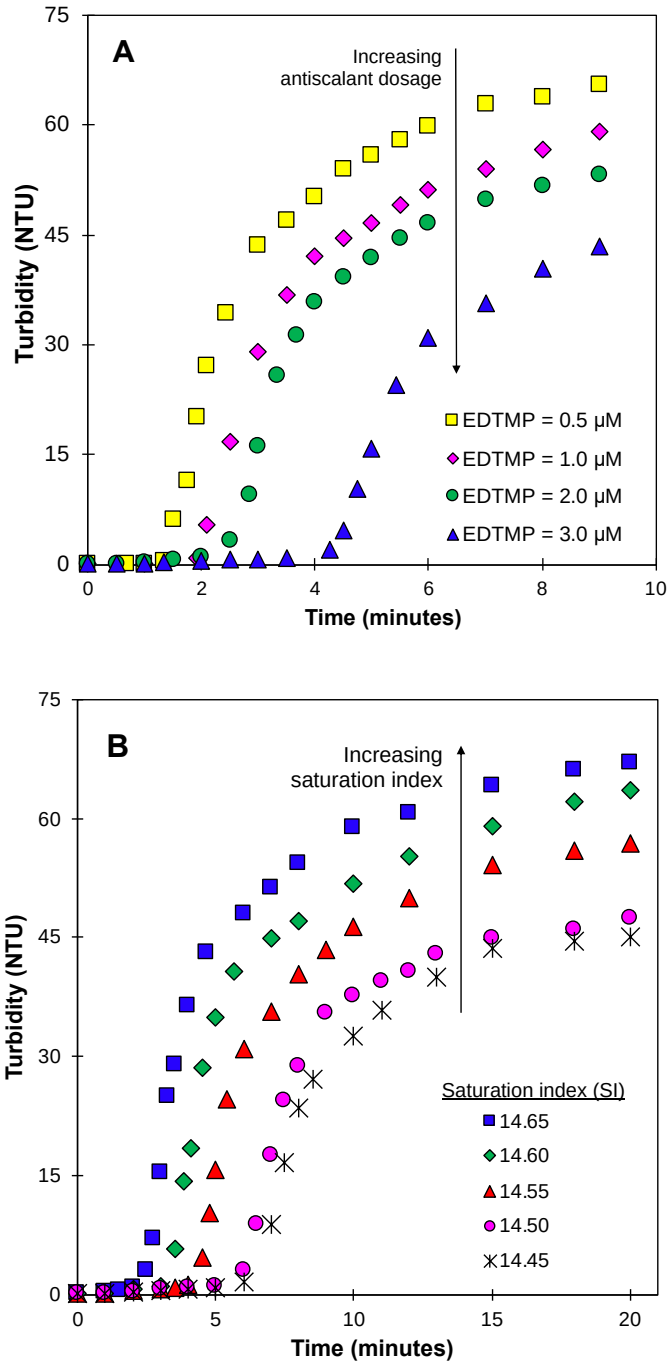

Figure 2. 2 The effects of EDTMP dosage and saturation index on induction time of precipitation of hydroxyapatite. (A) $[PO_4^{3-}]$ = 26 mg P/L; EDTMP = 0-3 µM. (B) $[PO_4^{3-}]$ = 22-25 mg P/L; EDTMP = 2 µM. $[Ca^{2+}]$ = 10 mM; pH = 7.8; ionic strength = 100 mM; [TRIS buffer] = 20 mM.

DTPMP was effective when saturation index was below 14.69 (Figure 2.3C). This effect was also observed for $CaSO_{4(s)}$ and $CaCO_{3(s)}$ precipitation, respectively (Figure S2.7). These critical saturation indices are significant in defining the inhibitive effects of antiscalants on scale formation in desalination concentrate. In addition, as the calcium oversaturation level was below the critical saturation index, different antiscalants accelerated the extension of induction time with respect to the saturation index in the order of NTMP > EDTMP > DTPMP (Figures 2.3A, 2.3B and 2.3C).

2.4.2 Thermodynamics of calcium crystallization in the presence of antiscalants

According to the theory of homogenous nucleation, the duration of induction time is intrinsically associated with the thermodynamics of nucleation reaction and crystal growth process. Specifically, the logarithm of induction time is linearly related to the square root of the saturation index of the corresponding solid as described in the equation below:[186,187]

$$\log(t_{ind}) = A\,[T^{-3}(SI)^{-2}] + B \qquad (1.5)$$

where t_{ind} is the induction time (second), T is the solution temperature (Kelvin), SI is the saturation index of the solution with respect to a calcium-containing solid (dimensionless), and both A and B are fitting parameters. This linear relationship was observed during the precipitation of $Ca_5(PO_4)_3OH_{(s)}$, $CaCO_{3(s)}$ and $CaSO_{4(s)}$ (Figure S2.8).

The surface energy of crystallization, γ (J/m^2), was calculated using the equation 1.6 below using the value of A obtained from equation 1.5:

$$\gamma = \left(\frac{A\,(2.3R)^3}{\beta V_m^2 N_A f(\theta)}\right)^{1/3} \qquad (1.6)$$

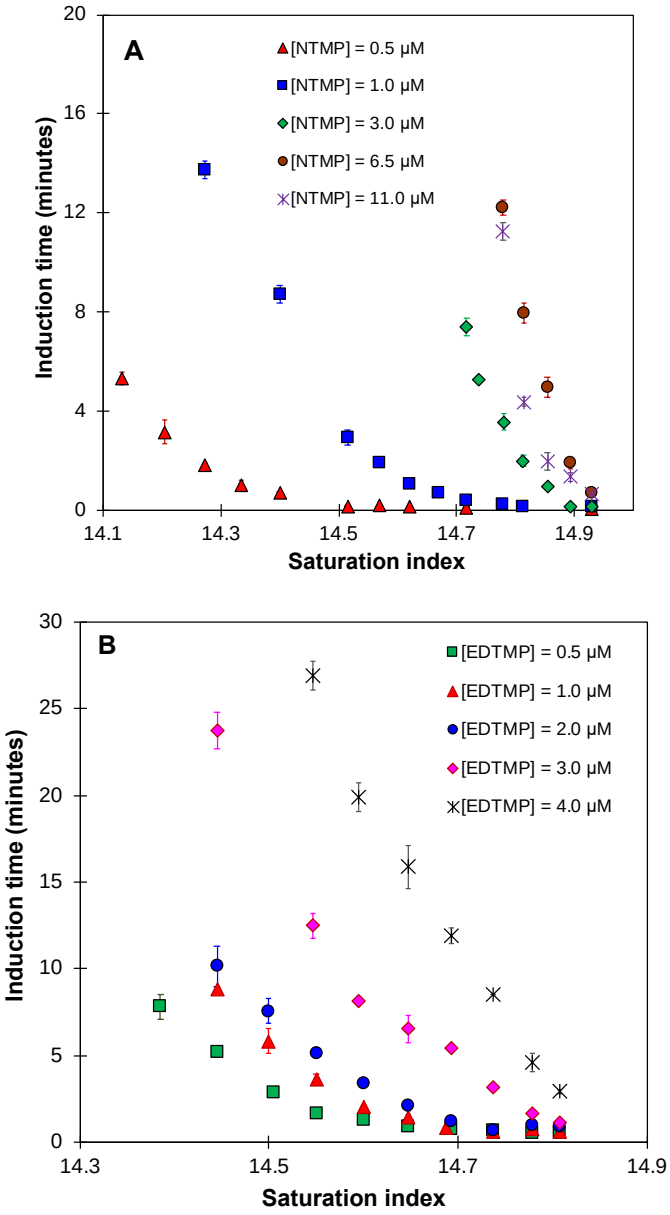

Figure 2. 3 The effect of antiscalant dosage on induction time of precipitation of hydroxyapatite. (A) $[PO_4^{3-}]$ = 17-34 mg-P/L; saturation index = 14.1-14.9. (B) $[PO_4^{3-}]$ = 22-31 mg-P/L; saturation index = 14.3-14.8.

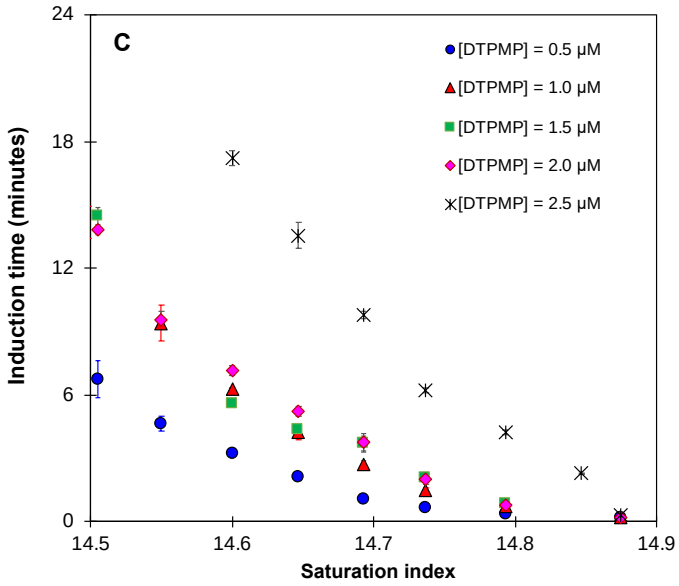

Figure 2.3 The effect of antiscalant dosage on induction time of precipitation of hydroxyapatite. (C) $[PO_4^{3-}]$ = 24-35 mg P/L; saturation index = 14.5-14.9. $[Ca^{2+}]$ = 10 mM; pH = 7.8; ionic strength = 100 mM; [TRIS buffer] = 20 mM.

where β is the geometry factor and has a value of $16\pi/3$ for a spherical nucleus, V_m is the molecular volume of the crystal (1.2×10^{-28} m^3/molecule for gypsum,[188] 6.1×10^{-29} m^3/molecule for vaterite,[189] and 2.6×10^{-28} m^3/molecule for hydroxyapatite[190,191]).

The Gibbs free energy of homogenous nucleation with respect to the radius of the nucleus is calculated as:[192-194]

$$\Delta G = -\frac{4\,\pi\,r^3\,k\,T\,\mathrm{SI}}{3\,V_m} + 4\,\pi\,r^2\gamma \qquad (1.7)$$

where k is the Boltzmann constant (1.38×10^{-23} $J\cdot K^{-1}$). The first term in Equation 7 represents the change in the bulk free energy. The second term is the change in the surface free energy that results from the formation of new interface between the new nuclei and the aqueous phase.

When the Gibbs free energy of nucleation reaches a maximum, the radius of the nucleus is defined as the critical radius of nucleation ($r_{critical}$), and the corresponding Gibbs free energy is defined as the activation energy of nucleation ($\Delta G_{critical}$). $r_{critical}$ is the minimal radius of the nucleus that is required for the initiation of crystal growth and precipitation. A typical calculated trend of the nucleation process is shown in Figure 2.4A. For Equation 7, when r = $r_{critical}$, (dΔG/dr) = 0. Therefore,

$$r_{critical} = \frac{2\gamma\, V_m}{kT\ \mathrm{SI}} \tag{1.8}$$

Accordingly, a combination of Equations 7 and 8 results in the following expression:

$$\Delta G_{critical} = \frac{16\pi\gamma^3 {V_m}^2}{3\, k^2 T^2 SI^2} \tag{1.9}$$

Calculations show that values of $\Delta G_{critical}$ and $r_{critical}$ decreased with an increase in saturation index (Figures S2.9-S2.10). A higher oversaturation level increases the probability of collisions between nuclei, and exerts a stronger driving force for nucleation, therefore decreasing the requirement on the size of subcritical nuclei reaching the $r_{critical}$. To understand the effect of antiscalants on the precipitation thermodynamics, the effect of antiscalant dosage on the activation energy of calcium solid nucleation was investigated. Figure 2.4B shows a plot of relative changes in activation energy of nucleation ($\Delta G_{critical}$) as a function of EDTMP dosage for different calcium solids. $CaCO_{3(s)}$ and $CaSO_{4(s)}$ showed a linear increase in the activation energy with an increasing EDTMP dosage. $Ca_5(PO_4)_3OH_{(s)}$, however, only showed a similar trend at a low EDTMP dosage up to 1

µM, and its activation energy decreased with a further increase in the EDTMP dosage from 1 µM to 4 µM (open circles, Figure 2.4B).

The decrease in the activation energy of nucleation of $Ca_5(PO_4)_3OH_{(s)}$ at higher EDTMP dosages can be attributed to a transition from homogenous to heterogeneous nucleation.

Plotting the log of induction time of hydroxyapatite in presence of EDTMP against the saturation ratio exhibited two distinct linear correlations (Figure S2.8A), suggesting a transition from homogenous to heterogenous nucleation when the saturation index decrease. This effect was only observed with lower saturation indices and higher antiscalant dosages. Similar findings were reported for the precipitation of calcium solids changing from homogeneous to heterogenous nucleation at lower saturation indices.[58,187] The heterogeneous nucleation can take place due to the presence of freshly formed hydroxyapatite acting as seeds for nucleation.[195] The free energy barrier is smaller for heterogeneous nucleation compared to that for homogeneous nucleation.[196] Thus, to calculate the homogeneous activation energy of hydroxyapatite nucleation the results with higher antiscalant dosage and lower saturation indices conditions were discarded. The recalculated results showed a linear increase with EDTMP dosage (closed circles, Figure 2.4B).

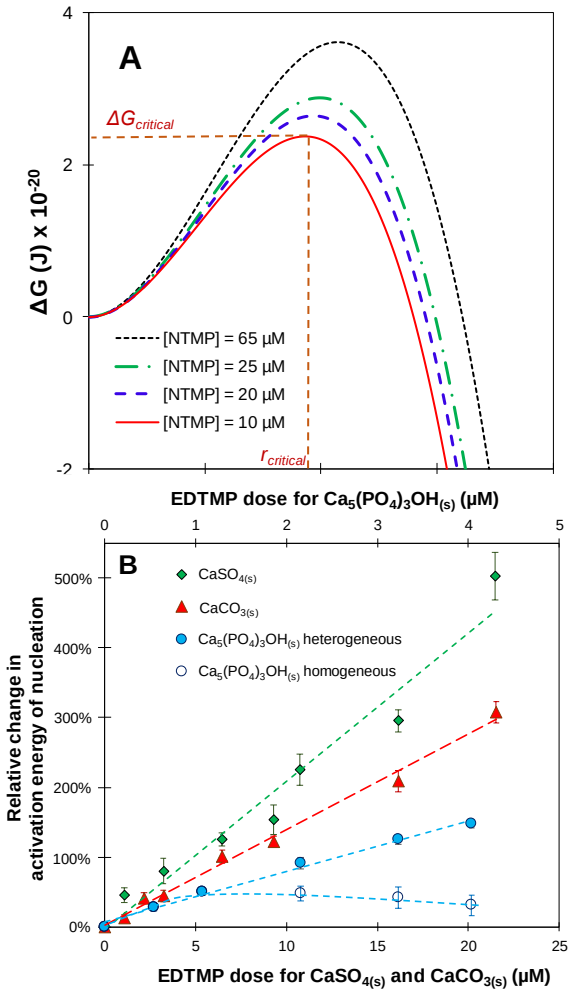

Figure 2. 4 (A) Gibbs free energy for homogeneous nucleation of $CaSO_{4(s)}$ at varying NTMP dosages. $[Ca^{2+}]$ = 37 mM; $[SO_4^{2-}]$ = 564 mM; Saturation index = 0.84; pH = 7.8. (B) Impact of EDTMP dose on activation energy of different calcium solids; Experimental conditions for $CaCO_{3(s)}$: $[Ca^{2+}]$ = 10 mM; $[CO_3^{2-}]$ = 10 mM; [EDTMP] = 0-21 µM; saturation index = 1.32; pH = 7.8; ionic strength = 100 mM; [TRIS buffer] = 50 mM; Experimental conditions for $CaSO_{4(s)}$: $[Ca^{2+}]$ = 37 mM; $[SO_4^{2-}]$ = 564 mM; [EDTMP] = 0-21 µM; saturation index = 7; pH = 7.8. Experimental conditions for $Ca_5(PO_4)_3OH_{(s)}$: homogeneous nucleation (closed circles), heterogeneous nucleation (open circles); $[Ca^{2+}]$ = 10 mM; $[PO_4^{3-}]$ = 0.6 mM; [EDTMP] = 0-4 µM; saturation index = 14.2; pH = 7.8; ionic strength = 100 mM; [TRIS buffer] = 20 mM.

2.4.3 Effect of antiscalant on the kinetics of calcium solids precipitation

The rate of hydroxyapatite precipitation depended on the antiscalant dosage and the saturation index (Figure 2.5). In general, at a fixed level of oversaturation, the rate of precipitation decreased with an increasing antiscalant dosage. Meanwhile, the rate of precipitation increased with a higher saturation index for any given antiscalant dosage.

In addition, different antiscalants exhibited distinct dosage-response behaviors on the precipitation rate. For example, NTMP showed a very strong dosage effect that highly depends on the level of oversaturation (Figure 2.5A). At a fixed NTMP dosage, as the saturation index increased beyond a critical value, the precipitation rate increased significantly

On the contrary, the dosage effect of EDTMP on the precipitation rate was moderate (Figure 2.5B), and that of DTPMP was insensitive to the saturation index (Figure 2.5C). EDTMP or DTPMP at a low dosage of 0.5 μM is as effective as other higher dosages in slowing down the precipitation kinetics regardless of calcium saturation, but NTMP at 0.5 μM was only effective at a low calcium saturation level. These trends suggest that EDTMP and DTPMP are more effective than NTMP in suppressing the rate of hydroxyapatite precipitation. This difference likely resulted from a higher surface blockage of nuclei by larger antiscalants molecules of EDTMP and DTPMP, and the consequently stronger inhibitive effects on the growth of calcium crystals.

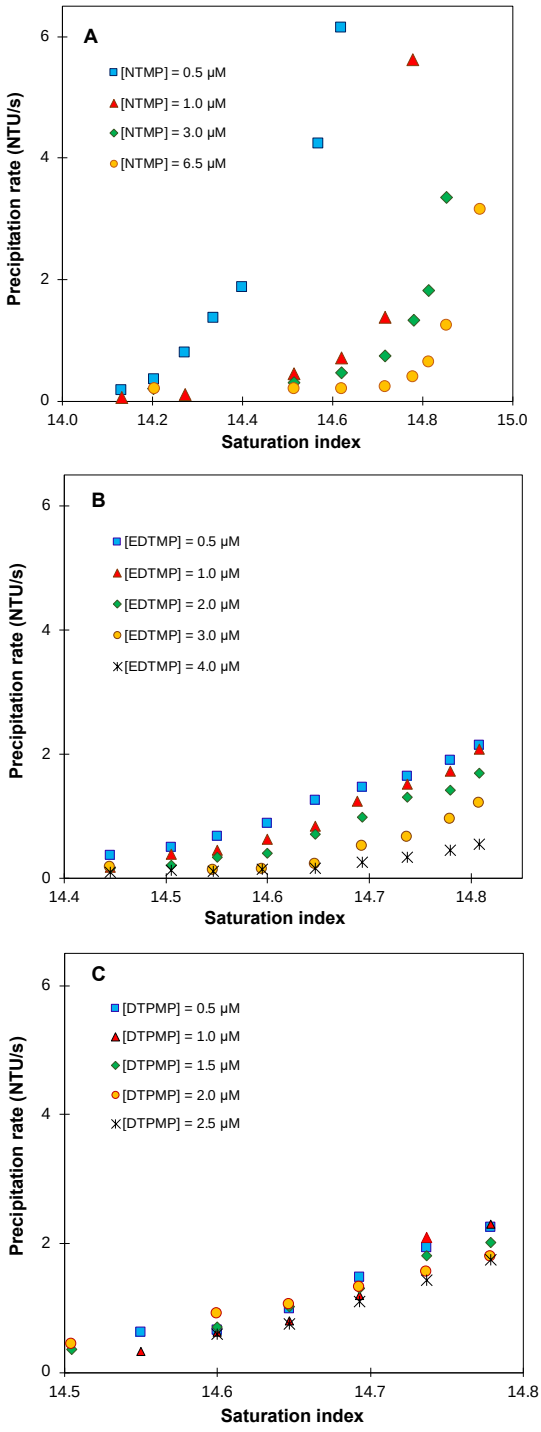

Figure 2. 5 Impact of antiscalant dosage on rate of precipitation of hydroxyapatite in presence of (A): NTMP (saturation index = 14.1-14.9); (B): EDTMP (saturation index = 14.3-14.8) and (C): DTPMP (saturation index = 14.5-14.8). [Ca^{2+}] = 10 mM; pH = 7.8; ionic strength = 100 mM; [TRIS buffer] = 20 mM.

2.5 Conclusions

These findings show that although all the three antiscalants have the active phosphonate functional groups, they affect the precipitation kinetics of calcium solids differently. Antiscalants are only effective in temporarily stabilizing the oversaturated desalination brine and delay the scale-forming substances (in this case, calcium solids) from precipitation. Results from this study established a quantitative relationship between the nucleation rate of three most commonly observed calcium-scaling solids and three most widely used antiscalants. Accordingly, it provided guidance on the threshold dosage of antiscalants that can hold a certain duration of time to prevent the oversaturated brine waste from scale formation. Furthermore, with an ever-increasing dependence on desalination especially in the inland areas and more desalination facilities targeting a near zero liquid discharge, brine demineralization (*i.e.*, TDS removal) is the key to increasing water recovery and managing the concentrate waste. The modeling of precipitation rate from this study provided crucial information on the relationship among the rate of precipitation, the antiscalant dosage and the critical saturation index, which can help to determine the targeted amount of antiscalant that needs to be removed to achieve a high rate of demineralization. The optimization of an efficient demineralization technique is crucial and will be further investigated in the future.

2.6 Acknowledgement

This research was partially supported by grants to H.L. from the National Science Foundation (Grant #1611306) and to T.J. from the National Water Research Institute

Fellowship. We also thank the assistance of Jesus Trujillo from San Bernardino Middle College High School and Osvaldo Mireles from San Bernardino Valley College.

Chapter 3

UV/oxidant enhanced precipitation of calcium sulfate in brackish water desalination brine concentrate

Manuscript in preparation for submission.

3.1 Abstract

Brackish water desalination has become increasingly important in arid inland regions for sustainable water supplies, but the management of desalination brine waste is costly. In particular, the presence of oversaturated calcium as scale-forming compounds in the brine is the most important factor limiting the recovery of water. Removal of these antiscalants from the brine can induce the precipitation of oversaturated scale-forming substances, enable additional water recovery from RO concentrate, and reduce the risk of eutrophication after brine disposal. This study investigated the impact of photochemical degradation of three widely used antiscalants, *i.e.,* nitrilotri-methylenephosphonic acid (NTMP), ethylenediaminetetra-methylenephosphonic acid (EDTMP) and diethylenetriaminepentakis-methylphosphonic acid (DTPMP) with hydrogen peroxide (H_2O_2) and persulfate ($S_2O_8^{2-}$) as the photo-oxidants, and the associated effects on inducing the precipitation of calcium sulfate ($CaSO_{4(s)}$). Results showed that the antiscalants could be effectively degraded at the optimized conditions. DTPMP degrades much slower compared to NTMP and EDTMP with both the photo-oxidants in this study. DTPMP also exhibited a much higher inhibition capacity in delaying the precipitation of gypsum. Results showed that the treatment efficiency of contaminants is higher with UV/$S_2O_8^{2-}$ than with UV/H_2O_2 under chemical conditions relevant to reverse osmosis desalination concentrate. The generation of $HO^{\cdot}$ was important in UV/H_2O_2, whereas both $SO4^{\cdot -}$ and $HO^{\cdot}$ were important in UV/$S_2O_8^{2-}$. It was also observed that induction time depended on the extent of UV exposure. This study shows an effective approach to potentially increase

the water recovery in desalination concentrate with the help of a UV/oxidant-assisted removal of TDS and thereby employing a secondary RO.

3.2 Introduction

During nanofiltration and reverse osmosis, antiscalant compounds are usually utilized to counteract membrane fouling by mineral scale. Phosphonate compounds are most widely used as antiscalants. Similar to phosphate, phosphonate compounds too have high affinity for Ca^{2+} and other scale forming ions, such as Ba^{2+}, Mg^{2+} and Fe^{3+}.[197] Phosphonate compounds hinder scale development by meddling with crystallization of scale shaping minerals and postponing or totally forestalling nucleation of mineral precipitates.[198] In multiple water treatment operations, the membrane concentrate is exposed to a subsequent stage reverse osmosis process. Water recuperation process can be increased by utilizing a multistage process that accommodates a precipitation step on the primary nano filtration and reverse osmosis concentrate.[199] Antiscalants are widely used in commercial applications since they have brilliant chelating properties[198] and helps in increasing the activation energy required by interacting with nucleating crystals. Moreover, antiscalants which contain phosphonate have been broadly utilized due to their stability and threshold adequacy.

Antiscalant compounds when utilized inhibit the mineral precipitation from the concentrate solution.[200] As a result, it is advisable that these compounds be removed from the primary concentrate before the precipitation stage. If the membrane concentrate has been discarded of in the ocean, phosphonate removal is also advisable to abstain from adding phosphonate that may advance algal blossoms.[201]

The management of the concentrated waste stream is one of the remaining obstacles for the implementation of desalination using RO membranes, since the concentrate is usually unusable and must be discharged or further treated. Currently, brine utilization has gained a lot of attention from both researchers and industries in the form of increasing water recovery and obtaining valuable components from the brackish desalinated water.[202,203,204,205] Several techniques have been proposed for separation of antiscalants. Some studies have reported that iron coated waste filtration sand and intermediate concentrate demineralization can eliminate antiscalant from the RO concentrate.[206,207] However, this method requires chemicals addition, generates sludge, low permeate quality, high operating costs, and the antiscalant in the RO concentrate is still not completely separated. Another study has investigated effect of antiscalant degradation using ozone on the salt precipitation in reverse osmosis concentrate and reported the changes in particle size distribution and the particle morphology. In this study, separation of antiscalant from reverse osmosis concentrates using advanced oxidation process was investigated. NTMP, EDTMP and DTPMP were used as models of antiscalants dissolved in reverse osmosis concentrate waste. Furthermore, persulfate and hydrogen peroxide were used as the oxidants to study the contribution of hydroxyl and sulfate radicals in the oxidation process.

3.3 Materials and methods

3.3.1 *Reagents*

All inorganic salts, acids and bases used in the experiments were analytical grade reagents. Calcium hydroxide, sodium sulfate and sodium persulfate were used were used to make synthetic test solutions. All the stock solutions were prepared with deionized (DI) water (18.2 MΩ/cm) produced from Milli-Q system (Millipore).

3.3.2 *$CaSO_{4(s)}$ precipitation via photochemical degradation of antiscalants.*

Batch experiments of photochemical antiscalant degradation were conducted in 10-mL quartz tubes under the irradiation of a 450-W UV immersion lamp (Ace Glass, Inc.). The lamp emitted photons with wavelengths ranging between 200 and 850 nm and has a UV intensity of 42 mW/cm^2 (Figure S3.1). All quartz tubes were placed in a carousel that rotated around the UV lamp. The dosage of all the antiscalants ranged from 0 to 15 mg P/L. To determine the steady-state radical concentrations generated during persulfate photolysis, 5 μM nitrobenzene (NB) and 5 μM benzoic acid (BA) were added as probe compounds. (Figure S3.2 and Figure S3.3) Prior to the experiment, the pH of the reaction solution was adjusted to a target value by adding $HClO_4$ or NaOH. The prepared reaction solution was transferred to quartz reaction tubes and placed in a carousel UV reactor (ACE Glass Inc.) equipped with a low-pressure UV mercury lamp (λ= 254 nm, 1.4 mW/cm^2)[208]. The experiments were conducted at 22±1° C. At predetermined time intervals, sacrificial tubes were withdrawn from the reactor for chemical analysis.

For UV-precipitation experiment with $CaSO_{4(s)}$, stock solutions of 500 mM $Ca(OH)_2$, 800 mM Na_2SO_4, 10 mM H_2O_2, 10 mM $Na_2S_2O_8$, 1 mM stock of each NTMP,

EDTMP and DTPMP, and 3 M $NaClO_4$ were prepared and adjusted to pH 7.8 with droplets of 2 M NaOH and 2 M $HClO_4$. This pH level is typical of brackish water desalination brine.[209] All the stock solutions were filtered through a 0.22-μm Millipore syringe filter prior to adding them before the start of the experiment. Turbidity of each stock solution was measured using a HACH 2100N turbidimeter. Initial ionic strength of the mixing solution was fixed at 1 M by adding targeted amount of $NaClO_4$. To start a UV reaction, all the chemicals viz. Na_2SO_4, antiscalant, $NaClO_4$ and the oxidant were added to the quartz tube except for the $Ca(OH)_2$. The pH of the solution was tested and adjusted to 7.8 if needed. $Ca(OH)_2$ was added just before placing the quartz tube in the UV reactor. The final mixed solution created a targeted antiscalant concentration ranging between 0 and 15 mg P/L, and a saturation ratio of 7 with respect to $CaSO_4$. The saturation ratio of $CaSO_{4(s)}$ is defined as:

$$SR_{CaSO_4} = \frac{\alpha_{Ca^{2+}} \times \alpha_{SO_4{}^{2-}}}{K_{sp,CaSO_{4(s)}}} \qquad (3.1)$$

Where $\alpha_{SO_4^{2-}}$ and $\alpha_{Ca^{2+}}$ are the activities of SO_4^{2-} and Ca^{2+}, respectively, while $K_{sp,CaSO_4}$ is the solubility product of calcium sulfate. ($K_{sp,CaSO_4} = 10^{-4.61}$).[210]

At pre-determined sampling intervals, one sacrificial quartz tube was taken out from the UV reactor. The suspension was immediately filtered through a 0.22-μm Millipore syringe filter to filter out the $CaSO_{4(s)}$ precipitated if any and further used to analyze the dissolved calcium concentration, inorganic phosphate and the antiscalant concentration in the filtrate. After filtering the $CaSO_{4(s)}$ out from the sample at the respective time interval,

the supernatant forms another precipitate of $CaSO_{4(s)}$ as the filtered supernatant is still supersaturated. To dissolve and extract all the calcium from the first filtered sample, one portion of concentrated HNO_3 is added to two portions of the sample. The solution obtained is then diluted to measure the dissolved calcium concentration.

3.3.3 *Modeling for determining the kinetics of calcium precipitation and induction time*

To quantitatively predict the induction time of nucleation and the kinetics of calcium precipitation, a multitarget model was established to describe the three-phase behavior using the equation 3.2. This model has been used to express typical viability loss profiles during disinfection of bacteria and Crytosporidium parvum oocysts and to predict the kinetics of disinfection of E coli.[211],[212]

$$N = N_0 \left\{ 1 - \frac{[1 - exp\,(-kt)]^m}{(N_0 p + 1)} \right\} \qquad (3.2)$$

Where, N is the dissolved calcium concentration (mM), N_0 is the initial calcium concentration before the onset of precipitation (mM), k is the rate constant for the exponential decay phase (minutes^{-1}), m and p are the intrinsic model fitting parameters with no physical significance. The value of k, m and p were obtained by fitting the model with experimental data using the Solver tool on the Microsoft Excel. The induction time (t_s) was defined as the period during which the dissolved calcium concentration dropped to 95% of the initial dissolved calcium concentration. Thus, when $N/N_0 = 0.95$. Consequently, t_s was calculated using equation 3.3:

$$t_s = \frac{-1}{k} LN\left\{1 - \left(\frac{100p + 1}{20}\right)^{1/m}\right\} \quad (3.3)$$

This kinetic model fits the precipitation of all calcium solids very well. Figure S3.4 shows a typically data fitting on the precipitation of gypsum in presence and absence of DTPMP. Figure S3.5 shows the model robustness comparing the predicted dissolved calcium concentration using the model against the experimentally measured concentration.

3.3.4 *Analytical methods*

Dissolved calcium was measured using a standard titration with ethylenediaminetetraacetic acid (EDTA) method.[213] All pH measurements were performed after calibrating the pH meter with standard buffers at pH 4, 7 and 10 adjusted to 1 M ionic strength simulating the experimental ionic strength to account for the pH deviation at elevated ionic strengths.[214,215] Thus, no recalculation of pH was further performed. The pH values reported in this work are presented as recorded based on the above procedure.

3.4 Results and discussion

3.4.1 *Antiscalant induced precipitation of calcium sulfate*

The dosage of hydrogen peroxide was optimized to achieve the optimal performance for antiscalant degradation in presence of medium pressure UV lamp. The antiscalant dosage was a key parameter because it impacted the induction time for nucleation and played a key role in the nucleation rate for different calcium minerals.[216] Details on the optimization of oxidation parameter were provided in Text S3.1 and Figure S3.6. The antiscalant degradation experiment released different degradation byproducts.

Inorganic orthophosphate is one of the primary oxidation products of this reaction. Figure 3.1 shows the fraction of the antiscalant degraded as depicted by the release of inorganic phosphorus. Owing to this, the concentration of inorganic phosphate increased with time. The saturation index of $Ca_5(PO_4)_3OH_{(s)}$ is defined as:

$$SI_{Ca_5(PO_4)_3OH} = log\left(\frac{\alpha^5_{Ca^{2+}} \times \alpha^3_{PO_4^{3-}} \times \alpha_{OH^-}}{K_{sp,Ca_5(PO_4)_3OH_{(s)}}}\right) \quad (3.4)$$

where $\alpha_{PO_4^{3-}}$, , α_{OH^-} and, $\alpha_{Ca^{2+}}$ are activities of PO_4^{3-}, OH^- and Ca^{2+}, respectively. $K_{sp,Ca_5(PO_4)_3OH_{(s)}}$ is the solubility product of hydroxyapatite ($10^{-44.33}$). Equilibrium calculations and stability constants were from the Visual MINTEQ software database.[217]

The saturation index of the solution with respect to hydroxyapatite thus increases with time as well. However, our previous studies have reported that hydroxyapatite doesn't precipitate within the experimental time below the saturation index of 12. To test this, an XRD analysis was performed at the precipitated minerals. XRD peaks showed that the precipitate existed as the gypsum and none of the peaks matched with hydroxyapatite Figure 3.2.

3.4.2 *Effect of antiscalant dosage on different precipitation properties of gypsum*

The impact of each antiscalant, NTMP, EDTMP and DTPMP was studied on their ability to induce precipitation of gypsum. Their concentrations were measured in terms of the amount of phosphorus content in each antiscalant as used in their commercial application. Thus, 3, 5, 8 and 15 mg P/L of each antiscalant was used as the initial dose. The antiscalant concentrations were measured and confirmed by different analytical methods. Inorganic phosphate was measured as a measure of antiscalant degradation as a function of time. All the three antiscalants were also measured directly using Ion chromatography as described in the materials and method to match with the inorganic phosphate measurement. This was further validated by fitting a degradation model based

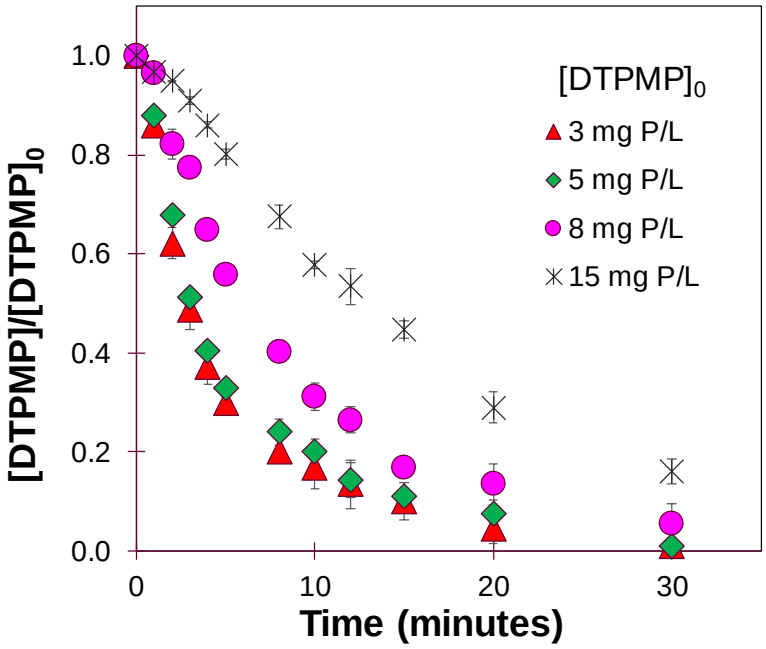

Figure 3. 1 Inorganic phosphate release profile with UV/PS degradation of DTPMP in presence of $CaSO_4$ precipitation $[S_2O_8]^{2-}{}_0$ = 3.8 mM; $[Ca^{2+}]$ = 37 mM; $[SO_4^{2-}]$ = 564 mM; pH = 7.8; medium pressure UV lamp.

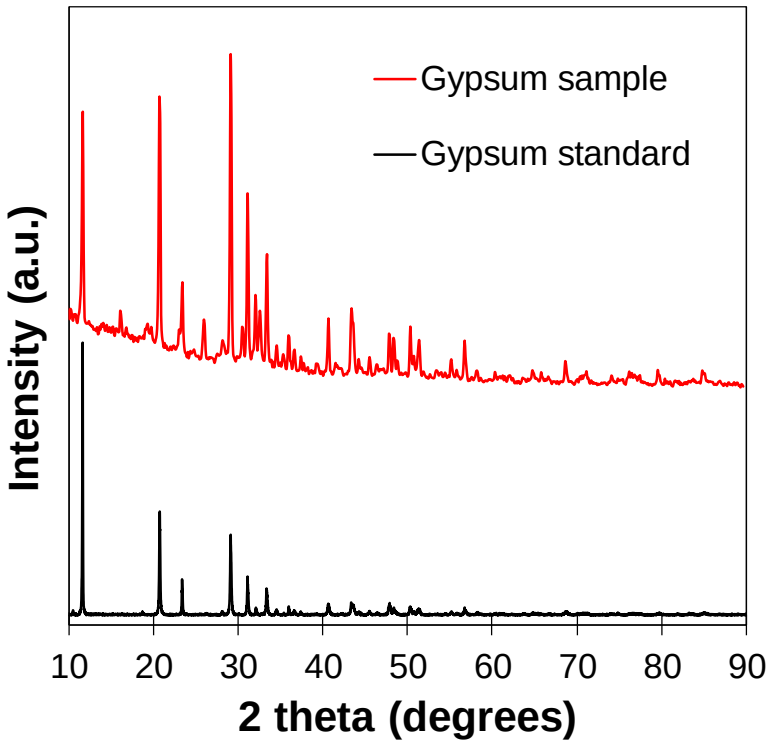

Figure 3. 2 Comparison of the XRD pattern for standard calcium sulfate with the solid precipitate after 60 minutes of oxidation of the antiscalant.

on the radical steady state concentration measurement (Figure S3.7). The dose response of each antiscalant was tested for its ability to delay the precipitation as well as the rate at which gypsum was precipitated in each case. were compared, and the fractional orthophosphate production increased as the concentration of antiscalant decreased. The thermodynamically stable form of calcium sulfate, gypsum is predicted to precipitate for the experimental conditions used (Figure 3.2). To compare the efficacy of the antiscalants, dissolved calcium was measured as a function of time to track the precipitation of gypsum. Typically, the onset of solid precipitation is delayed in the presence of antiscalants. The precipitation kinetics on the basis of the solution turbidity exhibited three distinct phases: an initial lag phase, a rapid precipitation phase and a final equilibrium phase. During the

lag stage, hydroxyapatite nuclei underwent a constant formation and dissolution until a critical radius (denoted as $r_{critical}$) was achieved. This initial phase was followed by a rapid precipitation phase where crystals grew quickly until reaching equilibrium and becoming stationary in the end. This delayed period, known as induction time, is controlled by the activation energy of the nucleation process.[218,219] With an initial antiscalant concentration of 3 mg P/L without any UV, there was no decrease in the dissolved calcium concentration for 30 minutes suggesting that without any decrease in the antiscalant concentration the supersaturated solution of calcium sulfate is stable and doesn't precipitate. Thus, the induction time is longer than the experimental time. Evidently, there won't be any decrease in the dissolved calcium concentration at higher antiscalant concentration without UV either. On the other hand, in absence of any antiscalant, the dissolved calcium concentration starts decreasing after 5 minutes. Suggesting that at the saturation conditions used in the experiments, the solution can hold only for 5 minutes. In presence of UV, as the antiscalant concentration decreased with time, so did the dissolved calcium concentration. As the initial antiscalant concentration increased, the induction time required for nucleation kept increasing. For example, the dissolved calcium concentration starts decreasing after 10 minutes when the initial antiscalant concentration was 3 mg P/L, while it took around 19 minutes when the initial antiscalant concentration was increased to 15 mg P/L (Figure 3.3). The same trend was observed for the two other phosphonate antiscalants, EDTMP and DTPMP tested in this study (Figure S3.8 and Figure S3.9). The residual antiscalant concentration which is the dynamic remaining concentration of antiscalant changes with time due to the antiscalant degradation. More importantly, for a

very low residual antiscalant concentration the induction time increases drastically with a slight increase in the residual antiscalant concentration. When the residual antiscalant concentration is high, the change is not this drastic.

In a system where the concentration of antiscalant doesn't change by operations like advanced oxidation processes, the induction time for precipitation is more sensitive to the antiscalant concentration at higher end of the spectrum unlike what we observed.[216] Usually when the concentration of antiscalant is high, the adsorption of these antiscalant molecules on the nucleating crystals have known to be increasing the activation energy of nucleation by retarding the precipitation of salts that have exceeded their solubility product,

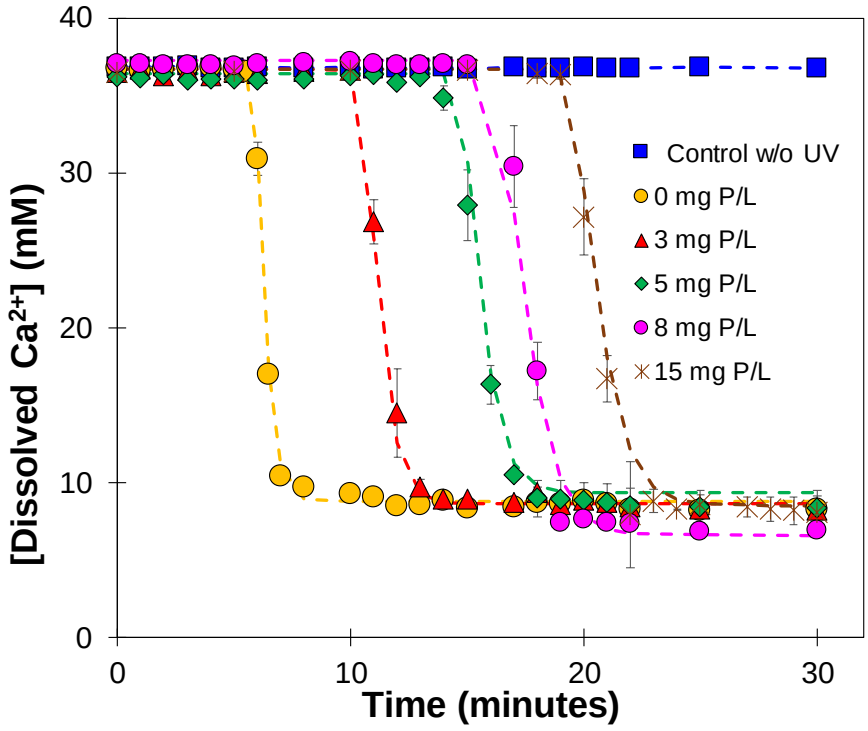

by distorting the normal crystal growth and producing an irregular crystal structure with

Figure 3. 3 Dissolved calcium release at different initial DTPMP concentrations; $[DTPMP]_0$ = 3-15 mg P/L; $[S_2O_8]^{2-}{}_0$ = 3.8 mM; $[Ca^{2+}]$ = 37 mM; $[SO_4^{2-}]$ = 564 mM; pH = 7.8; medium pressure UV lamp.

poor scale forming ability or by placing a surface charge on the crystals owing to which the crystals repel each other and are dispersed in the bulk.[220,221] However, in this dynamic experiment a synergistic effect between the nucleation of calcium sulfate crystals and degrading antiscalant is observed. When the antiscalant concentration decreases, the molecules of antiscalants are degraded they release packets of the nucleating crystals that were not available for nucleation. These newly freed crystals nucleate to form bigger crystals and eventually precipitate. Thus, between the two mechanisms of decreasing antiscalant concentration and nucleating crystals, the nucleation of crystals is more significant and hence the induction time of nucleation doesn't show strong dependence on

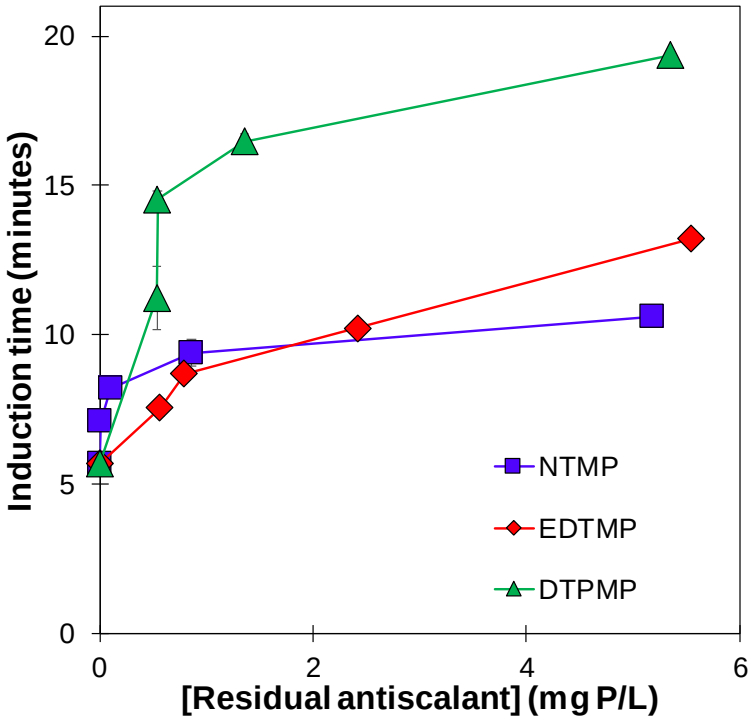

the residual antiscalant concentration (Figure 3.4). The critical radius of nucleation

Figure 3. 4 The effect of residual antiscalant concentration on the induction time of gypsum; $[antiscalant]_0$ = 3-15 mg P/L; $[S_2O_8^{2-}]_0$ = 3.8 mM; $[Ca^{2+}]$ = 37 mM; $[SO_4^{2-}]$ = 564 mM; pH = 7.8; medium pressure UV lamp.

required for the crystallization to occur is relatively smaller for lower antiscalant dosage. Thus, with slight decrease in the antiscalant concentration, the induction time decreases significantly.

3.4.3 *Effect of antiscalant type*

Figure 3.5 shows the kinetics of gypsum precipitation reaction in the presence of three antiscalants. In the presence of 15 mg P/L NTMP, EDTMP or DTPMP, the induction time for gypsum precipitation to occur ranged between 9 and 18 minutes. Phosphonate antiscalants can adsorb onto the incipient nuclei generated during the induction period, resulting in a distortion of crystal growth pattern and a delay of nucleation.[222-224]

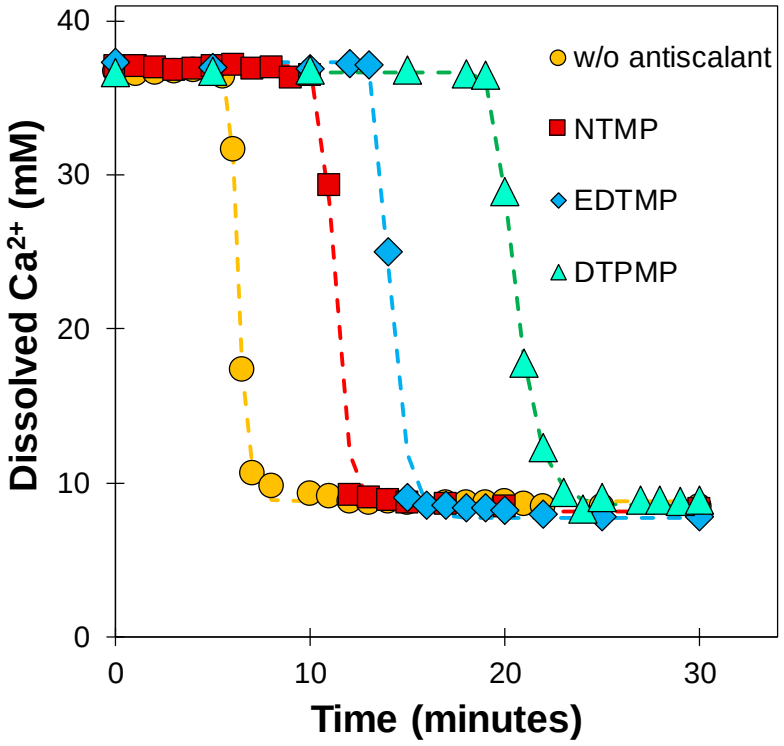

Figure 3. 5 Comparison among three antiscalants on their effects on the kinetics of gypsum precipitation in UV persulfate oxidation system. $[antiscalant]_0 = 15$ mg P/L; $[S_2O_8]^{2-}_0 = 3.8$ mM; $[Ca^{2+}] = 37$ mM; $[SO_4^{2-}] = 564$ mM; pH = 7.8; medium pressure UV lamp.

Antiscalants can also act as an impurity on the surface of a growing crystal, which slows down its further growth. The presence of antiscalants can increase the surface energy of the growing crystals, which decreases the rate of nucleation and increases the induction time.[225]

The induction time of gypsum precipitation without an antiscalant was only 5 minutes. It significantly increased in presence of an antiscalant by almost doubling compared to the control. Calculations showed that a majority of calcium under the brine chemical condition exists as the free ion form rather than aqueous calcium-antiscalant complexes in the presence of antiscalants (Text S2.2 and Figure S2.4), indicating that the inhibitive effect by antiscalants likely results from the adsorption of antiscalants onto the incipient nuclei of gypsum.

In addition, the effectiveness of antiscalant in extending the induction time followed the order of DTPMP > EDTMP > NTMP. The longer induction time of gypsum nucleation in the presence of DTPMP compared to NTMP or EDTMP is likely contributed by two factors. First, antiscalants differ from each other in the number of amine functional groups in their backbone structure and the number of phosphonate groups (Figure S2.1). High-molecular-weight antiscalants with a larger number of amine groups (*e.g.*, DTPMP) have a bigger molecular structure compared to the relatively low-molecular-weight antiscalants (*e.g.*, NTMP). When antiscalants adsorb on the incipient hydroxyapatite nuclei, the high-molecular-weight DTPMP molecules occupy a larger surface area of the nuclei structure, thus extending the induction time considerably.[69,226] Secondly, the degradation rate of the antiscalants follow the order of DTPMP < EDTMP < NTMP. Thus,

once the oxidation begins, at any given time, the concentration of DTPMP is relatively higher compared to EDTMP and NTMP.

3.4.4 *Effect of oxidant type on the precipitation kinetics and induction time for gypsum*

Most organic compounds are resistant to conventional chemical and biological treatments. The C-P bond in these antiscalants make them very durable in the environmental conditions.[227] Previous study have reported fission of this C-P bond as well as C-N bond using UV/persulfate.[228] To the best of our knowledge no investigation has been done on understanding the contribution of different radicals and UV/AOPs on the precipitation characteristics of scaling minerals.

All the experiments were conducted at pH 7.8 without addition of any buffer. All the three antiscalants showed complete removal at lower antiscalant dosage of 3 mg P/L within 30 minutes of UV/oxidant releasing orthophosphate as the degradation product. The degradation of NTMP and generation of orthophosphate both followed a pseudo first-order kinetics. The spontaneous release of orthophosphate and the decrease in the antiscalant concentration resulted due to the generation of highly reactive radicals in presence of UV/H_2O_2 and UV/persulfate in their respective systems.

The photochemical advanced oxidation process using UV light and hydrogen peroxide is a quite well-established technology for water and wastewater treatment[229,230,231] This process relies on the production of an effective oxidant, the hydroxyl radical (•OH), through the irradiation of the hydrogen peroxide with ultraviolet radiation.

$$H_2O_2 \xrightarrow{hv} 2HO^{\bullet} \quad (3.5)$$

$$S_2O_8^{2-} \xrightarrow{h\nu} 2SO_4^{\bullet-} \quad (3.6)$$

$$SO_4^{\bullet-} + H_2O \xrightarrow{h\nu} HO^{\bullet} + HSO_4^{-} \quad (3.7)$$

$HO^{\bullet}$ reacts non-selectively with organics at the near diffusion-limited rate constants[232] whereas, $SO_4^{\bullet-}$ is more reactive with compounds containing electron-donating functional groups including olefinic bonds, amine and hydroxyl groups.[233,234]

Several experiments were performed with a fixed oxidant dosage for both persulfate and peroxide varying the antiscalant type and dosage. Results for the antiscalant DTPMP are

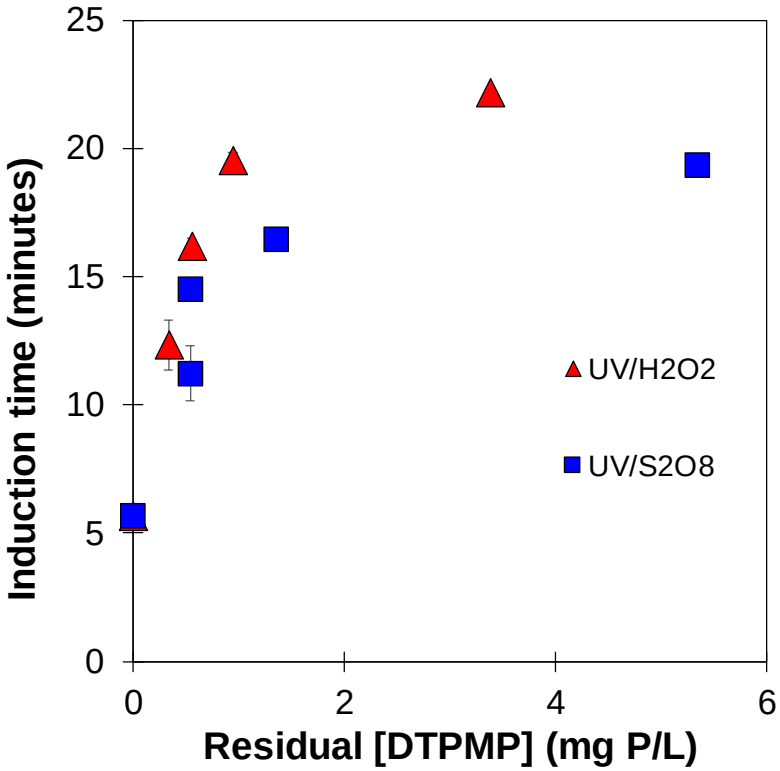

Figure 3. 6 Induction time of precipitation for gypsum as a function at varying residual DTPMP concentration. $[S_2O_8]^{2-}{}_0$ = 3.8 mM; $[Ca^{2+}]$ = 37 mM; $[SO_4^{2-}]$ = 564 mM; pH = 7.8; medium pressure UV lamp

shown in Figure 3.6 as the induction time of precipitation for gypsum as a function of the residual antiscalant concentration. The residual antiscalant concentration is the concentration of the antiscalant at the onset of precipitation. The onset of precipitation is determined by using equation 3.3 and the antiscalant concentration is estimated from the pseudo first order degradation rate profile of the antiscalant. UV/persulfate is slightly better with an induction time 10-15% longer compared to UV/H_2O_2. In order to quantify the performance of each system, steady state concentration of each radicals and hence their steady-state concentrations and intrinsic second-order reaction rate constants with DTPMP were determined based on competition reaction kinetics (Text S4.1). Nitrobenzene and

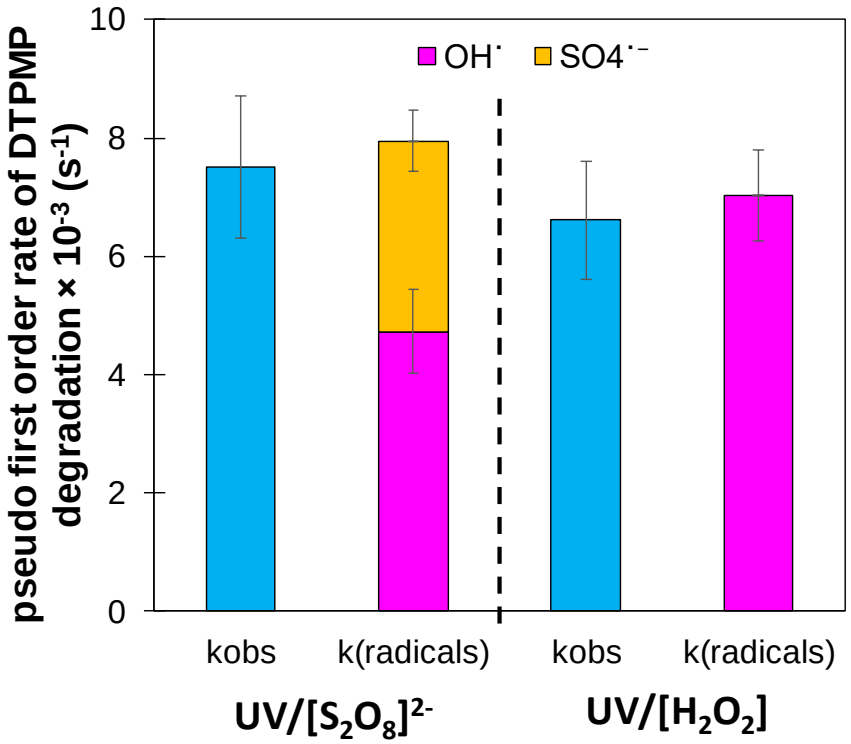

Figure 3. 7 Comparison of the pseudo first order rate constants in UV/H_2O_2 and UV/persulfate system. Color bars represent calculated radicals' contribution on $k_{obs\text{-}DTPMP}$ and patterned fill represents the observed pseudo first-order rates of DTPMP degradation. Experimental condition: $[oxidant]_0$ = 2.0 mM; [DTPMP] 15 mg P/L; pH = 7.8.

benzoic acid were used as the probes for measuring the steady state concentrations of HO• and $SO_4^{\bullet-}$.

Figure 3.7 shows the comparison of the pseudo first order rate constants in UV/H_2O_2 and UV/persulfate system. The pseudo-first order rate constant of UV/persulfate is ~13% higher compared to UV/H_2O_2. Although the second order rate constant for the reaction between sulfate radical and DTPMP ($k_{SO4\text{-}DTPMP}$ = 5.1×10^6 $M^{-1}s^{-1}$) is almost half of the second order rate constant for the reaction between hydroxyl radical and DTPMP ($k_{OH\text{-}DTPMP}$ = 11.6×10^7 $M^{-1}s^{-1}$) the radical steady state concentration of hydroxyl radicals decreases slightly in the UV/persulfate system but almost an equivalent amount of sulfate radicals is produced which compensates for the decreased hydroxyl radical steady state concentration. (Table S3.1)

3.5 Acknowledgement

This research was partially supported by grants to H.L. from the National Science Foundation (Grant #1611306) and to T.J. from the National Water Research Institute Fellowship. We also thank the assistance of Kiranmayi Mangalgiri and Samuel Patton with probe analysis, and Nadia Estrada from San Bernardino Valley College.

Chapter 4

Parameter effects on antiscalant degradation and precipitation of scale-forming constituents in brackish water desalination concentrate

Manuscript in preparation for submission.

4.1 Abstract

The integration advanced oxidation process on reverse osmosis membrane concentrate to degrade antiscalant while inducing the precipitation of gypsum was evaluated in this study. In addition, the impact of photochemical degradation of three widely used antiscalants, *i.e.*, nitrilotri-methylenephosphonic acid (NTMP), ethylenediaminetetra-methylenephosphonic acid (EDTMP) and diethylenetriaminepentakis-methylphosphonic acid (DTPMP) with hydrogen peroxide and persulfate as the photo-oxidants and on inducing the precipitation of calcium sulfate was studied while varying different water parameters such as pH, chloride, natural organic matter, bicarbonate. A systematic approach that included radical steady state distribution measurement for different radicals such as hydroxyl radical ($HO^{\cdot}$), sulfate radical ($SO_4^{\cdot -}$), reactive chlorine species and carbonate radical ($CO_3^{\cdot -}$) carbonate radical was examined The change of pH did not have any significant impact the radical steady state distribution in either oxidant system. Owing to which it did change the rate of precipitation or the induction time substantially. In the presence of chloride, natural organic matter, bicarbonate a considerable drop in the radical steady state concentration was observed for both, UV/$S_2O_8^{2-}$ as well as UV/H_2O_2 system. The combined experimental and modeling approach provided guidance for the design and optimization of UV/AOP systems for increasing the recovery of water in brackish water desalination systems.

4.2 Introduction

Groundwater is a significant wellspring of drinking water for mankind. 90% of the freshwater resources are contained by it and it is even a significant reserve of good quality water[235] and it is additionally utilized for farming, industrial, family unit, recreational and environmental activities everywhere throughout the world.[236] The groundwater quality is typically portrayed by physical attributes, concoction synthesis, and organic parameters. These quality parameters reflect contributions from regular sources including the environment, soil and water rock weathering, and also anthropogenic impacts of different activities, for example, mining, land leeway, agribusiness, corrosive precipitation, and household and industrial waste. These parameters change broadly because of the sort of contamination, seasonal fluctuation, groundwater extraction, and so on.[237] Groundwater generally contains dissolved mineral ions, for example, calcium, manganese, chromium, cadmium, copper, cobalt, zinc, lithium, sodium, potassium, nitrate, sulfate, bicarbonate and chloride which can influence the water quality.[238] A portion of these constituents such as chloride, bicarbonate and NOMs are available in very high percentage in the reverse osmosis brines. These water matrix segments have been accounted for, to adversely affect the radical based propelled oxidation processes.[239,240,241,242]

Past research has not efficiently assessed the impacts of these matrix components on AOP treatment. In fact, even the matrix effects were addressed, no study has evaluated the impact of these radicals on the precipitation pace of scaling minerals. It is important that a superior understanding be developed of the detailed mechanisms of radical distribution and transformation in UV/AOPs associated with antiscalant-degradation-

induced precipitation. Specific experiments were likewise directed to explain the effect of individual chemical parameters including pH, chloride, alkalinity and organic carbon on UV/AOP execution.

4.3 Materials and methods

4.3.1 *Reagents*

All inorganic salts, acids and bases used in the experiments were analytical grade reagents. Calcium hydroxide, sodium sulfate and sodium persulfate were used were used to make synthetic test solutions. All the stock solutions were prepared with deionized (DI) water (18.2 MΩ/cm) produced from Milli-Q system (Millipore).

4.3.2 *$CaSO_{4(s)}$ precipitation via photochemical degradation of antiscalants.*

Batch experiments of photochemical antiscalant degradation were conducted in 10-mL quartz tubes under the irradiation of a 450-W UV immersion lamp (Ace Glass, Inc.). The lamp emitted photons with wavelengths ranging between 200 and 850 nm and has a UV intensity of 42 mW/cm^2. All quartz tubes were placed in a carousel that rotated around the UV lamp. The dosage of all the antiscalants ranged from 0 to 15 mg P/L. The pH of the solutions was adjusted to 7.8 by adding concentrated sodium hydroxide or perchloric acid.

For UV-precipitation experiment with $CaSO_{4(s)}$, stock solutions of 500 mM $Ca(OH)_2$, 800 mM Na_2SO_4, 10 mM H_2O_2, 10 mM $Na_2S_2O_8$, 1 mM stock of each NTMP, EDTMP and DTPMP, and 3 M $NaClO_4$ were prepared and adjusted to pH 7.8 with droplets of 2 M NaOH and 2 M $HClO_4$. This pH level is typical of brackish water desalination brine.[243] All the stock solutions were filtered through a 0.22-μm Millipore syringe filter

prior to adding them before the start of the experiment. Turbidity of each stock solution was measured using a HACH 2100N turbidimeter. Initial ionic strength of the mixing solution was fixed at 1 M by adding targeted amount of $NaClO_4$.The solution chemical matrix for the precipitation experiments was selected based on the chemical composition of the brackish RO concentrate. A synthetic concentrate allowed us to precisely control and vary the saturation indices of different calcium minerals. Chemical structures of the antiscalants are as shown in Fig. S2.1.

4.3.3 *Steady state concentration measurement*

To determine the steady-state radical concentrations generated during persulfate photolysis, 5 μM nitrobenzene (NB), 5 μM benzoic acid (BA), 5 μM 4-chlorobenzoic acid (or para chlorobenzoic acid PCBA) and 5 μM of N,N Dimethylaniline (DMA) were added as probe compounds. Prior to the experiment, the pH of the reaction solution was adjusted to a target value between 6 and 9 by adding $HClO_4$ or NaOH, and chloride and bicarbonate levels were controlled between 0 to 20 mM. The prepared reaction solution was transferred to quartz reaction tubes and placed in a carousel UV reactor (ACE Glass Inc.) equipped with a medium pressure UV mercury lamp (λ= 200-800 nm, 42 mW/cm^2). The experiments were conducted at 22±1^o C. At predetermined time intervals, sacrificial tubes were withdrawn from the reactor for chemical analysis.

Prior to the analysis of NTMP, EDTMP, DTPMP and probe compounds, the residual persulfate in the sample was quickly quenched with excess sodium sulfite. The antiscalant concentration were determined by ion chromatography (Dionex ICS-5000) with optimized gradient elution (analytical details in Text S4.1); NB, PCBA, BA and DMA were

determined using a liquid chromatography (Agilent 1200) equipped with an Agilent Eclipse XDB-C18 column and a UV-Diode Array Detector (analytical details in Text S4.2). The concentration of orthophosphate was measured by analysis of phosphate using the standard molybdate blue spectrophotometric method.[244] The mineral phase of precipitated solid was analyzed and confirmed by X-ray diffraction (XRD).

4.4 Results and Discussions

4.4.1 *Effects of solution pH*

To investigate the effect of pH on the calcium sulfate precipitation induced by

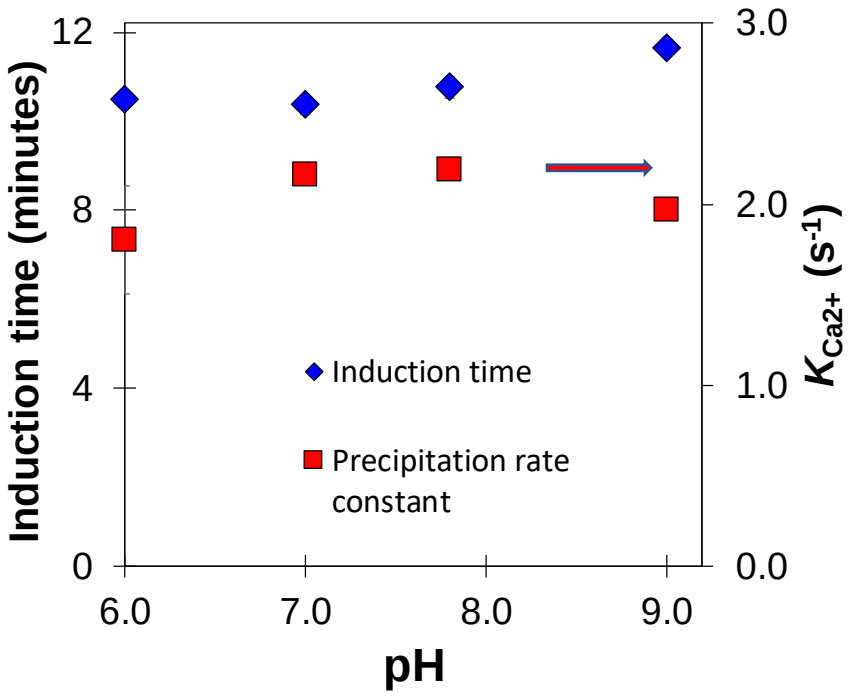

antiscalant degradation, several precipitation experiments were carried out at pH 6.0, 7.0,

Figure 4. 1 Effect of pH on the induction time and precipitation rate constant of calcium sulfate in UV/persulfate system. $[S_2O_8^{2-}]_0$ = 3.8 mM; $[Ca^{2+}]$ = 37 mM; $[SO_4^{2-}]$ = 564 mM; pH = 6.0-9.0; medium pressure UV lamp.

7.8 and 9.0. Since, the speciation of calcium or sulfate doesn't significantly change between this pH, the ionic activity of these ions shouldn't change in this range of pH. pKa of DTPMP on the other hand as a multiprotic acid are 1.52, 2.64, 3.10, 3.82, 5.38, 6.28, 7.07, 7.74, 9.36 and 11.12[245] Thus, with a change in the pH, it's speciation can change which can change the radical distribution and hence the degradation kinetics. Experimental results however, showed that the change of pH had no impact either on the degradation kinetics of DTPMP or the induction time of precipitation of calcium sulfate. The induction time slightly increased from 10.5 minutes at pH 6.0 to about 11.5 minutes at pH 9.0 (Figure 4.1, Figure S4.1) Thus, change of pH did not have any substantial effect on the photochemical demineralization of calcium sulfate. This is consistent with another study where the results showed that pH had little impact on the reactivity of SO4•− / HO· with NTMP despite the speciation change of NTMP ($k_{HO\cdot\text{-}NTMP}$ = 9.9 × 10^7 - 1.1× 10^8 M^{-1} s^{-1}; $k_{SO4\bullet-\cdot\text{-}NTMP}$ = 2.4 - 3.5 × 10^7 M^{-1} s)[228]. The contribution of $SO_4^{\bullet-}$ and $HO^{\bullet}$ to DTPMP degradation at different pHs was calculated, as shown in Figure S4.2. As expected, the calculated pseudo first order rates of DTPMP degradation (calculated sulfate radical contribution plus calculated hydroxyl radical contribution) were nearly identical to the directly observed pseudo first-order rates of DTPMP degradation (kobs-DTPMP), indicating DTPMP degradation is attributed to reactions with $SO_4^{\bullet-}$ and $HO^{\bullet}$.

4.4.2 *Effect of chloride*

To investigate the effect of chloride on the calcium sulfate precipitation induced by antiscalant degradation, several precipitation experiments were carried out at varying chloride levels ranging from 0 mM to 20 mM. Presence of chloride is known to interfere

with the radical steady state distribution as chloride is known to react with the primary radicals, $SO_4^{\bullet-}$ and $HO^{\bullet}$ formed in the UV/persulfate system. This leads to formation of different chloride radicals called as reactive chlorine species (RCS) shown as below:

$$SO_4^{\bullet-} + Cl^- \rightarrow SO_4^{2-} + Cl^{\bullet} \quad (4.1)$$

In presence of excess chloride, $Cl^{\bullet}$ further reacts with Cl^- to form chlorine dimer as shown in the reaction below:

$$Cl^{\bullet} + Cl^- \rightarrow Cl_2^{\bullet-} \quad (4.2)$$

In order to calculate the reaction rate constants of DTPMP reacting with $HO^{\bullet}$, the concentration of $HO^{\bullet}$ radical ($[HO^{\bullet}]_{ss}$) was first determined (Text S4.1). To quantify the contribution of $SO_4^{\bullet-}$ or $HO^{\bullet}$ to DTPMP degradation in UV/persulfate, their steady-state concentrations and intrinsic second-order reaction rate constants with DTPMP were determined based on competition reaction kinetics (Text S4). Nitrobenzene, benzoic acid and p-chlorobenzoic acid were used to probe the steady-state concentrations of $SO_4^{\bullet-}$, $Cl^{\bullet}$ and $HO^{\bullet}$

Addition of chloride was first tested on a controlled system where the precipitation of calcium sulfate was first with tested UV/persulfate in absence of any antiscalant (Figure S4.2). The induction time for calcium precipitation was not affected by presence of chloride in absence of any antiscalant. This is consistent with the fact that in presence of chloride, most of the calcium is still present as free calcium ion. Hence the presence of chloride

doesn't change the saturation index in the system. Figure 4.2 shows the change in induction time of in presence of DTPMP.

Addition of When DTPMP is added to the same system, chloride reacts with the free radicals such as $SO_4^{\bullet-}$ and $HO^{\bullet}$ produced during the UV/persulfate oxidation of antiscalant as shown in the reactions 4.1. Thus, chloride acts as scavenger for the parent radicals and forms daughter free reactive radicals which are less reactive with the antiscalant. Similar to the procedure in Figure 4.3, the contribution of $SO_4^{\bullet-}$, $HO^{\bullet}$ and $Cl^{\bullet}$ to DTPMP degradation at different chloride level was calculated, as shown in text S4.1.

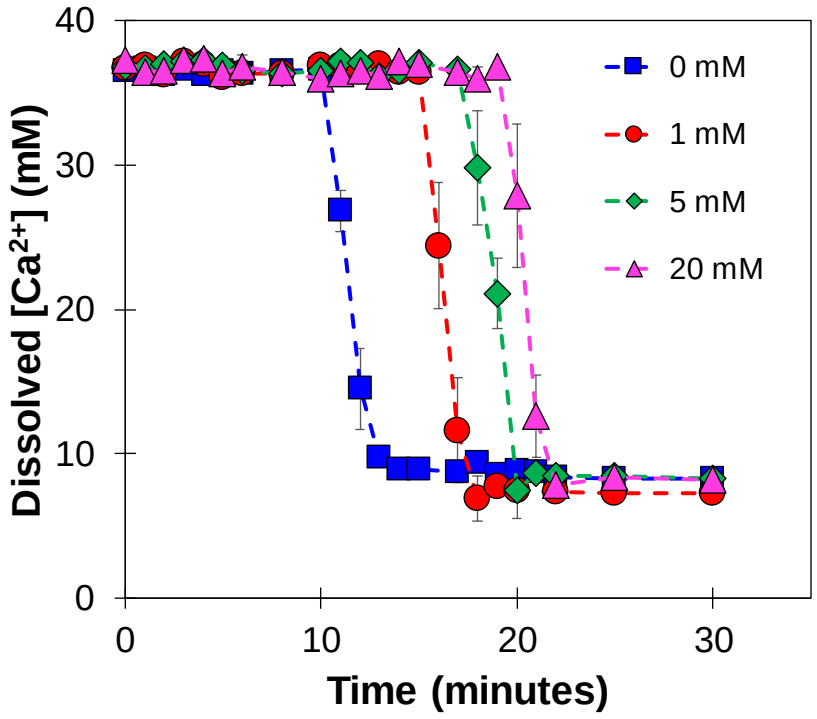

Figure 4.2 Effect of chloride dosage on the induction time of calcium sulfate in UV/persulfate system. $[DTPMP]_0$ = 3 mg P/L; $[S_2O_8]^{2-}{}_0$ = 3.8 mM; $[Ca^{2+}]$ = 37 mM; $[SO_4^{2-}]$ = 564 mM; pH = 7.8; medium pressure UV lamp

Figure 4.3 shows the contribution of each radical to the degradation rate constant of DTPMP in presence of chloride. With an increase in chloride dose from 0 to 1 mM, the contribution of sulfate radical significantly drops. This phenomenon is seen due to the scavenging of sulfate radicals by chloride ions. The radical steady state concentration of chlorine dimer is of the same order of magnitude as hydroxyl radical. However, the second order rate constant of chlorine dimer with DTPMP is $k_{Cl2\cdot\text{-}DTPMP} = 1.70 \times 10^3$; $k_{SO4\bullet-\text{-}DTPMP} = 5.11 \times 10^6$ M^{-1} s-1; $k_{HO\bullet-\text{-}DTPMP} = 1.16 \times 10^7$ M^{-1} s^{-1}) This significantly decreases the overall contribution of chlorine dimer towards the radical DTPMP degradation.

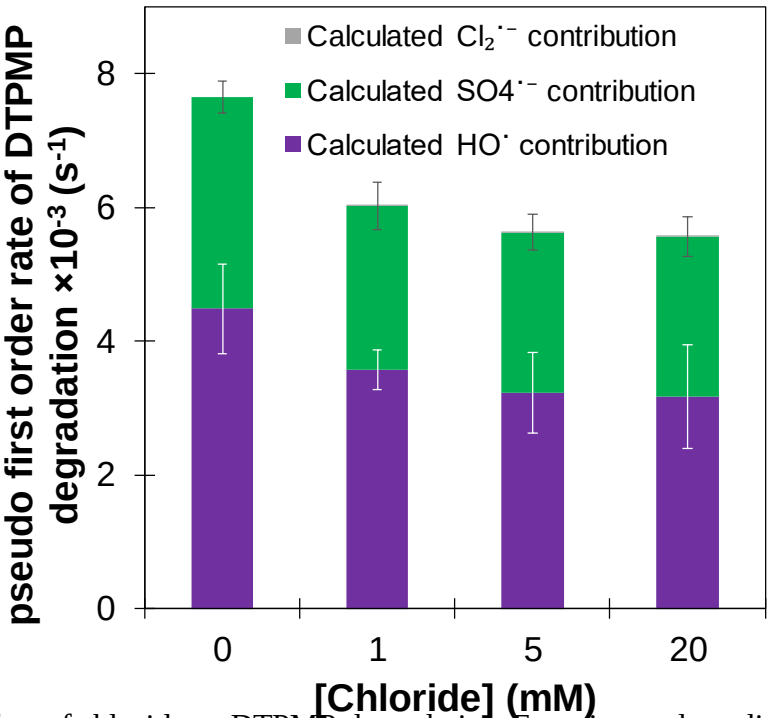

Figure 4. 3 Effect of chloride on DTPMP degradation. Experimental condition: $[oxidant]_0$ = 2.0 mM; pH = 7.8; $[DTPMP]_0$ = 3 mg P/L; $[Ca^{2+}]$ = 37 mM; $[SO_4^{2-}]$ = 564 mM; pH = 7.8; medium pressure UV lamp

Further, the effect of chloride was tested for NTMP and EDTMP as well (Figure S4.3). As expected, the addition of chloride increased the induction time for the gypsum precipitation.

4.4.3 *Effect of dissolved organic matters*

Dissolved organic matter (DOM) is commonly present in natural waters. It can absorb light, produce reactive intermediates, scavenge radical species (e.g., $SO_4^{\bullet-}$, $HO^{\bullet}$), and potentially impact the photochemical demineralization process. Suwannee river natural organic matter (SRNOM, 2R101N) was used as the model compound to investigate the impact of DOM. Induction time for calcium sulfate precipitation increased with increasing

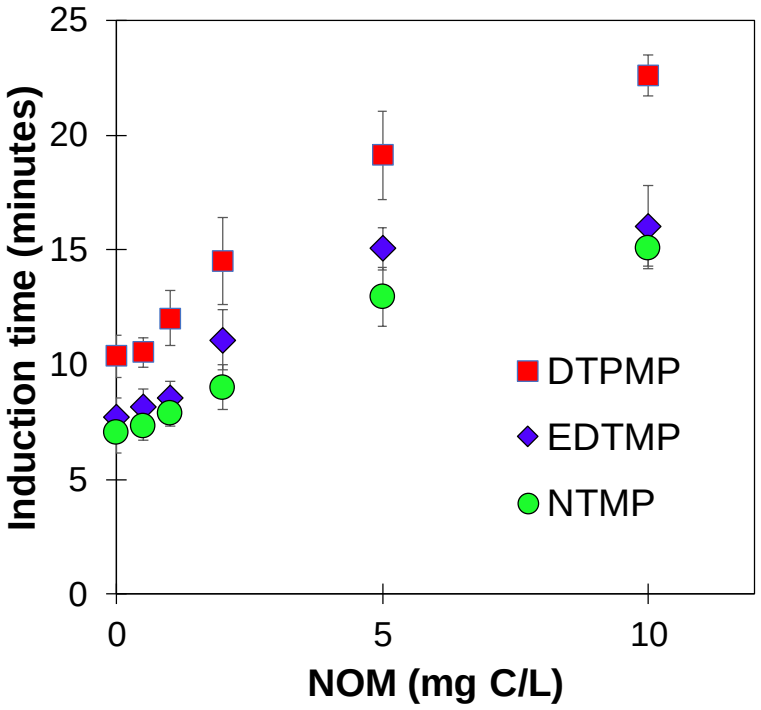

Figure 4. 4 Impact of dissolved organic matter (DOM) on photochemical demineralization of calcium sulfate. Experimental condition: $[persulfate]_0$ = 2.0 mM; pH = 7.8; $[antiscalant]_0$ = 3 mg P/L; $[Ca^{2+}]$ = 37 mM; $[SO_4^{2-}]$ = 564 mM; pH = 7.8; medium pressure UV lamp

DOM concentration for all the antiscalants. DOM impacted the demineralization process mainly because of its light-shading effect. To quantify the impact of DOM on demineralization process, $^{\cdot}OH$-scavenging, $SO_4^{\cdot-}$ scavenging and light-shading effects of DOM were considered. The degradation of antiscalant was also inhibited due to the presence of DOM. At lower DOM concentrations from 0.5 to 2 mg C/L, the impact of DOM is not very significant as the increase in the induction time for all the antiscalants is less than 9%. However, at higher DOM concentration ranging from 2 mg C/L to 10 mg C/L, there was a considerable increase in the induction time. This effect was particularly visible for DTPMP as the induction time increased from 10.3 minutes to 22.6 minutes. An increase of dissolved organic matter significantly increased the induction period for all the antiscalants (Figure 4.4, Figure S4.4, Figure S4.5 and Figure S4.6). The DOM, however, do not act as a scavenger for the radicals instead, it competes with the persulfate for the photon consumption. High concentrations of DOM shielded light from persulfate. The rate constants for the reaction of DOM with the hydroxyl radicals is around 5 times higher compared to that with sulfate radicals.[246],[247] Thus, if the DOM were to act as a scavenger for the radicals, it would have disproportionately changed the radical steady state concentration of hydroxyl and sulfate radicals. This is contrary to the observed ratio of the steady state concentrations of these radicals (Figure S4.7).

4.4.4 *Effect of UV irradiation time on induction time*

Advanced oxidation processes are widely recognized as highly efficient for recalcitrant wastewater treatment.[248,249] These processes involve the generation of the free radicals ($HO^{\bullet}$, $SO_4^{\bullet-}$, etc) which has a very high oxidation potential and is able to oxidize

almost all pollutant organic compounds. Unfortunately, these processes can be expensive as they are energy intensive due to the application of ultraviolet irradiation. Figure 3.4 shows that for most of the conditions, gypsum precipitation was seen even when all the antiscalant was not consumed. This is an important development considering that we need not achieve a complete oxidation of antiscalant in order to achieve precipitation. Thus, in this study we evaluated the prospect of partial irradiation of antiscalant to the UV to understand the precipitation behavior of gypsum with incomplete oxidation of the antiscalant. In order to evaluate the application of this process, the effectiveness of UV/persulfate based AOP as a treatment for demineralization of reverse osmosis desalination concentrate has been studied in this research.

Several demineralization experiments of calcium sulfate in presence of UV/persulfate were conducted with partial irradiation of UV. Based on the observed induction time for complete irradiation experiments which were in the range of 5 to 20 minutes, the range of irradiation time chosen for these set of experiments were 0, 2, 3, 4, 5, 8, 10 and 30 minutes. Each experiment was conducted in a sacrificial quartz tube as a batch reactor. With an initial antiscalant concentration of 3 mg P/L as DTPMP, shorter UV irradiation time showed relatively smaller degradation of antiscalant compared to a linger UV irradiation (Figure 4.5). For example, with 2 minutes of UV irradiation around 43% of DTPMP degradation was obtained. Only 10 minutes of UV irradiation were required to achieve 83% DTPMP degradation. Control experiments performed without any UV exposure showed no antiscalant degradation within the 30 minutes of the experiment time.

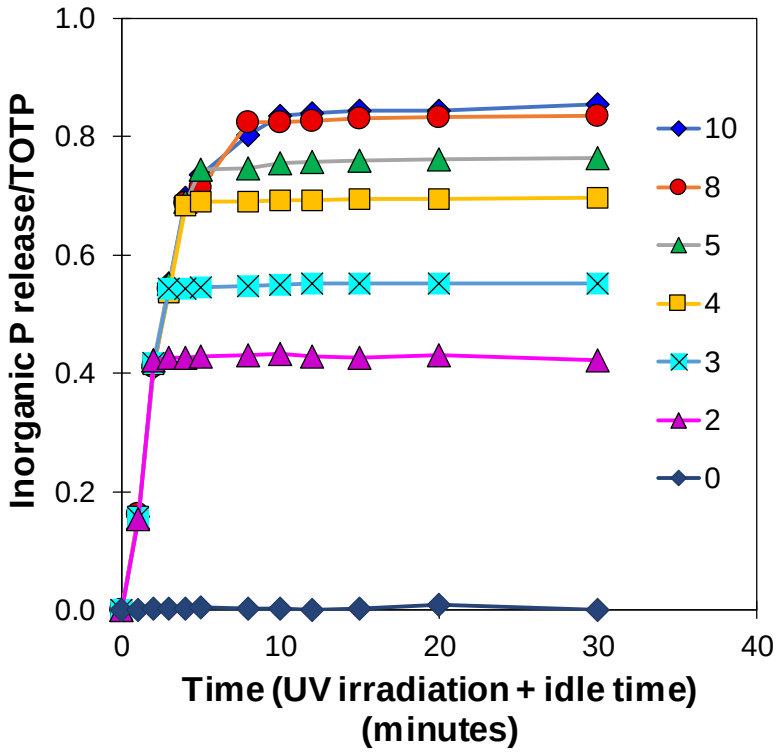

Figure 4. 5 DTPMP degradation at different UV irradiation time with [$S_2O_8^{2-}$] and 3 mg P/L DTPMP; values in the legend indicates the UV irradiation time; pH = 7.8; ionic strength = 1 M

With an initial calcium concentration of 37 mM, nearly 75% of calcium removal was obtained irrespective of the UV irradiation time (Figure 4.5). However, the time taken to achieve this extent of degradation was different for different UV irradiation times. Similar results were observed for NTMP as well as EDTMP experiments (Figures S4.4 and Figure S 4.5). In general, the induction time decreased with increasing UV irradiation time (Figure 4.6B)

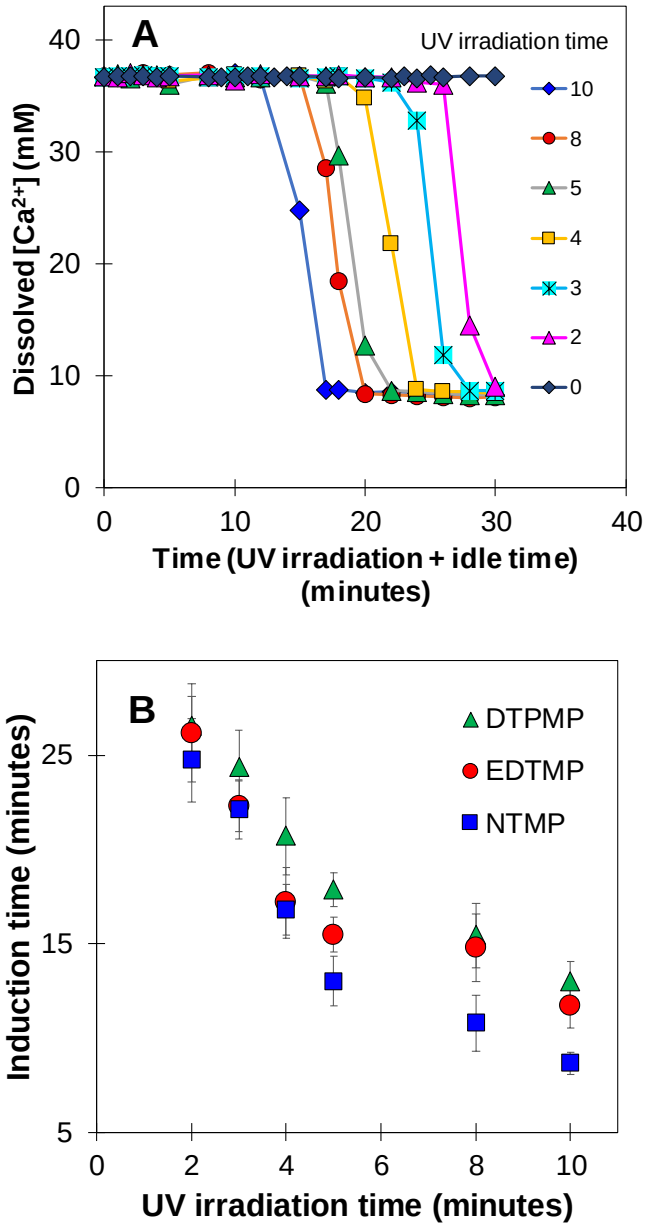

Figure 4. 6 (A) Dissolved calcium release at different UV irradiation times; values in the legend indicates the UV irradiation time; (B) Dependence of induction time on the UV irradiation time for each antiscalant. Experimental conditions: $[antiscalant]_0$ = 3 mg P/L; pH = 7.8; ionic strength = 1 M

4.5 Acknowledgements

This research was partially supported by grants to H.L. from the National Science Foundation (Grant #1611306) and to T.J. from the National Water Research Institute Fellowship. We also thank the assistance of Sheila Cervantes from University of California Riverside.

Chapter 5

Conclusions and Broader Impacts

The primary objective of this research was to develop a treatment process to treat a brackish RO concentrate, with the goals of reducing concentrate volume and increasing overall recovery of RO system. The concentrate treatment process consisted of three stages: antiscalant oxidation, salt precipitation, and solid/liquid separation. Three different phosphonate antiscalant compounds were tested. The antiscalants were chosen for their ability to reduce or eliminate calcium precipitation (as calcium carbonate, calcium sulfate and calcium phosphate). Two advanced oxidation processes were investigated as the oxidation system, and key parameters that affect antiscalant oxidation were identified and evaluated. Small doses of oxidants prior to precipitation allowed antiscalant deactivation and largely prevented the antiscalant from impacting the precipitation and separation steps. While results indicated that not all of the antiscalant molecules were completely oxidized, an evaluation of the precipitation and separation stages indicated that the partial oxidation products did not act in the same manner as whole antiscalant molecules.

Research in the area of concentrate treatment and volume reduction has received increased interest as reverse osmosis desalination becomes a more widespread technology and as more inland communities face water shortages. Current research ranges from basic experimental research to large-scale pilot system studies, and a common concern is the effects of specific concentrate constituents, such as antiscalants, concentrate pH, chloride levels, and NOM, on a concentrate treatment process. Most concentrate treatment processes use a controlled precipitation step to remove scaling salts. Hence, this research focuses on a relevant and critical aspect of RO concentrate treatment.

While the broad objective of the study was to develop an overall concentrate treatment process, the experiments resulted in a more detailed understanding of antiscalant oxidation and the effects of antiscalants on precipitation of scaling constituents. The results of this study provide a greater understanding of antiscalant chemistry within the framework of an applicable brackish RO concentrate treatment scheme.

Furthermore, phosphonate compounds are used not only as antiscalants for RO desalination, but as dispersion and scale inhibitor chemicals in many industrial and research applications. The oxidation results from this research provide insight into oxidation pathways, the influence of various cations (including calcium) on antiscalant chemistry, and the effects of operational parameters on phosphonate oxidation. Calcium is a ubiquitous component of natural waters and thus is the major ion involved in most scaling problems or precipitation events. Hence, the results of this research could allow advances not only in RO desalination but in other unrelated fields.

The study performed in this research suggested that, in addition to antiscalant, the presence of NOM, in large amounts, affects RO concentrate treatment. This result could be critical because depending on the geography and other aspects some brackish waters can have high NOM, and the NOM becomes concentrated in the RO concentrate. While a more detailed study of antiscalant and NOM interactions is necessary, it is clear that NOM plays an important role in precipitation-based RO concentrate treatment.

Appendix A

Supporting information for Chapter 2

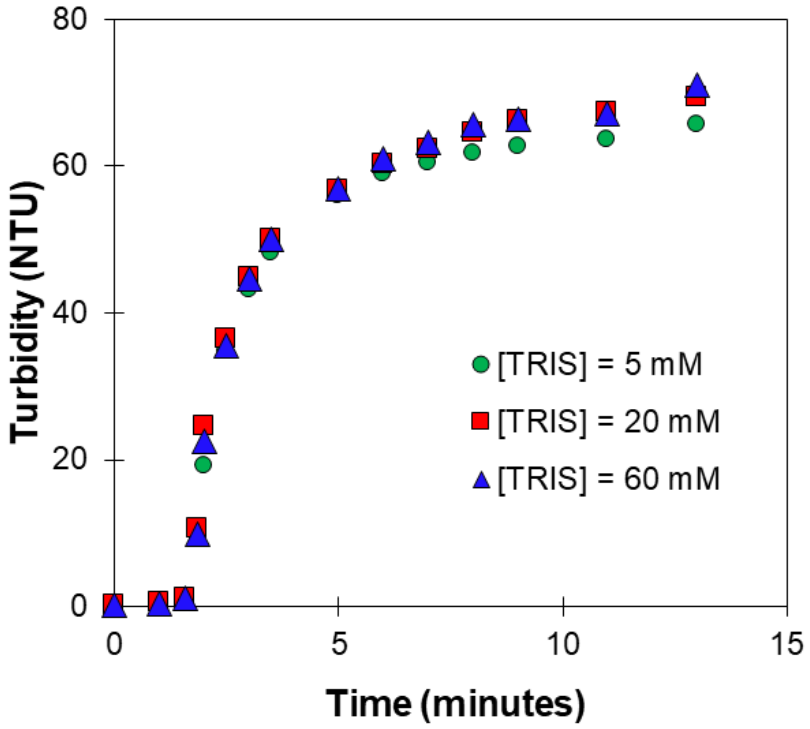

Figure S2. 1 The negligible effect of tris(hydroxymethyl)aminomethane (TRIS) pH buffer concentration on the precipitation of $Ca_5(PO_4)_3OH_{(s)}$ in presence of antiscalant EDTMP. Results showed that the presence of different TRIS buffer concentrations did not affect the precipitation kinetics. [Ca^{2+}] = 10 mM; [PO_4^{3-}] = 31 mg P/L; pH = 7.8; [EDTMP] = 3 µM; ionic strength = 100 mM.

Text S2.1 Kinetics modeling of the precipitation of calcium solids

The backbone of the model is the Michaelis-Menten equation that gives the relationship between the turbidity of the precipitation and the time of the precipitation reaction (Eqn. S2.1):

$$T = T_{max} \frac{t}{t + K_m} \quad \text{(S2.1)}$$

Where, T is the turbidity of the precipitation (NTU) at time t (seconds), T_{max} is the maximum turbidity of the precipitation reaction (NTU) and K_m is the Michaelis-Menten half-velocity constant (seconds).

Figure S2.3A shows the experimental data for the precipitation of hydroxyapatite in absence of antiscalant with time. The Michaelis-Menten type of model as described in equation S1.1 above is fit for the rapid-precipitation stage of the reaction. The constant, T_{max}/K_m gives the rate constant of the precipitation (NTU/second). This kinetic model fits the precipitation of all calcium solids very well. Figure S2.3B shows a typically data fitting on the precipitation of hydroxyapatite with different NTMP and phosphate dosages.

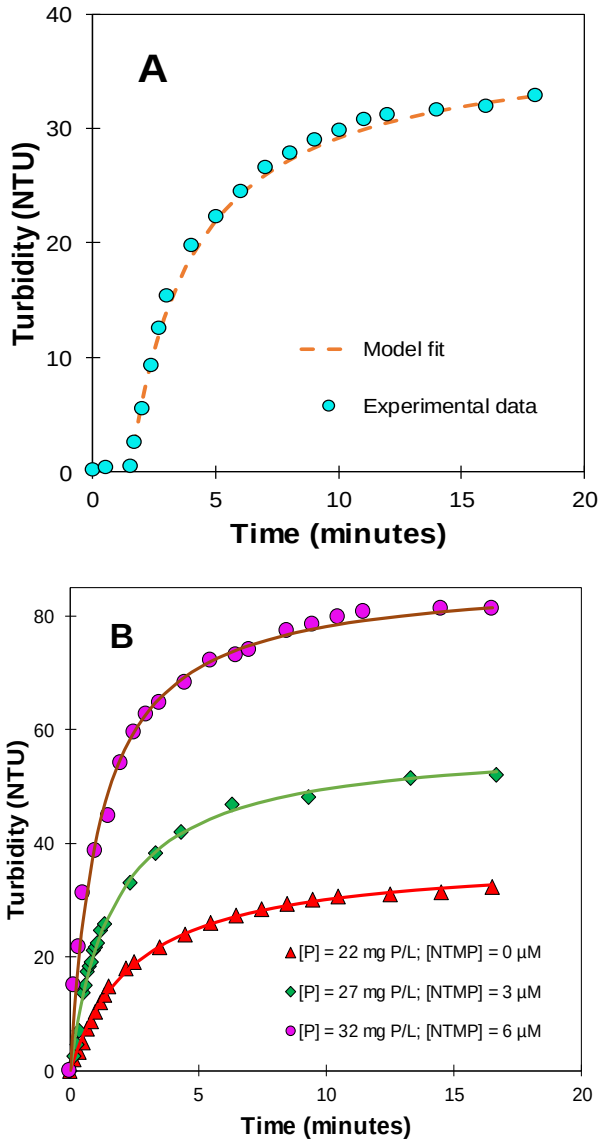

Figure S2.2 (A) Kinetic modeling on the precipitation of $Ca_5(PO_4)_3OH_{(s)}$. $[Ca^{2+}]$ = 10 mM; $[PO_4^{3-}]$ = 22 mg P/L; [NTMP] = 0 µM; pH = 7.8; saturation index = 14.46; [TRIS buffer] = 20 mM; ionic strength = 100 mM. (B) Michaelis-Menten model fitting for precipitation of $Ca_5(PO_4)_3OH_{(s)}$ at different saturation indices in the presence of varying dosages of

NTMP. [Ca^{2+}] = 10 mM; [PO_4^{3-}] = 20-32 mg P/L; [NTMP] = 0- 6 µM; pH = 7.8; [TRIS buffer] = 20 mM; ionic strength = 100 mM.

Text S2.2 Calculations on calcium complexation with different antiscalants

Mass balance for total calcium gives the equation below:

$$TOTCa = \{Ca^{2+}\} + \{CaHL\}^{3-} + \{CaH_2L\}^{2-} + \{CaH_3L\}^{-} + \cdots + \{CaH_iL\}^{i-4} + \{CaOH\}^{+} \quad \text{(S2.2)}$$

Where *TOT*Ca is the total dissolved calcium concentration, and L is the Ligand (NTMP in the above case, which has a negative six charges for its most deprotonated species L).

$$\beta_i = \frac{\{CaH_{i-1}L\}}{\{Ca^{2+}\}\{H\}^{(i-1)}\{L\}} \quad \text{(S2.3)}$$

The speciation equilibrium for $CaOH^+$, which has a pK_a of 12.7 (Visual MINTEQ) is calculated as below:

$$\{CaOH^+\} = \{Ca^{2+}\}\ \frac{10^{-12.7}}{\{H^+\}} \quad \text{(S2.4)}$$

In addition, calcium-antiscalant complexes for NTMP, EDTMP and DTPMP are listed in Table S2.1.

$$TOTCa = \{Ca^{2+}\}\left(1 + \left\{\frac{CaL^{4-}}{Ca^{2+}}\right\} + \left\{\frac{CaHL^{3-}}{Ca^{2+}}\right\} + \left\{\frac{CaH_2L^{2-}}{Ca^{2+}}\right\} + \left\{\frac{CaH_3L^{-}}{Ca^{2+}}\right\} + \left\{\frac{CaH_4L}{Ca^{2+}}\right\} + \left\{\frac{CaOH^{+}}{Ca^{2+}}\right\}\right) \quad \text{(S2.5)}$$

$$TOTCa = \{Ca^{2+}\}\Big(1 + \beta_1\{L\} + \beta_2\{H^+\}\{L\} + \beta_3\{H^+\}^2\{L\} + \beta_4\{H^+\}^3\{L\} + \beta_5\{H^+\}^4\{L\} + \frac{K}{\{H^+\}}\Big) \quad \text{(S2.6)}$$

Let $\Big(1 + \beta_1\{L\} + \beta_2\{H^+\}\{L\} + \beta_3\{H^+\}^2\{L\} + \beta_4\{H^+\}^3\{L\} + \beta_5\{H^+\}^4\{L\} + \frac{K}{\{H^+\}}\Big) = B$

$$\alpha_{Ca^{2+}} = \frac{1}{B} \quad \text{(S2.7)}$$

$$\alpha_{CaL^{4-}} = \frac{\beta_1\{L\}}{B} \quad \text{(S2.8)}$$

$$\alpha_{CaHL^{3-}} = \frac{\beta_2\{H^+\}\{L\}}{B} \quad \text{(S2.9)}$$

$$\alpha_{CaH_2L^{2-}} = \frac{\beta_3\{H^+\}^2\{L\}}{B} \quad \text{(S2.10)}$$

$$\alpha_{CaH_3L^{-}} = \frac{\beta_4\{H^+\}^3\{L\}}{B} \quad \text{(S2.11)}$$

$$\alpha_{CaH_4L} = \frac{\beta_5\{H^+\}^4\{L\}}{B} \quad \text{(S2.12)}$$

$$\alpha_{CaOH^+} = \frac{K}{\{H^+\}B} \quad \text{(S2.13)}$$

Where, $\alpha_{Ca^{2+}}$, $\alpha_{CaL^{4-}}$, $\alpha_{CaHL^{3-}}$, $\alpha_{CaH_2L^{2-}}$, $\alpha_{CaH_3L^{-}}$, α_{CaH_4L} and α_{CaOH^+} is the fraction of total dissolved calcium existing as Ca^{2+}, CaL^{4-}, $CaHL^{3-}$, CaH_2L^{2-}, CaH_3L^{-}, CaH_4L and $CaOH^+$, respectively.

The fraction of total dissolved calcium existing as Ca^{2+} as a function of solution pH is plotted in Figure S2.4.

Table S2.1 Calcium-antiscalant complexes and their stability constants.

#	Calcium ligand complexes with NTMP	Logβ_i [a]
(1)	$Ca^{2+} + L^{6-} \leftrightarrow CaL^{4-}$	7.6
(2)	$Ca^{2+} + H^{+} + L^{6-} \leftrightarrow CaHL^{3-}$	16.6
(3)	$Ca^{2+} + 2H^{+} + L^{6-} \leftrightarrow CaH_2L^{2-}$	22.9
(4)	$Ca^{2+} + 3H^{+} + L^{6-} \leftrightarrow CaH_3L^{-}$	28
(5)	$Ca^{2+} + 4H^{+} + L^{6-} \leftrightarrow CaH_4L$	32.1
	Calcium ligand complexes with EDTMP	Logβ_i [b]
(6)	$Ca^{2+} + L^{6-} \leftrightarrow CaL^{4-}$	9.29
(7)	$Ca^{2+} + H^{+} + L^{6-} \leftrightarrow CaHL^{3-}$	18.74
(8)	$Ca^{2+} + 2H^{+} + L^{6-} \leftrightarrow CaH_2L^{2-}$	26.98
(9)	$Ca^{2+} + 3H^{+} + L^{6-} \leftrightarrow CaH_3L^{-}$	33.72
(10)	$Ca^{2+} + 4H^{+} + L^{6-} \leftrightarrow CaH_4L$	39.21
	Calcium ligand complexes with DTPMP	Log$K$ [c]
(11)	$Ca^{2+} + H_2L^{8-} \leftrightarrow CaH_2L^{6-}$	5.04
(12)	$Ca^{2+} + H_3L^{7-} \leftrightarrow CaH_3L^{5-}$	4.41
(13)	$Ca^{2+} + H_4L^{6-} \leftrightarrow CaH_4L^{4-}$	3.78
(14)	$Ca^{2+} + H_5L^{5-} \leftrightarrow CaH_5L^{3-}$	3.5
(15)	$Ca^{2+} + H_6L^{4-} \leftrightarrow CaH_6L^{2-}$	2.52
(16)	$Ca^{2+} + H_7L^{3-} \leftrightarrow CaH_7L^{-}$	1.89
(17)	$Ca^{2+} + H_8L^{2-} \leftrightarrow CaH_8L$	1.26
(18)	$Ca^{2+} + H_9L^{+} \leftrightarrow CaH_9L^{+}$	0.63
	Calcium hydroxy complex	Log$K$ [c]
(19)	$Ca^{2+} + H_2O \leftrightarrow CaOH^{+} + H^{+}$	-12.697

[a] Taken from reference ([250]), [b] Taken from reference ([251]), [c] Taken from reference ([252]).

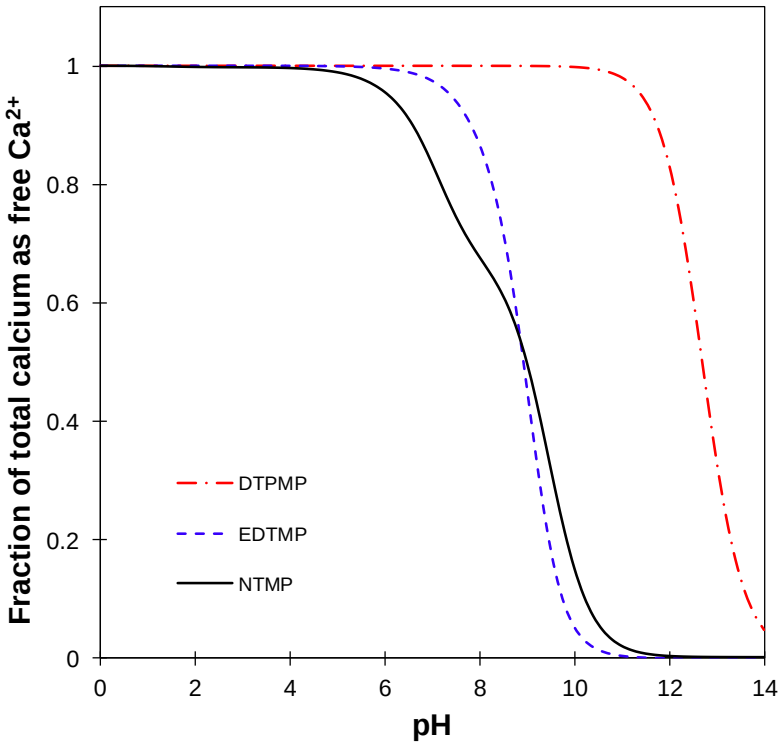

Figure S2.3 The impact of pH on the fraction of total dissolved calcium existing as free calcium in the presence of each antiscalant.

Text S2.3 Calculations for net charge of different antiscalants at different pH

Mass balance on the speciation of an antiscalant gives the equation below:

$$TOT\mathrm{L} = L^{6-} + \{HL\}^{5-} + \{H_2L\}^{4-} + \{H_3L\}^{3-} + \cdots + \{H_iL\}^{(n-i)-} \qquad \text{(S2.14)}$$

where L^{6-} is the most deprotonated form of NTMP. *TOT*L is defined as the sum of the concentration of all the species in the solution that contain an antiscalant, *n* is the charge of the most deprotonated species and *i* varies from 0 to *n*.

Speciation constants for NTMP, EDTMP and DTPMP are shown in Table S2 below.

Table S2.2 Protonation constants of NTMP, EDTMP and DTPMP

#	NTMP	pK_a [d]
(1)	$H_5L^- + H^+ \leftrightarrow H_6L$	0.30
(2)	$H_4L^{2-} + H^+ \leftrightarrow H_5L^-$	1.50
(3)	$H_3L^{3-} + H^+ \leftrightarrow H_4L^{2-}$	4.64
(4)	$H_2L^{4-} + H^+ \leftrightarrow H_3L^{3-}$	5.86
(5)	$HL^{5-} + H^+ \leftrightarrow H_2L^{4-}$	7.30
(6)	$L^{6-} + H^+ \leftrightarrow HL^{5-}$	12.10
	EDTMP	pK_a [e]
(7)	$H_6L^- + H^+ \leftrightarrow H_7L$	1.30
(8)	$H_5L^{2-} + H^+ \leftrightarrow H_6L^-$	2.96
(9)	$H_4L^{3-} + H^+ \leftrightarrow H_5L^{2-}$	5.12
(10)	$H_3L^{4-} + H^+ \leftrightarrow H_4L^{3-}$	6.40
(11)	$H_2L^{5-} + H^+ \leftrightarrow H_3L^{4-}$	7.87
(12)	$HL^{6-} + H^+ \leftrightarrow H_2L^{5-}$	7.85
(13)	$L^{7-} + H^+ \leftrightarrow HL^{6-}$	13.01
	DTPMP	pKa [f]
(14)	$H_9L^- + H^+ \leftrightarrow H_{10}L$	1.04
(15)	$H_8L^{2-} + H^+ \leftrightarrow H_9L^-$	2.08
(16)	$H_7L^{3-} + H^+ \leftrightarrow H_8L^{2-}$	3.11
(17)	$H_6L^{4-} + H^+ \leftrightarrow H_7L^{3-}$	4.15
(18)	$H_5L^{5-} + H^+ \leftrightarrow H_6L^{4-}$	5.19
(19)	$H_4L^{6-} + H^+ \leftrightarrow H_5L^{5-}$	6.23
(20)	$H_3L^{7-} + H^+ \leftrightarrow H_4L^{6-}$	7.23
(21)	$H_2L^{8-} + H^+ \leftrightarrow H_3L^{7-}$	8.30
(22)	$HL^{9-} + H^+ \leftrightarrow H_2L^{8-}$	11.18
(23)	$L^{10-} + H^+ \leftrightarrow HL^{9-}$	12.58

[d] Taken from literature ([253]), [e] Taken from literature (251), [f] Taken from literature ([254])

$$pKa_i = -\log\left(\frac{\{H_{n-i+1}L\}^{1-i}}{\{H^+\}\{H_{n-i}L\}^{-i}}\right) \quad \text{(S2.15)}$$

where L is the most deprotonated form of the ligand (NTMP, EDTMP or DTPMP), *n* is the charge of the most deprotonated form of the ligand (n = 6, 8 and 10 for NTMP, EDTMP and DTPMP, respectively) and *i* varies from 0 to *n*.

$$\alpha_i = \frac{\{H^+\}^{n-i}\prod_{j=0}^{i}K_{aj}}{\sum_{k=0}^{n}(\{H^+\}^{n-k}\prod_{j=0}^{k}K_{aj})} \quad \text{(S2.16)}$$

Where α_i is defined as the fraction of *TOT*L that is in a form that has lost *i* protons, *n* is the number of protons in the most protonated state, K_{a0} = 1.0. Thus, for NTMP, the value of α for the species H_6L is defined as:

$$\alpha_0 = \frac{\{H^+\}^6}{\{H^+\}^6 + \{H^+\}^5K_{a1} + \{H^+\}^4K_{a1}K_{a2} + \cdots + K_{a1}K_{a2}K_{a3}K_{a4}K_{a5}K_{a6}} \quad \text{(S2.17)}$$

Using the pK_a values from Table S2 and equation (15), (16) and (17) the fraction of each species is calculated at different pHs. Accordingly, the net charge of each antiscalant molecule is calculated by using the equation below:

$$molecular\ charge\ per\ mole = \sum_{i=0}^{i=n}\alpha_i z_i \quad \text{(S2.18)}$$

Where z_i is the charge of species that has lost *i* protons, n is the number of protons in the most protonated species.

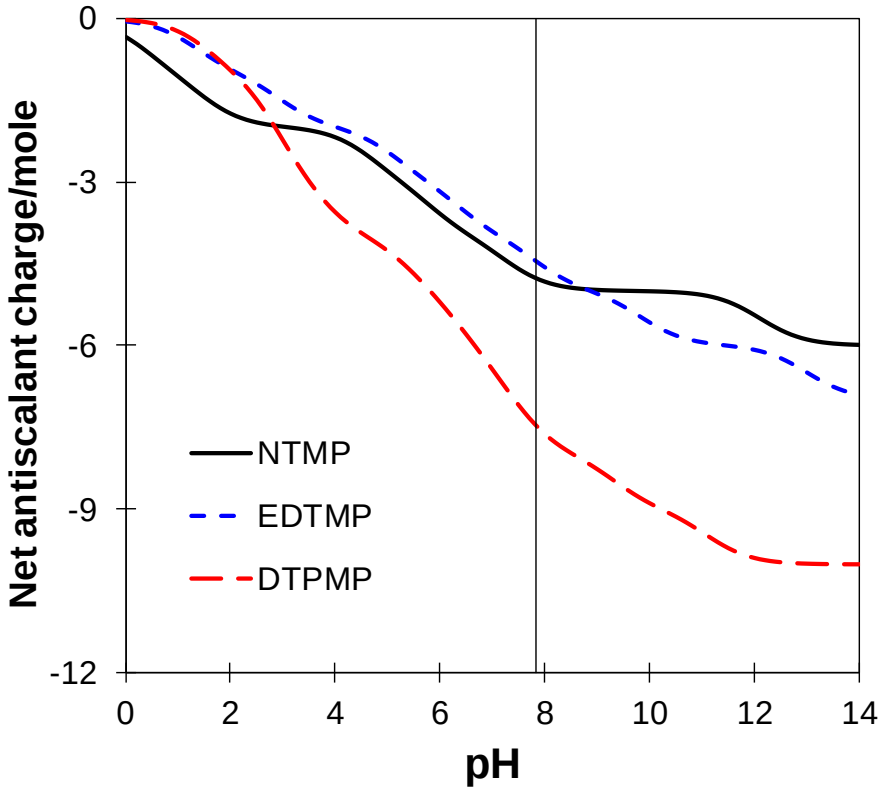

Figure S2.4 The impact of pH on the charge of each antiscalant. The charge is normalized to the molar concentration of the antiscalant and shown as the ratio of charge to molar concentration of antiscalant in the y-axis.

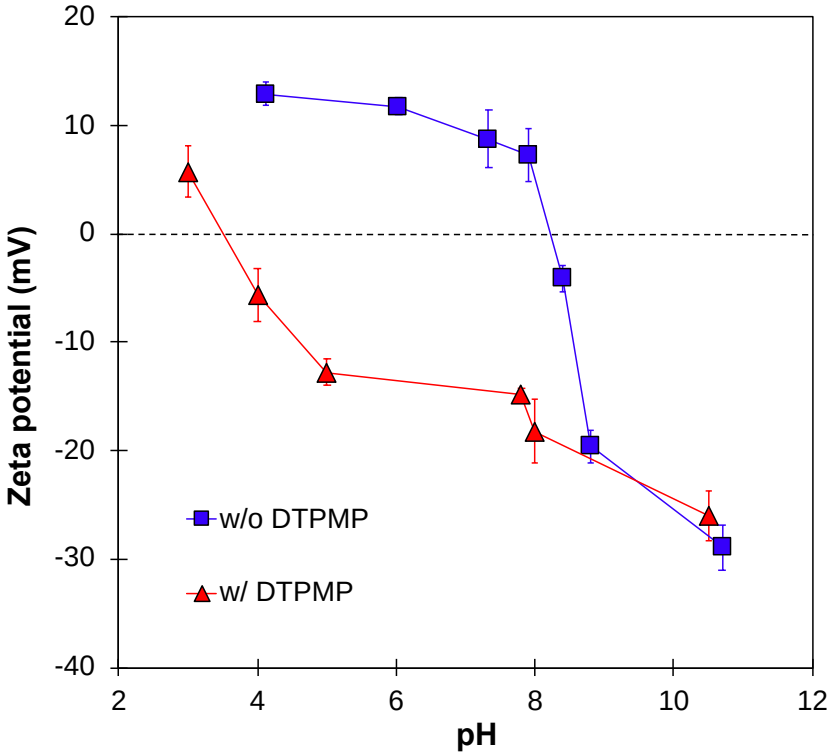

Figure S2.5 Impact of the antiscalant DTPMP on the zeta potential of hydroxyapatite at different pHs**.** [DTPMP] = 1 μM; $[Ca^{2+}]$ = 10 mM; $[PO_4^{3-}]$ = 26 mg P/L; saturation index = 14.2; ionic strength=100 mM.

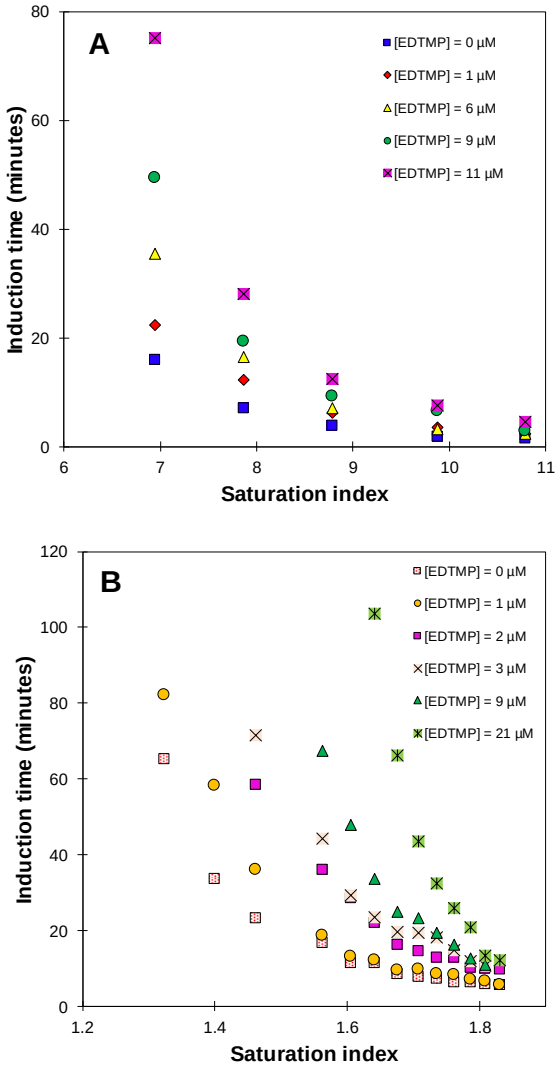

Figure S2.6 The effect of EDTMP dosage on the extension of induction time for CaSO4(s) and CaCO3(s) precipitation. Experimental conditions: (A) $[Ca^{2+}]$ = 37-58 mM; $[SO_4^{2-}]$ = 564 mM; ionic strength = 1 M pH = 7.8. (B) $[Ca^{2+}]$ = 10 mM; $[CO_3^{2-}]$ = 10-30 mg CO_3/L; pH = 7.8; ionic strength = 100 mM; [TRIS buffer] = 50 mM.

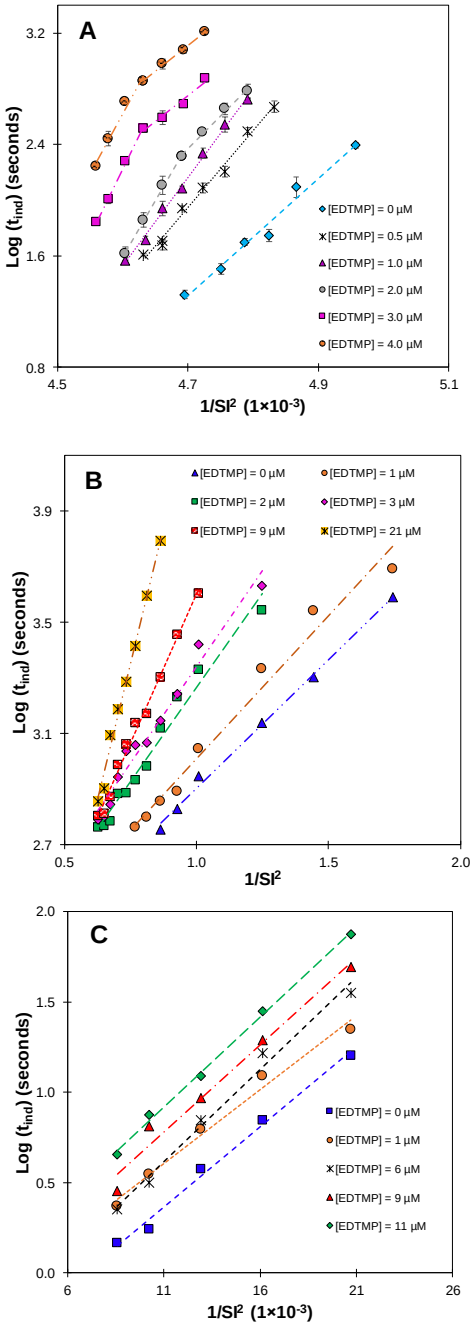

Figure S2.7 The impact of varying dosage of EDTMP at different saturation indices on the induction time for Ca5(PO4)3OH(s), CaCO3(s) and CaSO4(s) nucleation. (A) $[Ca^{2+}]$ = 10 mM; $[PO_4^{3-}]$ = 18-30 mg P/L; pH = 7.8; ionic strength = 100 mM; [TRIS buffer] = 20 mM. (B) $[Ca^{2+}]$ = 10 mM; $[CO_3^{2-}]$ = 10-30 mg/L; pH = 7.8; ionic strength = 100 mM; [TRIS buffer] = 50 mM. (C) $[Ca^{2+}]$ = 37-80 mM; $[SO_4^{2-}]$ = 560 mM; ionic strength = 1 M; pH = 7.8.

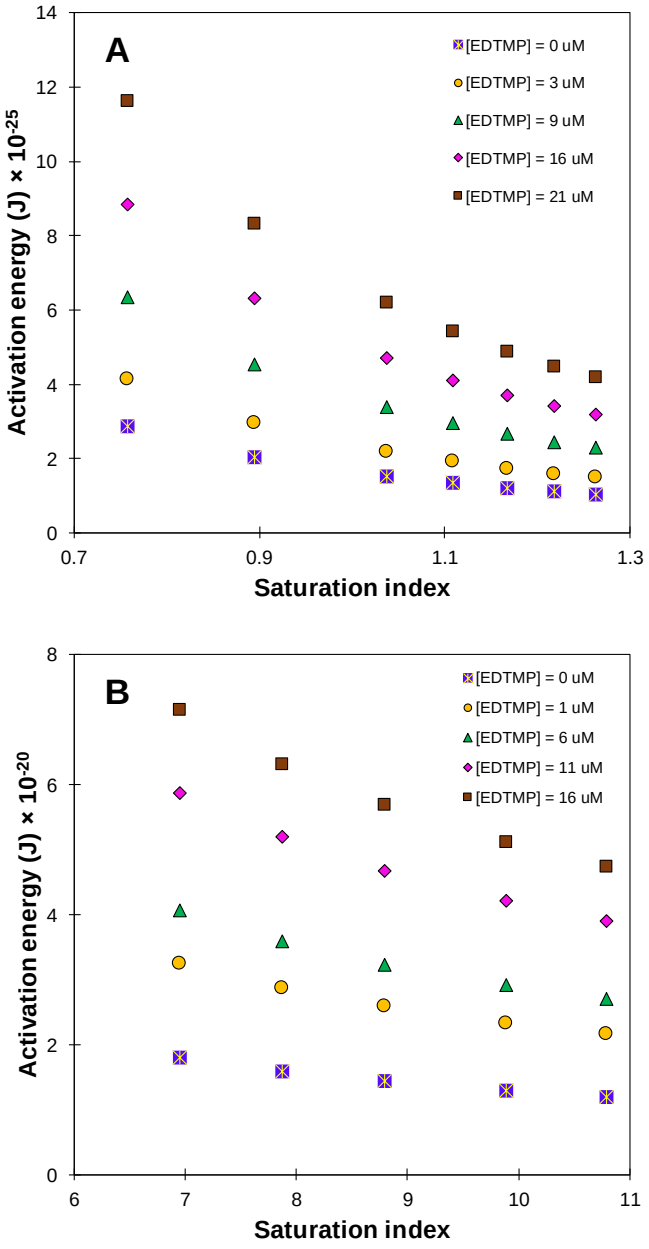

Figure S2.8 Impact of saturation index of CaCO3(s) and CaSO4(s) on activation energy of nucleation at varying EDTMP dose. (A) $[Ca^{2+}]$ = 10 mM; $[CO_3^{2-}]$ = 10 mM; pH = 7.8; ionic strength = 100 mM; [TRIS buffer] = 50 mM. (B) $[Ca^{2+}]$ = 37 mM; $[SO_4^{2-}]$ = 564 mM; ionic strength = 100 mM; pH = 7.8.

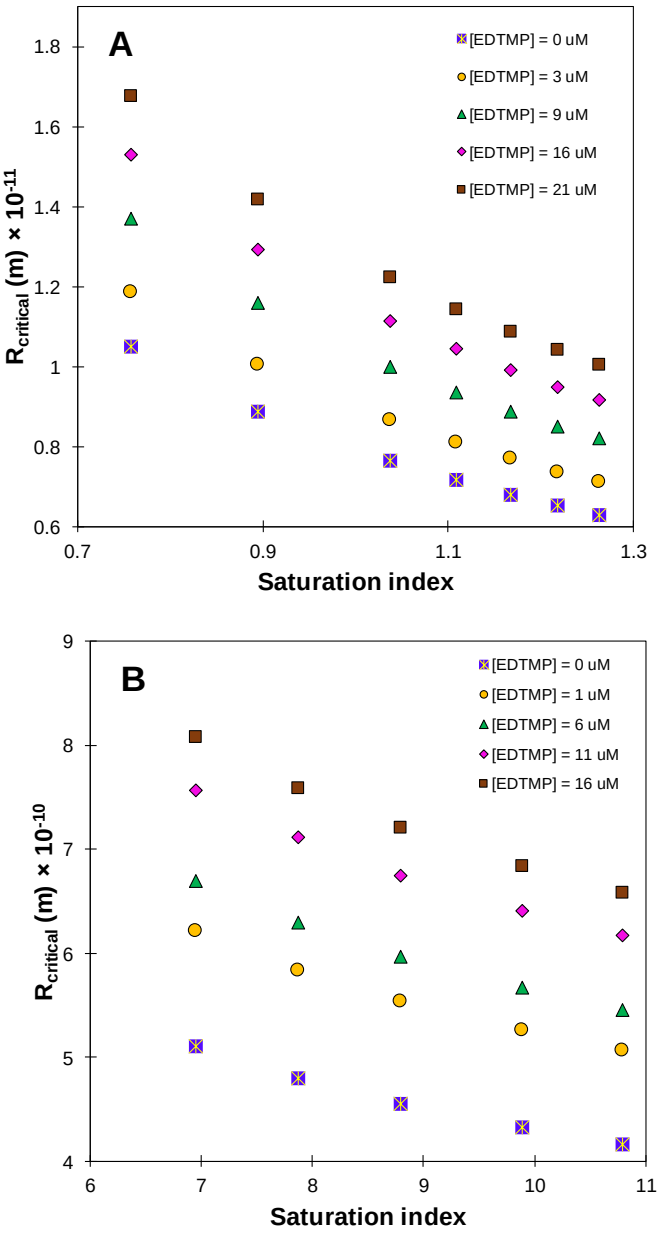

Figure S2.9 Impact of saturation index of CaCO3(s) and CaSO4(s) on critical radius of nucleation at varying EDTMP dose. A: Experimental conditions for $CaCO_{3(s)}$: [Ca^{2+}] = 10 mM; [CO_3^{2-}] = 10 mM; [EDTMP] = 0-21 µM; Saturation index = 1.32; pH = 7.8; Ionic strength = 100 mM; TRIS= 50 mM; B: Experimental conditions for $CaSO_{4(s)}$: [Ca^{2+}] = 37 mM; [SO_4^{2-}] = 564 mM; [EDTMP] = 0-16 µM; Saturation index = 7; pH = 7.8.

Appendix B

Supporting Information for Chapter 3

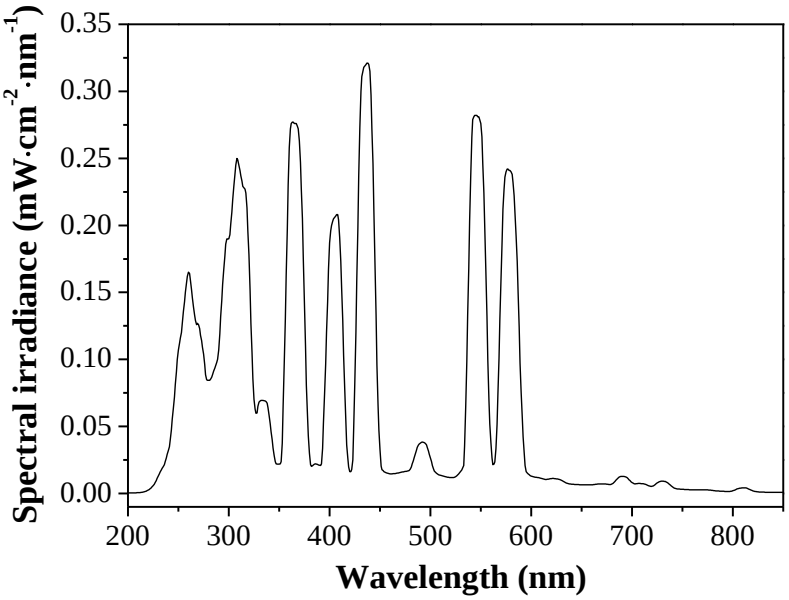

Figure S3. 1 Spectra of the 450-W UV immersion lamp used for photochemical antiscalant oxidation experiments.

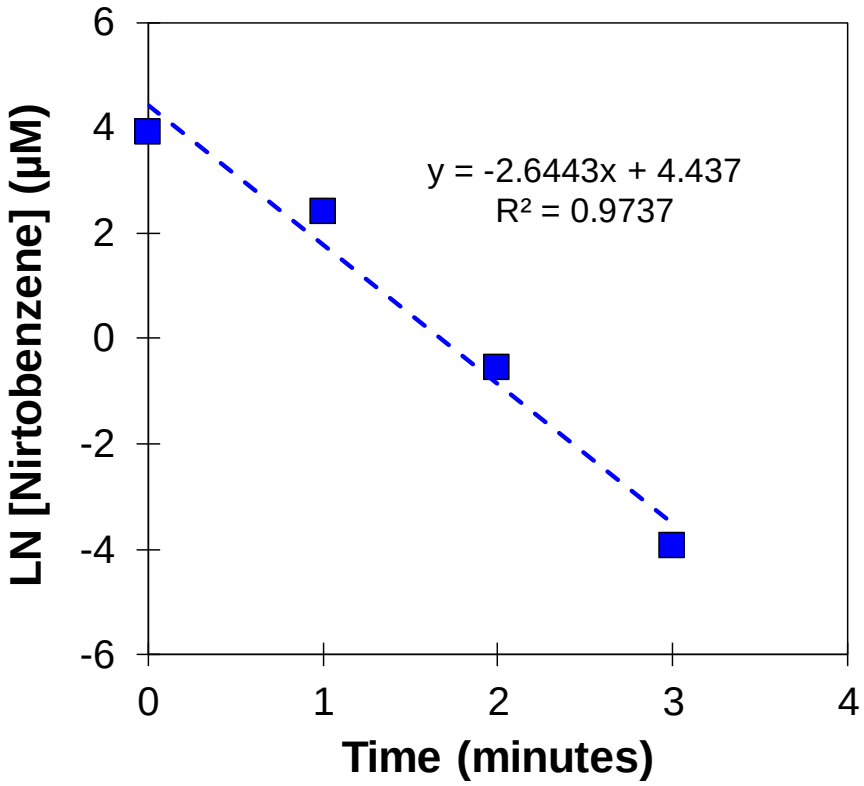

Figure S3. 2 Nitrobenzene probe analysis for hydroxyl radical steady state measurement. Nitrobenzene = 5 µM; NTMP= 2 mM; H_2O_2= 3.8 mM pH= 7.8

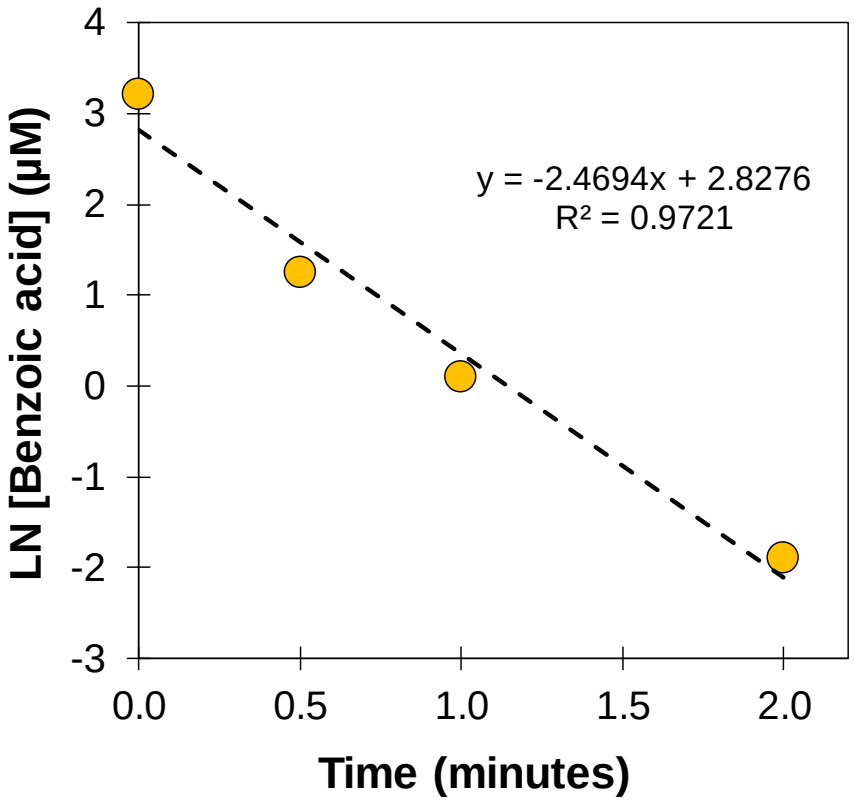

Figure S3. 3 Benzoic acid probe analysis for sulfate and hydroxyl radical steady state measurement. Benzoic acid = 5µM; NTMP= 2 mM; [$S_2O_8^{2-}$] = 2 mM pH= 7.8

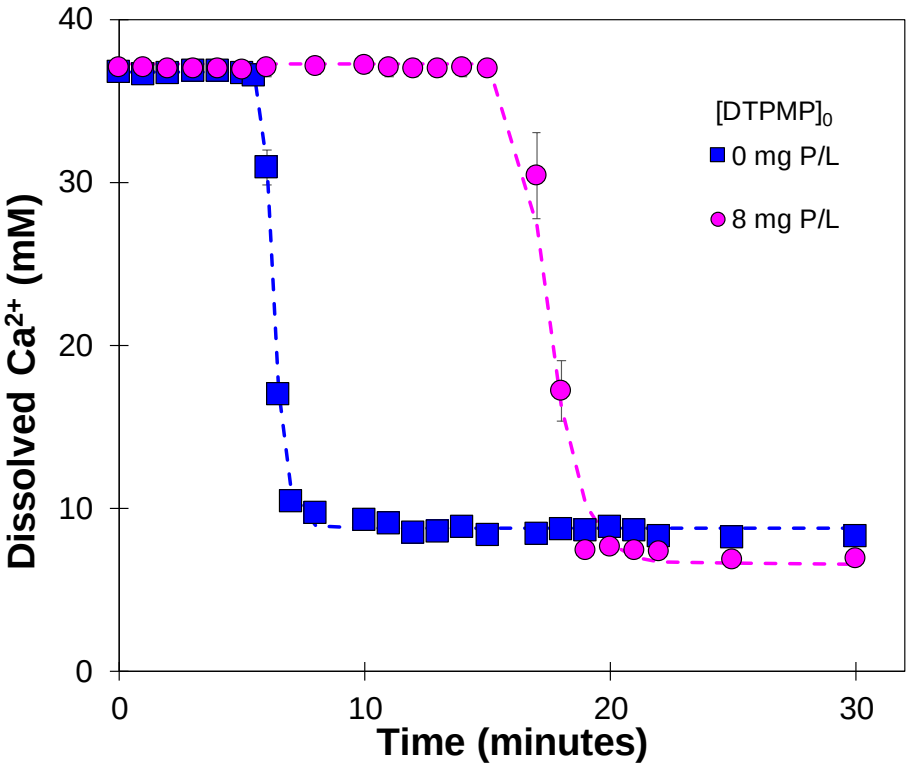

Figure S3. 4 Kinetic modeling on the precipitation of gypsum in presence and absence of DTPMP; $[S_2O_8]^{2-}{}_0$ = 3.8 mM; $[Ca^{2+}]$ = 37 mM; $[SO_4^{2-}]$ = 564 mM; pH = 7.8; medium pressure UV lamp

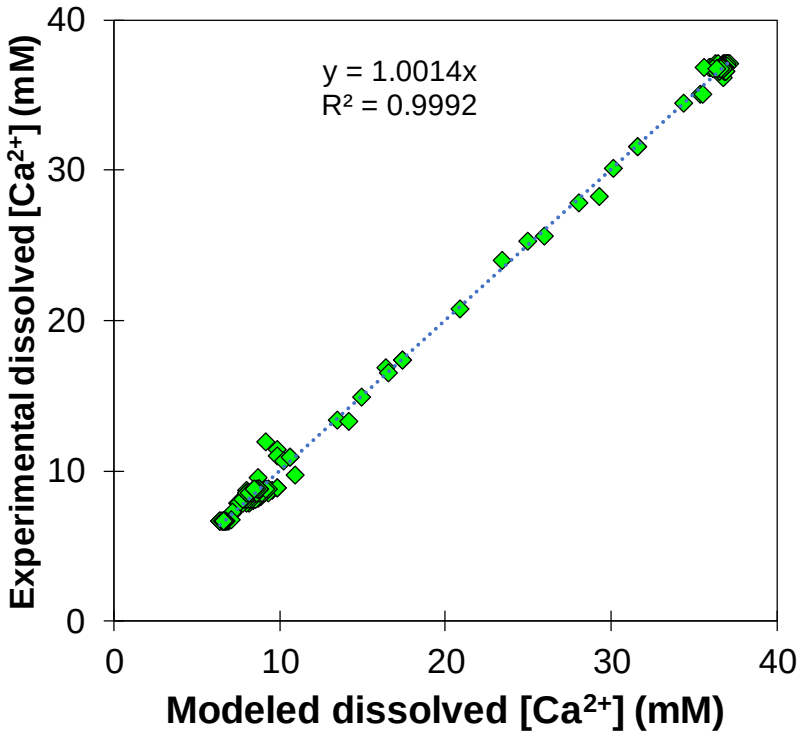

Figure S3. 5 Model robustness for the dissolved calcium prediction. $[DTPMP]_0$ = 3-15 mg P/L; $[S_2O_8]^{2-}{}_0$ = 3.8 mM; $[Ca^{2+}]$ = 37 mM; $[SO_4^{2-}]$ = 564 mM; pH = 7.8; medium pressure UV lamp

Text S3.1 Optimization of antiscalant oxidation parameters

Hydrogen peroxide and NTMP were used as the model oxidant and antiscalant respectively to optimize the oxidative degradation of antiscalant. Varying experiments were conducted to have different molar ratios of oxidant to the antiscalant. Figure S3.2 shows the impact of NTMP:Hydrogen peroxide on the degradation rate constant of NTMP. It can be seen that as the molar ratio increased from 5 to 40, the degradation rate constant increases and on further increasing the oxidant dosage, the degradation rate constant decreases. This phenomenon is due to the scavenging of hydroxyl radical by hydrogen peroxide.[255] Thus a molar ratio of 1:40 as NTMP : Hydrogen peroxide is the optimum ratio for the degradation of NTMP. At this condition, the oxidant concentration was 3.8 mM and an antiscalant concentration of 3 mg P/L. Thus for all the other conditions, an oxidant dosage of 3.8 mM was chosen while the antiscalant concentration was varied from 3 mg P/L to 15 mg P/L. To compare the degradation efficiency of hydrogen peroxide and persulfate, experiments were carried out at equimolar concentrations.

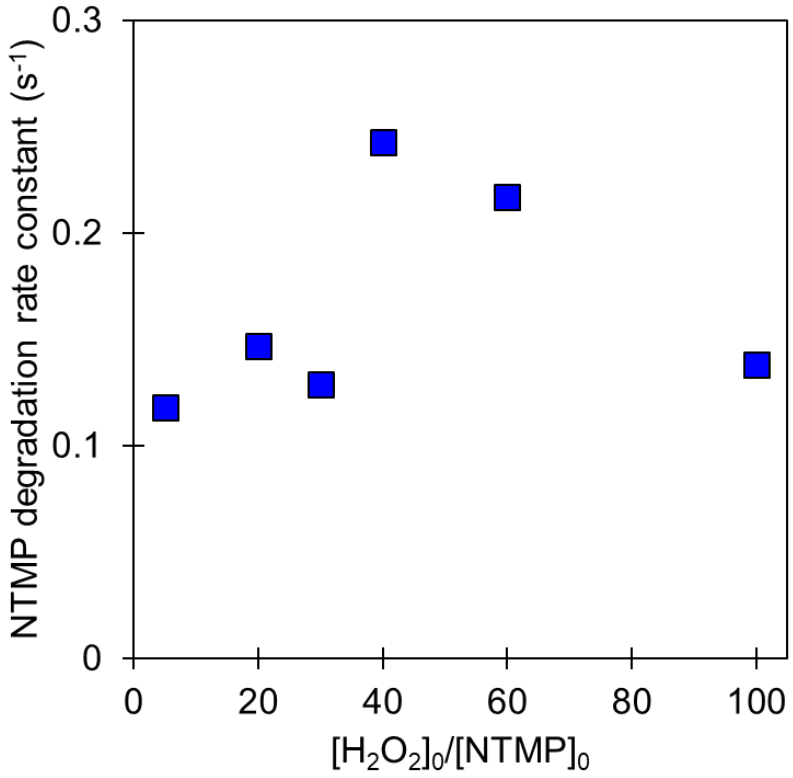

Figure S3. 6 $[NTMP]_0$ = 3 mg P/L; $[H_2O_2]_0$ = 0.47 - 9.50 mM; pH = 7.8; ionic strength = 1M

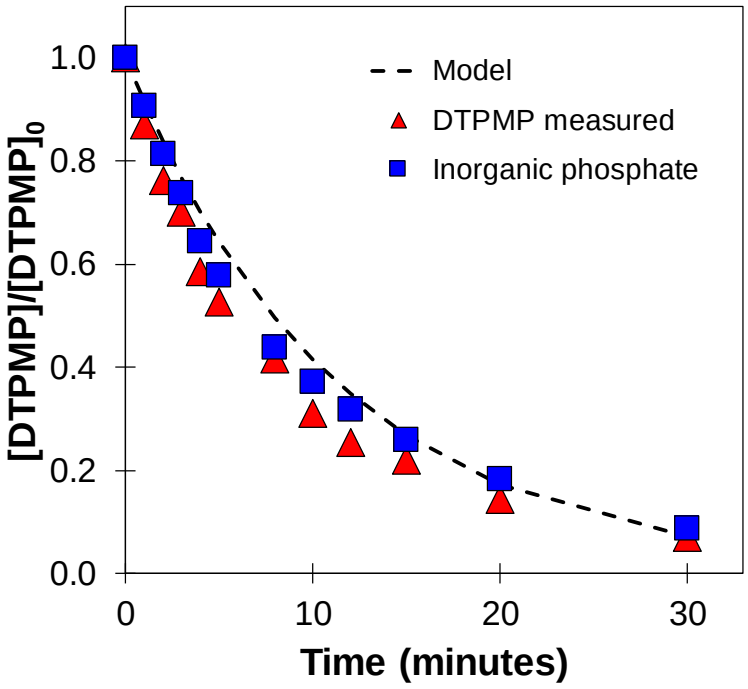

Figure S3. 7 Inorganic phosphate release profile with UV/PS degradation of DTPMP in presence of $CaSO_4$ precipitation $[S_2O_8^{2}]^{-}_0$ = 3.8 mM; $[Ca^{2+}]$ = 37 mM; $[SO_4^{2-}]$ = 564 mM; pH = 7.8; medium pressure UV lamp

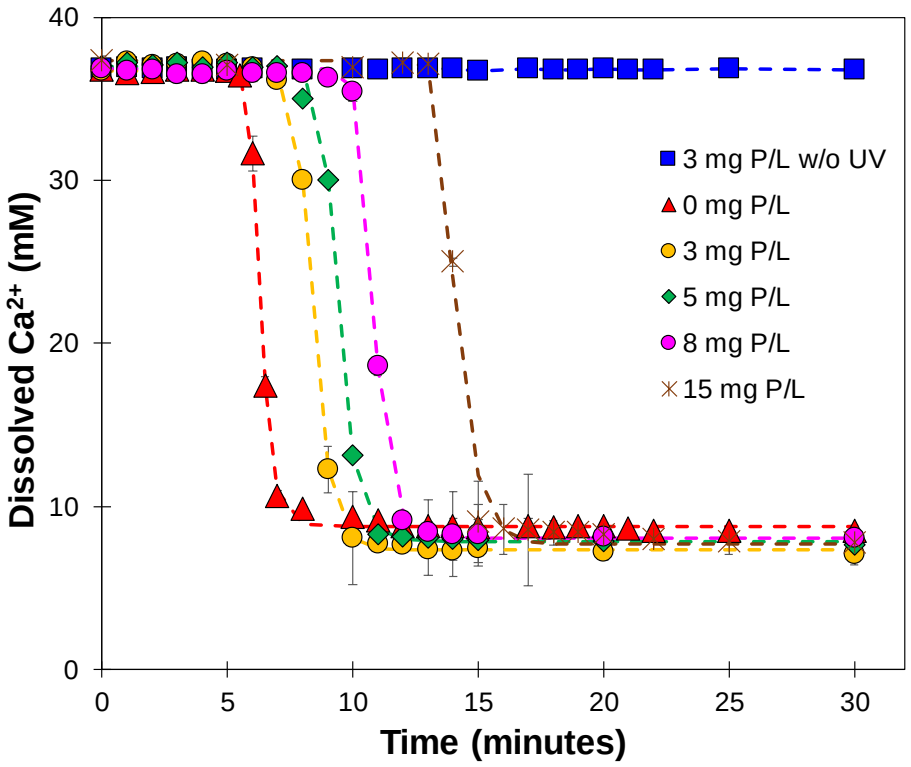

Figure S3. 8 Dissolved calcium release at different initial EDTMP concentrations; $[EDTMP]_0$ = 3-15 mg P/L; $[H_2O_2]_0$ = 3.8 mM; $[Ca^{2+}]$ = 37 mM; $[SO_4^{2-}]$ = 564 mM; pH = 7.8; medium pressure UV lamp

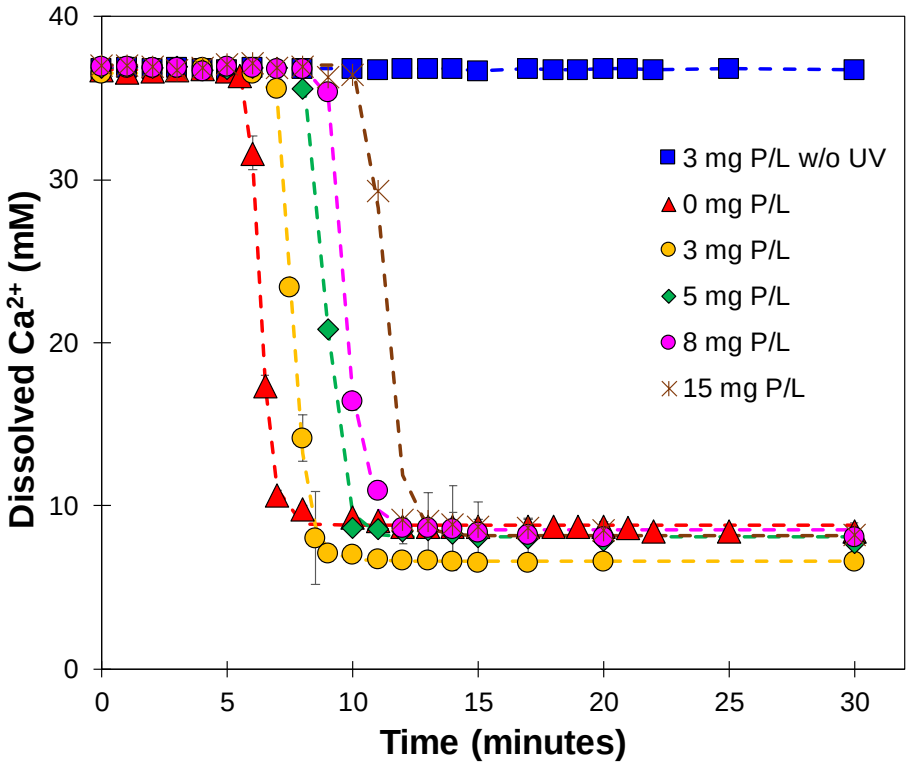

Figure S3. 9 Dissolved calcium release at different initial NTMP concentrations; $[NTMP]_0$ = 3-15 mg P/L; $[H_2O_2]_0$ = 3.8 mM; $[Ca^{2+}]$ = 37 mM; $[SO_4^{2-}]$ = 564 mM; pH = 7.8; medium pressure UV lamp

Table S3.1 Radical steady state concentration in UV/persulfate and UV/H_2O_2 system during the oxidation of DTPMP

	UV/persulfate	UV/H_2O_2
$[HO\bullet]_{ss}$ [M]	4.07×10^{-10}	5.58×10^{-10}
$[SO_4^{\bullet-}]_{ss}$ [M]	6.32×10^{-10}	0

Appendix C

Supporting Information for Chapter 4

Text S4.1 Probe method to determine steady state concentration of radicals

Nitrobenzene, benzoic acid p-chlorobenzoic acid and N,N-dimethylaniline were utilized to probe the steady state concentration of HO•, SO4 •-, reactive chlorine species and CO3•- radicals. Control experiments were performed for each probe compounds and was accounted for when calculating the decay rate of each probe. Nitrobenzene exclusively reacts with HO•, therefore is the best probe for HO•. First, the experimentally observed pseudo first order decay rate of nitrobenzene (k_{obs}) was obtained and $[HO^{\bullet}]_{ss}$ was calculated based on Equation S4.1

$$-\frac{d[NB]}{dt} = k_{OH\bullet,\mathrm{NB}}[OH^{\bullet}]_{ss}[NB]_t = k_{obs-NB}[NB]_t \quad \text{(S4.1)}$$

$$[OH^{\bullet}]_{ss} = k_{obs-NB}/k_{OH\bullet,\mathrm{NB}} \quad \text{(S4.2)}$$

$[NB]_t$ is the concentration of nitrobenzene at a given reaction time t; $[NB]_0$ is the initial concentration of nitrobenzene (5 μM); $k_{OH\bullet,NB}$ is the second-order rate constant between HO• and NB, which is known as 4.7×10^9 $M^{-1}s^{-1}$. $k_{obs\text{-}NB}$ is the experimentally obtained pseudo first-order decay rate of NB.

Similarly, the steady-state concentration of $SO_4^{\bullet-}$ ($[SO_4^{\bullet-}]_{ss}$) was calculated using benzoic acid (BA) as the probe. The *pseudo* first-order decay rate of BA ($k_{obs\text{-}NB}$) was obtained based on experimental measurements. $[SO_4^{\bullet-}]_{ss}$ was calculated as below:

$$-\frac{d[BA]}{dt} = k_{OH\bullet,\mathrm{BA}}[OH^{\bullet}]_{ss}[BA]_t + k_{SO4\bullet,\mathrm{BA}}[SO_4^{\bullet-}]_{ss}[BA]_t = k_{obs-BA}[BA]_t \quad \text{(S4.3)}$$

$$[SO_4^{\bullet-}]_{ss} = (k_{obs-BA} - k_{OH\bullet,\mathrm{BA}}[OH^{\bullet}]_{ss})/k_{SO4\bullet,BA} \quad \text{(S4.4)}$$

$[BA]_t$ is the concentration of benzoic acid at a given reaction time t; $[BA]_0$ is the initial concentration of benzoic acid (5 µM); $k_{OH\bullet,BA}$ is the second-order rate constant between $HO^{\bullet}$ and BA, which is known as 4.2×10^9 $M^{-1}s^{-1}$; $k_{SO4\bullet,BA}$ is the second-order rate constant between $SO_4^{\bullet-}$ and BA, which is known as 1.2×10^9 $M^{-1}s^{-1}$; $k_{obs\text{-}BA}$ is the experimentally obtained *pseudo* first-order decay rate of BA.

In presence of chloride, following equations were simultaneously solved to calculate the steady state concentrations of the radicals:

$$-\frac{d[BA]}{dt} = k_{OH\bullet,\mathrm{BA}}[OH^{\bullet}]_{ss}[BA]_t + k_{SO4\bullet,\mathrm{BA}}[SO_4^{\bullet-}]_{ss}[BA]_t + k_{Cl\bullet,\mathrm{BA}}[Cl^{\bullet}]_{ss}[BA]_t \quad \text{(S4.5)}$$

$$-\frac{d[PCBA]}{dt} = k_{OH\bullet,PCBA}[OH^{\bullet}]_{ss}[PCBA]_t + k_{SO4\bullet,PCBA}[SO_4^{\bullet-}]_{ss}[PCBA]_t + k_{Cl\bullet,PCBA}[Cl^{\bullet}]_{ss}[PCBA]_t \quad \text{(S4.6)}$$

$[PCBA]_t$ is the concentration of p-chlorobenzoic acid at a given reaction time t; $[PCBA]_0$ is the initial concentration of p-chlorobenzoic acid (5 µM); $k_{Cl\bullet,BA}$ is the second-order rate constant between $Cl^{\bullet}$ and BA, which is known as 1.8×10^{10} $M^{-1}s^{-1}$; $k_{Cl\bullet,PCBA}$ is the second-

order rate constant between $Cl^{\bullet}$ and PCBA, which is known as 1.2×10^{9} $M^{-1}s^{-1}$; $k_{obs\text{-}PCBA}$ is the experimentally obtained *pseudo* first-order decay rate of PCBA.

In a similar fashion, N,N Dimethyl aniline (DMA) was added as a probe instead of PCBA in the bicarbonate system.

Thus,

$$-\frac{d[BA]}{dt} = k_{OH\bullet,\mathrm{BA}}[OH^{\bullet}]_{ss}[BA]_t + k_{SO4\bullet,\mathrm{BA}}[SO_4^{\bullet-}]_{ss}[BA]_t + k_{CO3\bullet-,\mathrm{BA}}[CO_3^{\bullet-}]_{ss}[BA]_t \quad \text{(S4.5)}$$

$$-\frac{d[DMA]}{dt} = k_{OH\bullet,DMA}[OH^{\bullet}]_{ss}[DMA]_t + k_{SO4\bullet,DMA}[SO_4^{\bullet-}]_{ss}[DMA]_t + k_{Cl\bullet,DMA}[CO_3^{\bullet-}]_{ss}[DMA]_t \quad \text{(S4.6)}$$

$[DMA]_t$ is the concentration of N,N Dimethyl aniline (DMA) at a given reaction time t; $[DMA]_0$ is the initial concentration of N,N Dimethyl aniline (DMA) (5 µM); $k_{OH\bullet,DMA}$ is the second-order rate constant between $OH^{\bullet}$ and DMA, which is known as 1.8×10^{10} $M^{-1}s^{-1}$; $k_{CO3\bullet,DMA}$ is the second-order rate constant between $CO_3^{\bullet-}$ and DMA, which is known as 1.2×10^{9} $M^{-1}s^{-1}$ 256 $k_{obs\text{-}DMA}$ is the experimentally obtained *pseudo* first-order decay rate of DMA.

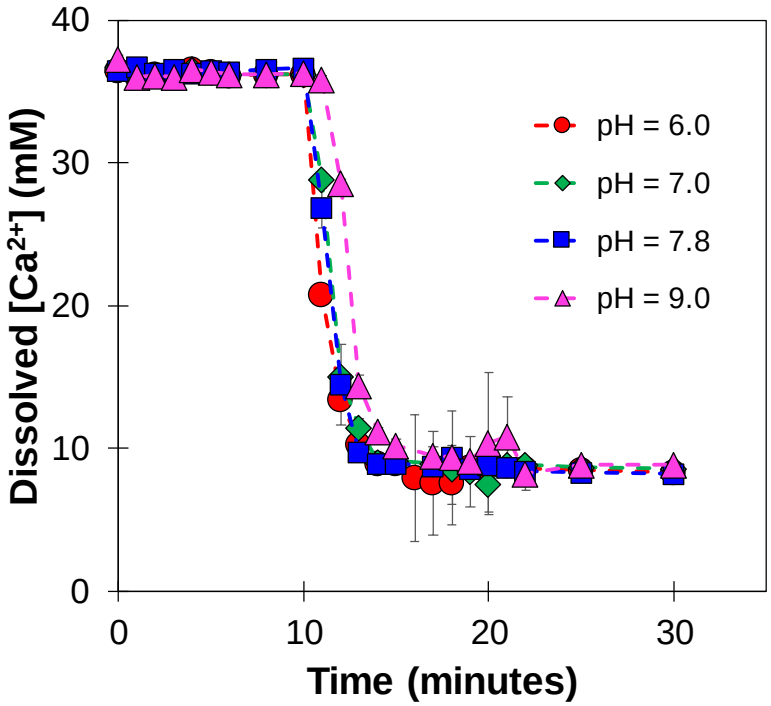

Figure S4. 1 Effect of pH on the dissolved calcium release at different initial initial pH; $[DTPMP]_0$ = 15 mg P/L; $[S_2O_8]^{2-}{}_0$ = 3.8 mM; $[Ca^{2+}]$ = 37 mM; $[SO_4^{2-}]$ = 564 mM; pH = 7.8; medium pressure UV lamp

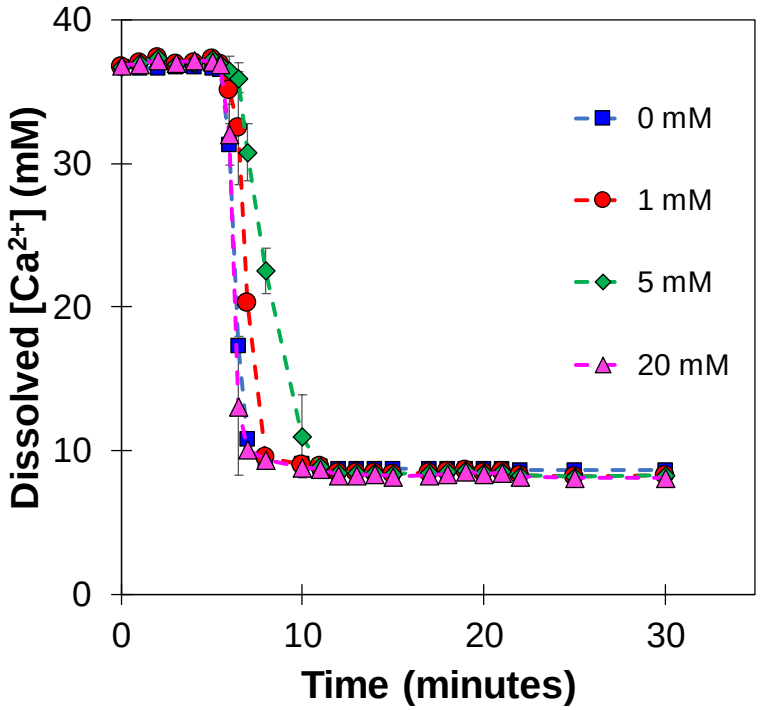

Figure S4. 2 Effect of chloride dosage on the induction time of calcium sulfate in UV/persulfate system. $[DTPMP]_0$ = 0 mg P/L; $[S_2O_8]^{2-}{}_0$ = 3.8 mM; $[Ca^{2+}]$ = 37 mM; $[SO_4^{2-}]$ = 564 mM; pH = 7.8; medium pressure UV lamp

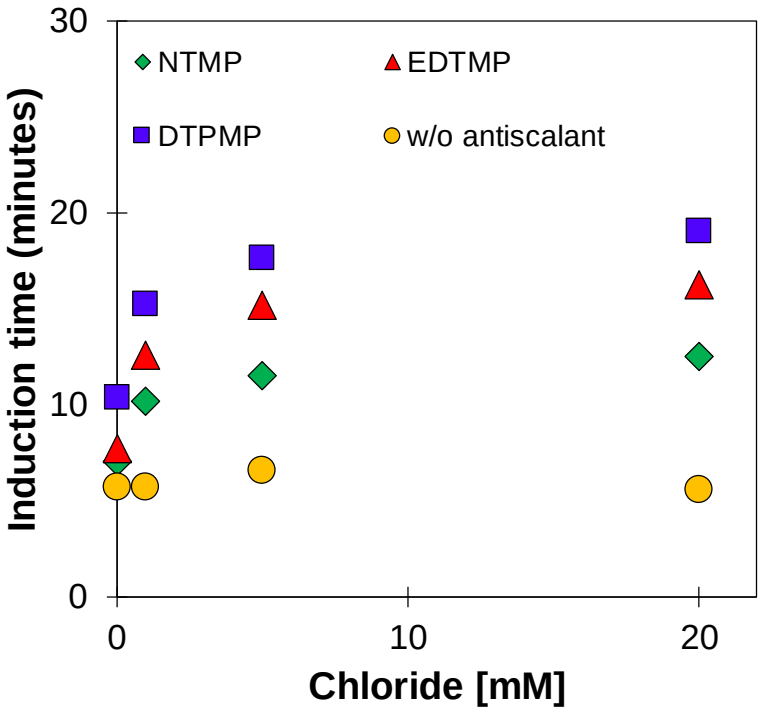

Figure S4. 3 Effect of chloride dosage on the induction time of calcium sulfate in UV/persulfate system. $[antiscalant]_0$ = 0 mg P/L; $[S_2O_8]^{2-}_0$ = 3.8 mM; $[Ca^{2+}]$ = 37 mM; $[SO_4^{2-}]$ = 564 mM; pH = 7.8; medium pressure UV lamp

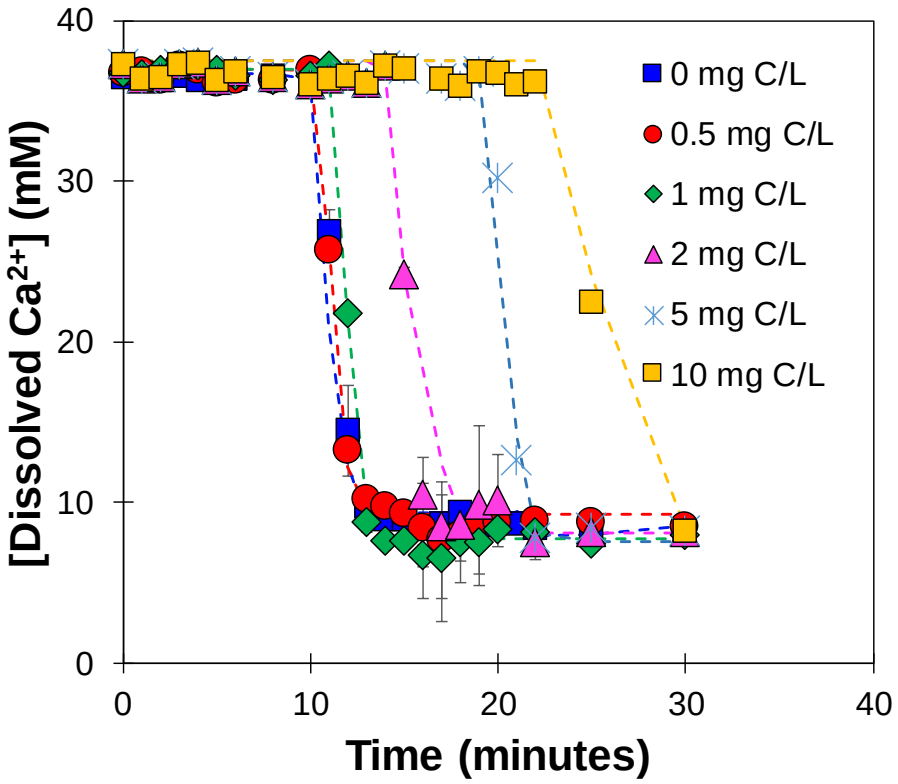

Figure S4. 4 Impact of dissolved organic matter (DOM) on photochemical demineralization of calcium sulfate in presence of DTPMP. Experimental condition: $[persulfate]_0$ = 2.0 mM; pH = 7.8; $[DTPMP]_0$ = 3 mg P/L; $[Ca^{2+}]$ = 37 mM; $[SO_4^{2-}]$ = 564 mM; pH = 7.8; medium pressure UV lamp

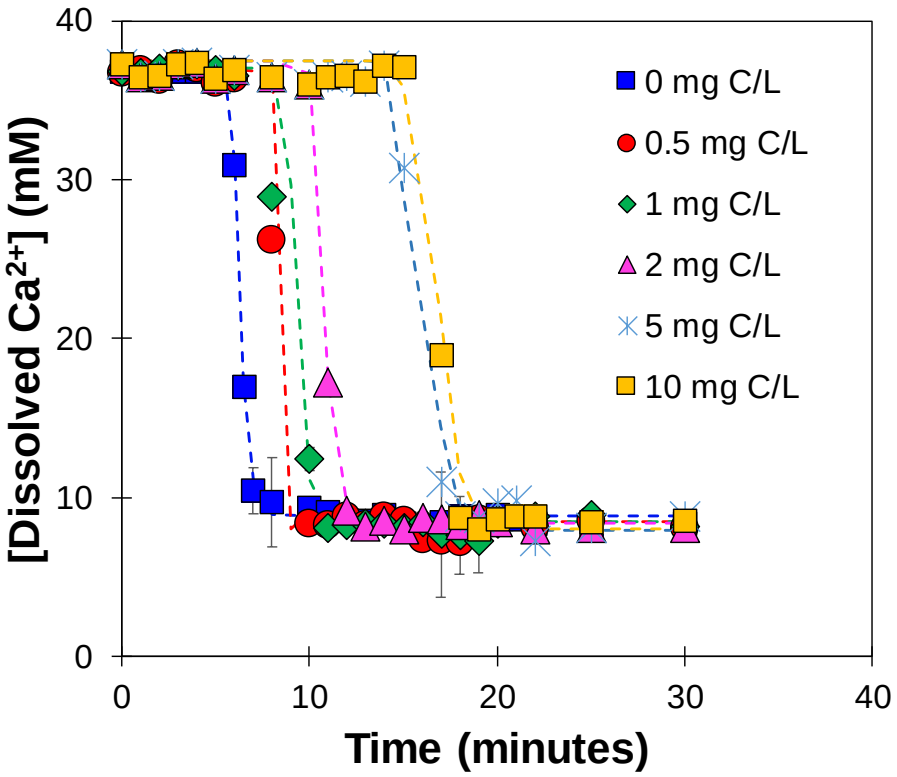

Figure S4. 5 Impact of dissolved organic matter (DOM) on photochemical demineralization of calcium sulfate in presence of EDTMP. Experimental condition: $[persulfate]_0$ = 2.0 mM; pH = 7.8; $[EDTMP]_0$ = 3 mg P/L; $[Ca^{2+}]$ = 37 mM; $[SO_4^{2-}]$ = 564 mM; pH = 7.8; medium pressure UV lamp

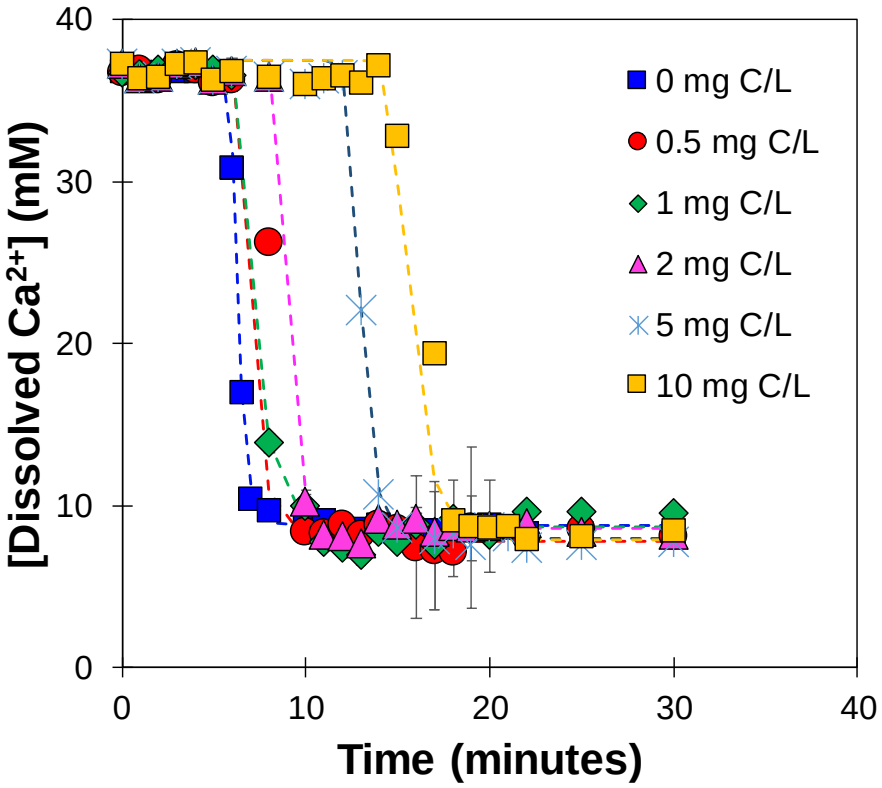

Figure S4. 6 Impact of dissolved organic matter (DOM) on photochemical demineralization of calcium sulfate in presence of NDTMP. Experimental condition: $[persulfate]_0$ = 2.0 mM; pH = 7.8; $[NTMP]_0$ = 3 mg P/L; $[Ca^{2+}]$ = 37 mM; $[SO_4^{2-}]$ = 564 mM; pH = 7.8; medium pressure UV lamp

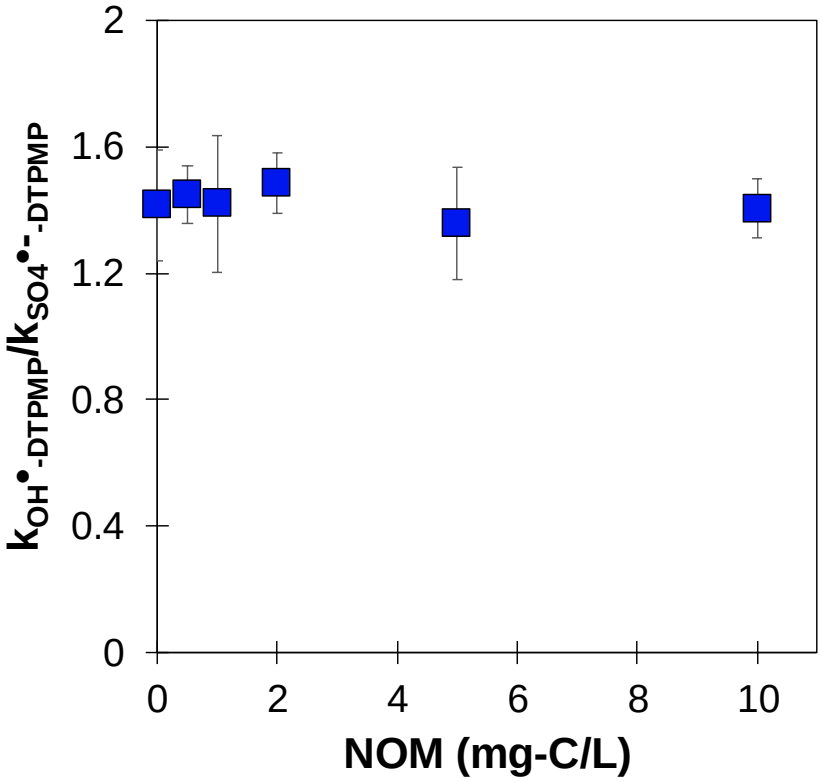

Figure S4. 7 Effect of NOM on the ratio of contribution of sulfate radical and hydroxyl radical on DTPMP degradation. Experimental condition: $[persulfate]_0$ = 2.0 mM; pH = 7.8; $[DTPMP]_0$ = 3 mg P/L; $[Ca^{2+}]$ = 37 mM; $[SO_4^{2-}]$ = 564 mM; pH = 7.8; medium pressure UV lamp

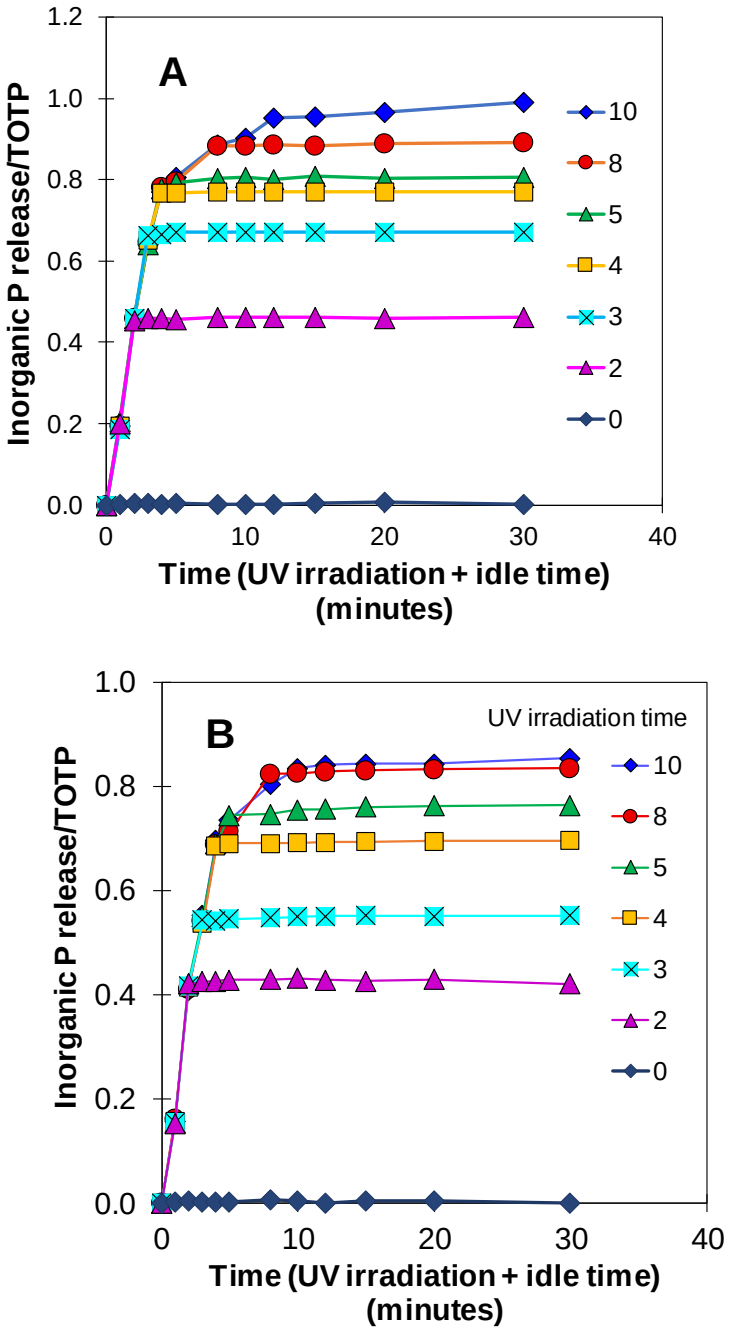

Figure S4. 8 Antiscalant degradation at different UV irradiation time with H_2O_2 and 3mg P/L; values in the legend indicates the UV irradiation time; pH = 7.8; ionic strength = 1 M

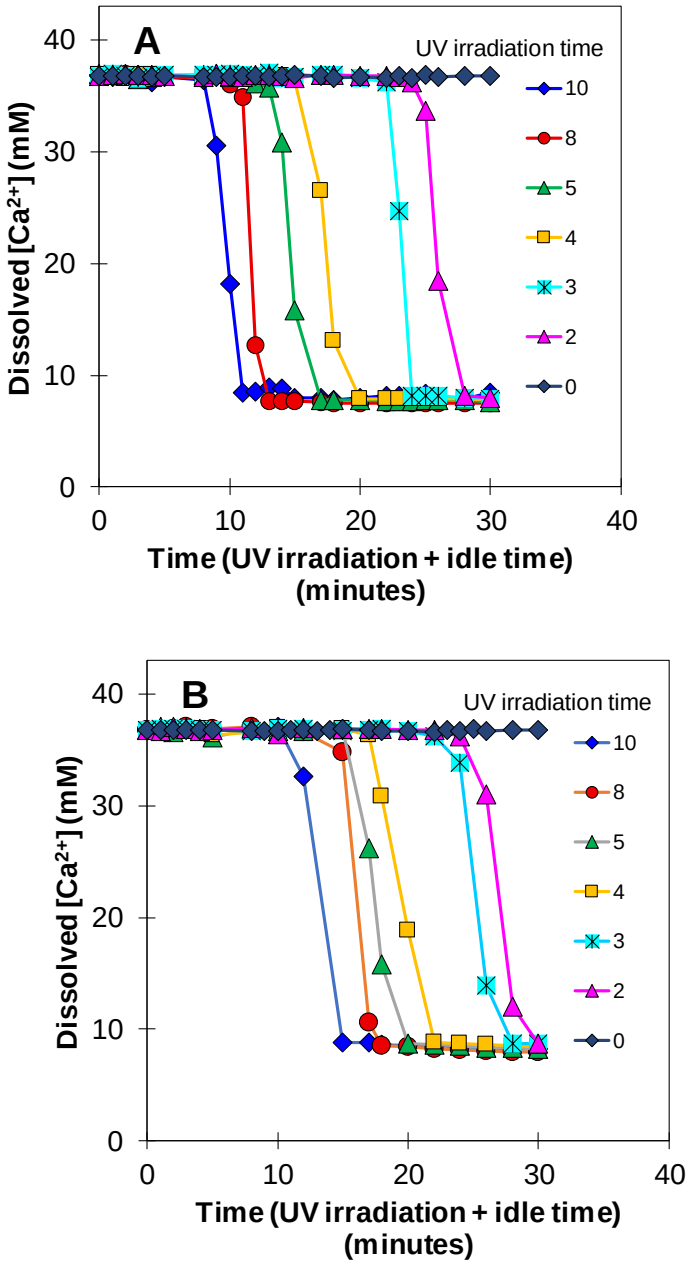

Figure S4. 9 Dissolved calcium release at different UV irradiation times; values in the legend indicates the UV irradiation time. Experimental conditions: $[antiscalant]_0$ = 3 mg P/L; pH = 7.8; ionic strength = 1 M

References

1. Abdelkareem, M.A.; Assad, M.E.; Sayed, E.T.; Soudan, B., Recent progress in the use of renewable energy sources to power water desalination plants. *Desalination* **2018,** 435, 97-113.

2. Alkaisi, A; Mossad, R; Sharifian-Barforoush A., A review of the water desalination systems integrated with renewable energy. *Energy Procedia* **2017**, 74, 110-268.

3. World Health Organization, Progress on drinking water, sanitation and hygiene: **2017** update and SDG baselines.

4. Jamaly, S.; Darwish, N.N.; Ahmed, I.; Hasan, S.W., A short review on reverse osmosis pretreatment technologies. *Desalination* **2014**, 354, 30-38.

5. Shenvi, S.S.; Isloor, A.M.; Ismail, A.F., A review on RO membrane technology: developments and challenges. *Desalination* **2015**, 368, 10-26.

6. Population Action International (PAI). People in the Balance Update **2004**: Population and Natural Resources at the Turn of the Millennium. Washington, DC: PAI

7. Gannon, J.P.; Bailey, S.W.; McGuire, K.J., Organizing groundwater regimes and response thresholds by soils: A framework for understanding runoff generation in a headwater catchment. *Water Resources Research* **2014**, 50, 8403-8419.

8. Famiglietti, J.S., Lo, M., Ho, S.L., Bethune, J., Anderson, K.J., Syed, T.H., Swenson, S.C., de Linage, C.R. and Rodell, M., Satellites measure recent rates of groundwater depletion in California's Central Valley. *Geophysical Research Letters* **2011**, 38.

9. Fuchs, B.; Wood, D.; Ebbeka, D., From too much to too little: How the central US drought of 2012 evolved out of one of the most devastating floods on record in 2011. **2015**

10. Alcott, B., Population matters in ecological economics. *Ecological Economics* **2012**, 80, 109-120.

11. Post, V.E., Groen, J., Kooi, H., Person; M., Ge, S., Edmunds, W.M., Offshore fresh groundwater reserves as a global phenomenon. *Nature* **2013**, 504, 71.

12. Olsson, G. Water and energy: threats and opportunities. IWA publishing **2015**.

13. Roy, S.B., Chen, L., Girvetz, E.H., Maurer, E.P., Mills, W.B. and Grieb, T.M., Projecting water withdrawal and supply for future decades in the US under climate change scenarios. *Environmental science & technology* **2012**, 46, 2545-2556.

14. McNabb, D.E., Water Resource Management: Sustainability in an Era of Climate Change. *Springer* **2017**.

15. Vörösmarty, C. J.; Green, P.; Salisbury, J.; Lammers, R. B. Global water resources: vulnerability from climate change and population growth. *Science* **2000**, 289, 284-288.

16. Trenberth, K. E., Changes in precipitation with climate change. *Climate Research* **2011**, 47, 123-138.

17. Hardy, D.; Cubillo, F.; Han, M.; Li, H., Alternative water resources: a review of concepts, solutions and experiences. *International Water Association (IWA)* **2015**.

18. Post, V.E.A., Fresh and saline groundwater interaction in coastal aquifers: is our technology ready for the problems ahead?. *Hydrogeology Journal* **2005**, 13, 120-123.

19. Stuyfzand, P.J.; Raat, K.J., Benefits and hurdles of using brackish groundwater as a drinking water source in the Netherlands. *Hydrogeology Journal* **2010**, 18, 117-130.

20. Buono, R.M.; Zodrow, K.R.; Alvarez, P.J.; Li, Q., Brackish groundwater: current status and potential benefits for water management. *Issue Brief* **2016**.

21. Elimelech, M.; Phillip, W.A., The future of seawater desalination: energy, technology, and the environment. Science **2011**, 712-717.

22. Shenvi, S.S.; Isloor, A.M.; Ismail, A.F., A review on RO membrane technology: developments and challenges. *Desalination* **2015**, 368, 10-26.

23. https://water.usgs.gov/ogw/gwrp/brackishgw/brackish.html

24. Ahmed, M.; Shayya, W. H.; Hoey, D.; Al-Handaly, J. Brine disposal from reverse osmosis desalination plants in Oman and the United Arab Emirates. *Desalination* **2001**, 133, 135-147.

25. Ruiz-García, A.; Ruiz-Saavedra, E.; Feo-García, J. Start-up of brackish water desalination for agricultural irrigation in the Canary Islands (Spain). *Desalination and Water Treatment* **2016**, 57, 22734-22742.

26. Seckin, G.; Yilmaz, T.; Sari, B.; Ersu, C. B., Groundwater hydrochemistry at the Mediterranean coastal plains - the case of Silifke, Turkey. *Desalination* **2010**, 253, 164-169.

27. Giambastiani, B. M. S.; Colombani, N.; Mastrocicco, M.; Fidelibus, M. D. Characterization of the lowland coastal aquifer of Comacchio (Ferrara, Italy): hydrology, hydrochemistry and evolution of the system. *Journal of hydrology* **2013**, 501, 35-44.

28. Barlow, P. M.; Reichard, E. G., Saltwater intrusion in coastal regions of North America. *Hydrogeology Journal* **2010**, 18, 247-260.

29. Vörösmarty, C. J.; Green, P.; Salisbury, J.; Lammers, R. B., Global water resources: vulnerability from climate change and population growth. *Science* **2000**, 289, 284-288.

30. Trenberth, K. E., Changes in precipitation with climate change. *Climate Research* **2011**, 47, 123-138.

31. Park, P.K.; Lee, S.; Cho, J.S.; Kim, J.H., Full-scale simulation of seawater reverse osmosis desalination processes for boron removal: Effect of membrane fouling. *Water research* **2012**, 46, 3796-3804.

32. Atab, M.S.; Smallbone, A.J.; Roskilly, A.P., An operational and economic study of a reverse osmosis desalination system for potable water and land irrigation. *Desalination* **2016**, 397, 174-184.

33. Goh P.S.; Lau W.J.; Othman M.H.D.; Ismail A.F., Membrane fouling in desalination and its mitigation strategies, *Desalination* **2018**, 425, 130-155

34. Burn, S.; Gray, S., Efficient Desalination by Reverse Osmosis: A guide to RO practice. *IWA Publishing*, **2016**.

35 Ahmed, M., Shayya, W.H., Hoey, D. and Al-Handaly, J., Brine disposal from reverse osmosis desalination plants in Oman and the United Arab Emirates. *Desalination*, **2001**, *133*(2), 135-147.

36. Shannon, M. A.; Bohn, P. W.; Elimelech, M.; Georgiadis, J. G.; Marinas, B. J.; Mayes, A. M. Science and technology for water purification in the coming decades. *Nature* **2008**, 452, 301-310.

37. Côté, P.; Siverns, S.; Monti, S. Comparison of membrane-based solutions for water reclamation and desalination. *Desalination* **2005**, 182, 251-257.

38. Werber, J. R.; Osuji, C. O.; Elimelech, M. Materials for next-generation desalination and water purification membranes. *Nature Reviews Materials* **2016**, 1, 16018.

39. Famiglietti, J. S., The global groundwater crisis. *Nature Climate Change* **2014**, 4, 945-8.

40. El Saliby, I.; Okour, Y.; Shon, H. K.; Kandasamy, J.; Kim, I. S. Desalination plants in Australia, review and facts. *Desalination*. **2009**, 247, 1-4.

41. "Desalination (Brackish and Sea Water)." California Water Plan Update 2013. http://www.water.ca.gov/waterplan/docs/cwpu2013/Final/Vol3_Ch10_Desalination.pdf.

42. Reilly, T.E.; Dennehy, K.F.; Alley, W.M.; Cunningham, W.L., Ground-water availability in the United States (No. 1323). *Geological Survey (US)* **2008**.

43. Meixner, T.; Manning, A.H.; Stonestrom, D.A.; Allen, D.M., Ajami, H., Blasch, K.W., Brookfield, A.E., Castro, C.L., Clark, J.F., Gochis, D.J.; Flint, A.L., Implications of projected climate change for groundwater recharge in the western United States. *Journal of Hydrology* **2016**, 534, 124-138.

44. Mickley, M., US municipal desalination plants: number, types, locations, sizes, and concentrate management practices. *IDA Journal of Desalination and Water Reuse* **2013**, 4, 44-51.

45. Wenten, I.G., Reverse osmosis applications: prospect and challenges. *Desalination* **2016**, 391, 112-125.

46. McCool, B.C.; Rahardianto, A.; Cohen, Y., Antiscalant removal in accelerated desupersaturation of RO concentrate via chemically-enhanced seeded precipitation (CESP). *Water research* **2012**, 46, 4261-4271.

47. Maupin, M.A.; Kenny, J.F.; Hutson, S.S.; Lovelace, J.K.; Barber, N.L.; Linsey, K.S., Estimated use of water in the United States in 2010 (No. 1405). *US Geological Survey* **2014**.

48. Van de Lisdonk, C. A. C.; Van Paassen, J. A. M.; Schippers, J. C. Monitoring scaling in nanofiltration and reverse osmsis membrane systems. *Desalination* **2000**, 132, 101-108.

49. Shirazi, S.; Lin, C. J.; Chen, D., Inorganic fouling of pressure-driven membrane processes—a critical review. *Desalination* **2010**, 250, 236-248.

50. Greenlee, L. F.; Lawler, D. F.; Freeman, B. D.; Marrot, B.; Moulin, P., Reverse osmosis desalination: water sources, technology, and today's challenges. *Water research* **2009**, 43, 2317-2348.

51. Cartmell, D. Desalination: Antiscalants keep the water flowing in reverse osmosis. *Filtration+ Separation* **2012**, 49, 22-24.

52. Neveux, T.; Bretaud, M.; Chhim, N.; Shakourzadeh, K.; Rapenne, S., Pilot plant experiments and modeling of CaCO3 growth inhibition by the use of antiscalant polymers in recirculating cooling circuits. *Desalination* **2016**, 397, 43-52.

53. Vrouwenvelder, J.S.; Manolarakis, S.A.; Veenendaal, H.R.; Van der Kooij, D., Biofouling potential of chemicals used for scale control in RO and NF membranes. *Desalination* **2000**, 132, 1-10.

54. Sheikhi, A.; Li, N.; van de Ven, T. G.; Kakkar, A. Macromolecule-based platforms for developing tailor-made formulations for scale inhibition. *Environmental Science: Water Research & Technology* **2016**, 2, 71-84.

55. Ahmed, M.; Arakel, A.; Hoey, D.; Thumarukudy, M. R.; Goosen, M. F.; Al-Haddabi, M.; Al-Belushi, A. Feasibility of salt production from inland RO desalination plant reject brine: a case study. *Desalination* **2003**, 158, 109-117.

56. Van der Bruggen, B.; Lejon, L.; Vandecasteele, C., Reuse, treatment, and discharge of the concentrate of pressure-driven membrane processes. *Environmental science & technology* **2003**, 37, 3733-3738.

57. Santa Ana Watershed Project Authority Website; http://www.sawpa.org/brineline/what-is-it/

58. Owens-Bennett, E. L.; Trussell, B.; Monroy, I.; Trussell, R. Proposed solids formation recovery formula for the inland empire brine line; **2016**.

59. Benjamin, M. M.; Lawler, D. F.; Tobiason, J. E. Inland empire brine line expert panel, **2011**.

60. Greenlee, L. F.; Testa, F.; Lawler, D. F.; Freeman, B. D.; Moulin, P. Effect of antiscalants on precipitation of an RO concentrate: metals precipitated and particle characteristics for several water compositions. *Water research* **2010**, 44 (8), 2672-2684.

61. Greenlee, L. F.; Testa, F.; Lawler, D. F.; Freeman, B. D.; Moulin, P. The effect of antiscalant addition on calcium carbonate precipitation for a simplified synthetic brackish water reverse osmosis concentrate. *Water research* **2010**, 44, 2957-2969.

62. Hasson, D.; Drak, A.; Semiat, R. Induction times induced in an RO system by antiscalants delaying CaSO4 precipitation. *Desalination* **2003**, 157, 193-207.

63. Mansour, S.; Arafat, H. A.; Hasan, S. W. Chapter 5, Brine management in desalination plants, Desalination Sustainability, A Technical, Socioeconomic, and Environmental Approach **2017**, 207-236.

64. Giwa, A.; Dufour, V.; Al Marzooqi, F.; Al Kaabi, M.; Hasan, S. W. Brine management methods: Recent innovations and current status. *Desalination* **2017**, 407, 1-23.

65. Khudair, K. M.; Eraibi, N. A. Environmental impact of RO units installation in main water treatment plants of Basrah city/south of Iraq. *Desalination* **2017**, 404, 270-279.

66 Alawadhi, A.A., Pretreatment plant design—Key to a successful reverse osmosis desalination plant. *Desalination*, **1997**, *110*(1-2), 1-10.

67. Darton, E. G.; Scale inhibition techniques used in membrane systems. *Desalination* **1997**, 113, 227-229.

68. Austin, A. E.; Miller, J. F.; Vaughan, D.A.; Kircher, J.F. Chemical additives for calcium sulfate scale control. *Desalination* **1975**, 16, 345-357.

69. Ketrane, R.; Saidani, B.; Gil, O.; Leleyter, L.; Baraud, F. Efficiency of five scale inhibitors on calcium carbonate precipitation from hard water: effect of temperature and concentration. *Desalination* **2009**, 249, 1397-1404.

70. Abd-El-Khalek, D. E.; Abd-El-Nabey, B. A. Evaluation of sodium hexametaphosphate as scale and corrosion inhibitor in cooling water using electrochemical techniques. *Desalination* **2013**, 311, 227-233.

71. He, F.; Sirkar, K. K.; Gilron, J. Effects of antiscalants to mitigate membrane scaling by direct contact membrane distillation. *Journal of Membrane Science* **2009**, 345, 53-58.

72. Nowack, B. The behavior of phosphonates in wastewater treatment plants of Switzerland. *Water research* **1998**, 32, 1271-1279.

73. Sweeney, F. M.; Cooper, S.D. The development of a novel scale inhibitor for severe water chemistries. In SPE *International Symposium on Oilfield Chemistry* **1993**.

74. Carter Jr, R. P.; Carroll, R. L.; Irani, R. R. Nitrilotri (methylenephosphonic acid), ethyliminodi-(methylenephosphonic acid), and diethylaminomethylphosphonic acid: acidity and calcium (II) and magnesium (II) complexing. *Inorganic Chemistry* **1967**, 6, 939-942.

75. Pairat, R.; Sumeath, C.; Browning, F. H.; Fogler, H. S. Precipitation and dissolution of calcium− ATMP precipitates for the inhibition of scale formation in porous media. *Langmuir* **1997**, 13, 1791-1798.

76. Knepper, T. P., Synthetic chelating agents and compounds exhibiting complexing properties in the aquatic environment. *TrAC: Trends in Analytical Chemistry* **2003**, 22, 708-724.

77. Duan, W.; Oota, H.; Sawada, K. Stability and structure of ethylenedinitrilopoly (methylphosphonate) complexes of the alkaline-earth metal ions in aqueous solution. *Journal of the Chemical Society, Dalton Transactions* **1999**, 17, 3075-3080.

78. Deluchat, V.; Bollinger, J. C.; Serpaud, B.; Caullet, C. Divalent cations speciation with three phosphonate ligands in the pH-range of natural waters. *Talanta* **1997**, 44, 897-907.

79. Popov, K.; Rönkkömäki, H.; Lajunen, L.H. Critical evaluation of stability constants of phosphonic acids (IUPAC technical report). *Pure and applied chemistry* **2001**, 73, 1641-1677.

80 Popov, K., Rönkkömäki, H. and Lajunen, L.H., Critical evaluation of stability constants of phosphonic acids (IUPAC technical report). *Pure and applied chemistry*, **2001**, 73(10), 1641-1677.

81 Ramachandran, V.S., Lowery, M.S., Wise, T. and Polomark, G.M., The role of phosphonates in the hydration of Portland cement. *Materials and structures*, **1993**, 26(7), 425-432.

82 Gratz AJ, Hillner PE. Poisoning of calcite growth viewed in the atomic force microscope (AFM). J Cryst Growth **1993**, 129:789–93.

83. Kappel, C.; Kemperman, A.J.; Temmink, H.; Zwijnenburg, A.; Rijnaarts, H.H.M.; Nijmeijer, K., Impacts of NF concentrate recirculation on membrane performance in an integrated MBR and NF membrane process for wastewater treatment. *Journal of membrane science* **2014**, 453, 359-368.

84. Acero, J.L.; Benitez, F.J., Real, F.J.; Teva, F., Coupling of adsorption, coagulation, and ultrafiltration processes for the removal of emerging contaminants in a secondary effluent. *Chemical Engineering Journal* **2012**, 210, 1-8.

85. Bagastyo, A.Y.; Radjenovic, J.; Mu, Y.; Rozendal, R.A.; Batstone, D.J.; Rabaey, K., Electrochemical oxidation of reverse osmosis concentrate on mixed metal oxide (MMO) titanium coated electrodes. *Water research* **2011**, 45, 4951-4959.

86. Bagastyo, A.Y.; Keller, J.; Poussade, Y.; Batstone, D.J., Characterisation and removal of recalcitrants in reverse osmosis concentrates from water reclamation plants. *Water Research* **2011**, 45, 2415-2427.

87. Umar, M., Roddick, F.; Fan, L., Effect of coagulation on treatment of municipal wastewater reverse osmosis concentrate by UVC/H2O2. *Journal of hazardous materials* **2014**, 266, 10-18.

88. Wert, E.C.; Gonzales, S.; Dong, M.M.; Rosario-Ortiz, F.L., Evaluation of enhanced coagulation pretreatment to improve ozone oxidation efficiency in wastewater. *Water research* **2011**, 45, 5191-5199.

89. Arola, K.; Van der Bruggen, B.; Mänttäri, M.; Kallioinen, M., Treatment options for nanofiltration and reverse osmosis concentrates from municipal wastewater treatment: A review. *Critical Reviews in Environmental Science and Technology* **2019**, 1-68.

90. Joo, S.H.; Tansel, B., Novel technologies for reverse osmosis concentrate treatment: A review. *Journal of Environmental Management* **2015**, 150, 322-335.

91. Ahmed, M.; Shayya, W.H.; Hoey, D.; Al-Handaly, J., Brine disposal from reverse osmosis desalination plants in Oman and the United Arab Emirates. *Desalination* **2001**, 133, 135-147.

92. Arnal, J.M.; Sancho, M.; Iborra, I.; Gozálvez, J.M., Santafé, A.; Lora, J., Concentration of brines from RO desalination plants by natural evaporation. *Desalination* **2005**, 182, 435-439.

93. Yen, F.C.; You, S.J.; Chang, T.C., Performance of electrodialysis reversal and reverse osmosis for reclaiming wastewater from high-tech industrial parks in Taiwan: A pilot-scale study. *Journal of environmental management* **2017**, 187, 393-400.

94. Subramani, A.; Jacangelo, J.G., Treatment technologies for reverse osmosis concentrate volume minimization: A review. *Separation and Purification Technology* **2014**, 122, 472-489.

95. Sethi, S.; Zacheis, A.; Juby, G., State-of-science and emerging and promising technologies for brine disposal and minimization for reverse osmosis desalination. *ACE* **2005**.

96. Lamei, A.; Von Münch, E.; Van der Zaag, P., Environmental impact and economic costs of brine disposal from RO desalination plants in arid coastal regions. *In Proc. IDA World Congress* **2009**, 7-12.

97. Gabelich, C.J.; Williams, M.D., Rahardianto, A., Franklin, J.C.; Cohen, Y., High-recovery reverse osmosis desalination using intermediate chemical demineralization. *Journal of Membrane Science* **2007**, 301, 131-141.

98. Ordóñez, R.; Moral, A.; Hermosilla, D.; Blanco, Á., Combining coagulation, softening and flocculation to dispose reverse osmosis retentates. *Journal of Industrial and Engineering Chemistry* **2012**, 18, 926-933.

99. Rahardianto, A.; Gao, J.; Gabelich, C. J.; Williams, M.D.; Cohen, Y., High recovery membrane desalting of low-salinity brackish water: integration of accelerated precipitation softening with membrane RO. *Journal of Membrane Science* **2007**, 289, 123-137.

100. Rahardianto, A.; McCool, B.C.; Cohen, Y., Accelerated desupersaturation of reverse osmosis concentrate by chemically-enhanced seeded precipitation. *Desalination* **2010**, 264, 256-267.

101. McCool, B.C.; Rahardianto, A.; Cohen, Y., Antiscalant removal in accelerated desupersaturation of RO concentrate via chemically-enhanced seeded precipitation (CESP). *Water research* **2012**, 46, 4261-4271.

102. Sanciolo, P.; Ostarcevic, E.; Atherton, P.; Leslie, G.; Fane, T.; Cohen, Y.; Payne. M; Gray. S., Enhancement of reverse osmosis water recovery using interstage calcium precipitation. *Desalination* **2012**, 295, 43-52.

103. Gabelich, C.J.; Xu, P.; Cohen, Y., Concentrate treatment for inland desalting. *Sustainability science and engineering* **2010**, 2, 295-326.

104. Ashraf, S.N.; Rajapakse, J.; Dawes, L.A.; Millar, G.J., Electrocoagulation for the purification of highly concentrated brine produced from reverse osmosis desalination of coal seam gas associated water. *Journal of Water Process Engineering* **2019**, 28, 300-310.

105. Azerrad, S.P.; Isaacs, M.; Dosoretz, C.G., Integrated treatment of reverse osmosis brines coupling electrocoagulation with advanced oxidation processes. *Chemical Engineering Journal* **2019**, 356, 771-780.

106. Den, W.; Wang, C.J., Removal of silica from brackish water by electrocoagulation pretreatment to prevent fouling of reverse osmosis membranes. *Separation and Purification Technology* **2008**, 59, 318-325.

107. Jegatheesan, V.; Pramanik, B.K.; Chen, J.; Navaratna, D.; Chang, C.Y.; Shu, L., Treatment of textile wastewater with membrane bioreactor: a critical review. *Bioresource technology* **2016**, 204, 202-212.

108. Aktaş, Ö.; Sahinkaya, E.; Yurtsever, A.; Demir, S.; Yüceyurt, M.; Çakmak, A.; Külekci, Ç.; Tahmaz, Ş.; Uludağ, M., Treatment of a chemical industry effluent by nanofiltration and reverse osmosis. *Desalination and Water Treatment* **2017**, 75, 274-283.

109 Boels, L., Tervahauta, T. and Witkamp, G.J., Adsorptive removal of nitrilotris (methylenephosphonic acid) antiscalant from membrane concentrates by iron-coated waste filtration sand. *Journal of hazardous materials*, **2010**, 182(1-3), 855-862.

110. Weng, J.; Jia, H.; Wu, B.; and Pan, B.; Is ozonation environmentally benign for reverse osmosis concentrate treatment? Four-level analysis on toxicity reduction based on organic matter fractionation. *Chemosphere* **2018**, 191, 971-978.

111. Greenlee, L.F.; Testa, F.; Lawler, D.F.; Freeman, B.D.; Moulin, P., Effect of antiscalant degradation on salt precipitation and solid/liquid separation of RO concentrate. *Journal of membrane science* **2011**, 366(1-2), pp.48-61.

112. Van Geluwe, S.; Braeken, L.; Van der Bruggen, B., Ozone oxidation for the alleviation of membrane fouling by natural organic matter: A review. *Water research* **2011**, 45(12), 3551-3570.

113. Vatankhah, H.; Murray, C.C.; Brannum, J. W., Vanneste, J.; Bellona, C., Effect of pre-ozonation on nanofiltration membrane fouling during water reuse applications. *Separation and Purification Technology* **2018**, 205, 203-211.

114. Lee, L.Y.; Ng, H.Y.; Ong, S.L.; Hu, J.Y.; Tao, G.; Kekre, K.; Viswanath, B.; Lay, W.; Seah, H., Ozone-biological activated carbon as a pretreatment process for reverse osmosis brine treatment and recovery. *Water research* **2009**, 43(16), 3948-3955.

115 Yang, Q., Choi, H., Chen, Y. and Dionysiou, D.D., Heterogeneous activation of peroxymonosulfate by supported cobalt catalysts for the degradation of 2, 4-dichlorophenol in water: the effect of support, cobalt precursor, and UV radiation. *Applied Catalysis B: Environmental*, **2008**, 77(3-4), 300-307.

116. Giwa, A.; Dufour, V.; Al Marzooqi, F.; Al Kaabi, M.; Hasan, S. W., Brine management methods: Recent innovations and current status. *Desalination* **2017**, 407, 1-23.

117. Khudair, K. M.; Eraibi, N. A., Environmental impact of RO units installation in main water treatment plants of Basrah city/south of Iraq. *Desalination* **2017**, 404, 270-279.

118. Vörösmarty, C. J.; Green, P.; Salisbury, J.; Lammers, R. B. Global water resources: vulnerability from climate change and population growth. *Science* **2000**, 289 (5477), 284-288.

119. Trenberth, K. E. Changes in precipitation with climate change. *Climate Research* **2011**, 47, 123-138.

120. Seckin, G.; Yilmaz, T.; Sari, B.; Ersu, C. B. Groundwater hydrochemistry at the Mediterranean coastal plains—the case of Silifke, Turkey. *Desalination* **2010**, 253 (1), 164-169.

121. Giambastiani, B. M. S.; Colombani, N.; Mastrocicco, M.; Fidelibus, M. D. Characterization of the lowland coastal aquifer of Comacchio (Ferrara, Italy): hydrology, hydrochemistry and evolution of the system. *Journal of hydrology* **2013**, 501, 35-44.

122. Barlow, P. M.; Reichard, E. G. Saltwater intrusion in coastal regions of North America. *Hydrogeology Journal* **2010**, 18 (1), 247-260.

123. https://water.usgs.gov/ogw/gwrp/brackishgw/brackish.html

124. Ahmed, M.; Shayya, W. H.; Hoey, D.; Al-Handaly, J. Brine disposal from reverse osmosis desalination plants in Oman and the United Arab Emirates. *Desalination* **2001**, 133 (2), 135-147.

125. Ruiz-García, A.; Ruiz-Saavedra, E.; Feo-García, J. Start-up of brackish water desalination for agricultural irrigation in the Canary Islands (Spain). *Desalination and Water Treatment* **2016**, 57 (48-49), 22734-22742.

126. Shannon, M. A.; Bohn, P. W.; Elimelech, M.; Georgiadis, J. G.; Marinas, B. J.; Mayes, A. M. Science and technology for water purification in the coming decades. *Nature* **2008**, 452 (7185), 301-310.

127. Côté, P.; Siverns, S.; Monti, S. Comparison of membrane-based solutions for water reclamation and desalination. *Desalination* **2005**, 182 (1-3), 251-257.

128. Werber, J. R.; Osuji, C. O.; Elimelech, M. Materials for next-generation desalination and water purification membranes. *Nature Reviews Materials* **2016**, 1, 16018.

129. Famiglietti, J.; S. The global groundwater crisis. *Nature Climate Change*. **2014**,4, 945-8.

130. El Saliby, I.; Okour, Y.; Shon, H. K.; Kandasamy, J.; Kim, I. S. Desalination plants in Australia, review and facts. *Desalination*. **2009**, 247, 1-4.

131. "Desalination (Brackish and Sea Water)." California Water Plan Update 2013. Retrieved November 28, 2018 from http://www.water.ca.gov/waterplan/docs/cwpu2013/Final/Vol3_Ch10_Desalination.pdf.

132. Van de Lisdonk, C. A. C.; Van Paassen, J. A. M.; Schippers, J. C. Monitoring scaling in nanofiltration and reverse osmsis membrane systems. *Desalination* **2000**, 132 (1-3), 101-108.

133. Shirazi, S.; Lin, C. J.; Chen, D. Inorganic fouling of pressure-driven membrane processes—a critical review. *Desalination* **2010**, 250 (1), 236-248.

134. Greenlee, L. F.; Lawler, D. F.; Freeman, B. D.; Marrot, B.; Moulin, P. Reverse osmosis desalination: water sources, technology, and today's challenges. *Water research* **2009**, 43 (9), 2317-2348.

135. Cartmell, D. Desalination: Antiscalants keep the water flowing in reverse osmosis. *Filtration+ Separation* **2012**, 49 (5), 22-24.

136. Neveux, T.; Bretaud, M.; Chhim, N.; Shakourzadeh, K.; Rapenne, S. Pilot plant experiments and modeling of CaCO3 growth inhibition by the use of antiscalant polymers in recirculating cooling circuits. *Desalination* **2016**, 397, 43-52.

137. Sheikhi, A.; Li, N.; van de Ven, T. G.; Kakkar, A. Macromolecule-based platforms for developing tailor-made formulations for scale inhibition. *Environmental Science: Water Research & Technology* **2016**, 2 (1), 71-84.

138. Ahmed, M.; Arakel, A.; Hoey, D.; Thumarukudy, M. R.; Goosen, M. F.; Al-Haddabi, M.; Al-Belushi, A. Feasibility of salt production from inland RO desalination plant reject brine: a case study. *Desalination* **2003**, 158 (1-3), 109-117.

139. Van der Bruggen, B.; Lejon, L.; Vandecasteele, C. Reuse, treatment, and discharge of the concentrate of pressure-driven membrane processes. *Environmental science & technology* **2003**, 37 (17), 3733-3738.

140. Santa Ana Watershed Project Authority Website; http://www.sawpa.org/brineline/what-is-it/

141. Owens-Bennett, E. L.; Trussell, B.; Monroy, I.; Trussell, R. Proposed solids formation recovery formula for the inland empire brine line; October 10, **2016**.

142. Benjamin, M. M.; Lawler, D. F.; Tobiason, J. E. Inland empire brine line expert panel; June 29-30, **2011**.

143. Greenlee, L. F.; Testa, F.; Lawler, D. F.; Freeman, B. D.; Moulin, P. Effect of antiscalants on precipitation of an RO concentrate: metals precipitated and particle characteristics for several water compositions. *Water research* **2010**, 44 (8), 2672-2684.

144. Greenlee, L. F.; Testa, F.; Lawler, D. F.; Freeman, B. D.; Moulin, P. The effect of antiscalant addition on calcium carbonate precipitation for a simplified synthetic brackish water reverse osmosis concentrate. *Water research* **2010**, 44 (9), 2957-2969.

145. Hasson, D.; Drak, A.; Semiat, R. Induction times induced in an RO system by antiscalants delaying CaSO4 precipitation. *Desalination* **2003**, 157 (1-3), 193-207.

146. Mansour, S.; Arafat, H. A.; Hasan, S. W. Chapter 5, Brine management in desalination plants, Desalination Sustainability, A Technical, Socioeconomic, and Environmental Approach **2017**, 207-236.

147. Giwa, A.; Dufour, V.; Al Marzooqi, F.; Al Kaabi, M.; Hasan, S. W. Brine management methods: Recent innovations and current status. *Desalination* **2017**, 407, 1-23.

148. Khudair, K. M.; Eraibi, N. A. Environmental impact of RO units installation in main water treatment plants of Basrah city/south of Iraq. *Desalination* **2017**, 404, 270-279.

149. Darton, E. G.; Scale inhibition techniques used in membrane systems. *Desalination* **1997**, 113 (2), 227-229.

150. Austin, A. E.; Miller, J. F.; Vaughan, D.A.; Kircher, J.F. Chemical additives for calcium sulfate scale control. *Desalination* **1975**, 16 (3), 345-357.

151. Ketrane, R.; Saidani, B.; Gil, O.; Leleyter, L.; Baraud, F. Efficiency of five scale inhibitors on calcium carbonate precipitation from hard water: effect of temperature and concentration. *Desalination* **2009**, 249 (3), 1397-1404.

152. Abd-El-Khalek, D. E.; Abd-El-Nabey, B. A. Evaluation of sodium hexametaphosphate as scale and corrosion inhibitor in cooling water using electrochemical techniques. *Desalination* **2013**, 311, 227-233.

153. He, F.; Sirkar, K. K.; Gilron, J. Effects of antiscalants to mitigate membrane scaling by direct contact membrane distillation. *Journal of Membrane Science* **2009**, 345 (1), 53-58.

154. Nowack, B. The behavior of phosphonates in wastewater treatment plants of Switzerland. *Water research* **1998**, 32 (4), 1271-1279.

155. Sweeney, F. M.; Cooper, S.D. The development of a novel scale inhibitor for severe water chemistries. In SPE *International Symposium on Oilfield Chemistry* **1993**. Society of Petroleum Engineers.

156. Carter Jr, R. P.; Carroll, R. L.; Irani, R. R. Nitrilotri (methylenephosphonic acid), ethyliminodi-(methylenephosphonic acid), and diethylaminomethylphosphonic acid: acidity and calcium (II) and magnesium (II) complexing. *Inorganic Chemistry* **1967**, 6 (5), 939-942.

157. Pairat, R.; Sumeath, C.; Browning, F. H.; Fogler, H. S. Precipitation and dissolution of calcium− ATMP precipitates for the inhibition of scale formation in porous media. *Langmuir* **1997**, 13 (6), 1791-1798.

158. Knepper, T. P. Synthetic chelating agents and compounds exhibiting complexing properties in the aquatic environment. *TrAC Trends in Analytical Chemistry* **2003**, 22 (10), 708-724.

159. Duan, W.; Oota, H.; Sawada, K. Stability and structure of ethylenedinitrilopoly (methylphosphonate) complexes of the alkaline-earth metal ions in aqueous solution. *Journal of the Chemical Society, Dalton Transactions* **1999**, (17), 3075-3080.

160. Deluchat, V.; Bollinger, J. C.; Serpaud, B.; Caullet, C. Divalent cations speciation with three phosphonate ligands in the pH-range of natural waters. *Talanta* **1997**, 44 (5), 897-907.

161. Popov, K.; Rönkkömäki, H.; Lajunen, L.H. Critical evaluation of stability constants of phosphonic acids (IUPAC technical report). *Pure and applied chemistry* **2001**, 73 (10), 1641-1677.

162. Lin, Y. P.; Singer, P.C. Inhibition of calcite crystal growth by polyphosphates. *Water Research* **2005**, 39 (19), 4835-4843.

163. Peters, E. M.; Chivavava, J.; Rodriguez-Pascual, M.; Lewis, A. E. Effect of a Phosphonate Antiscalant during Eutectic Freeze Crystallization of a Sodium Sulfate Aqueous Stream. *Industrial & Engineering Chemistry Research* **2016**, 55 (35), 9378-9386.

164. Rosenberg, Y. O.; Reznik, I. J.; Zmora-Nahum, S.; Ganor, J. The effect of pH on the formation of a gypsum scale in the presence of a phosphonate antiscalant. *Desalination* **2012**, *284*, 207-220.

165. Greenlee, L. F.; Testa, F.; Lawler, D. F.; Freeman, B. D.; Moulin, P. The effect of antiscalant addition on calcium carbonate precipitation for a simplified synthetic brackish water reverse osmosis concentrate. *Water research* **2010**, 44 (9), 2957-2969.

166. Shih, W. Y.; Albrecht, K.; Glater, J.; Cohen, Y. A dual-probe approach for evaluation of gypsum crystallization in response to antiscalant treatment. *Desalination* **2004**, 169 (3), 213-221.

167. Wang, F.; Davis, T. E.; Tarabara, V. V. Crystallization of calcium sulfate dihydrate in the presence of colloidal silica. *Industrial & Engineering Chemistry Research* **2010**, *49* (22), 11344-11350.

168. Söhnel, O.; Mullin, J.W. Interpretation of crystallization induction periods. *Journal of colloid and interface science* **1988**, 123 (1), 43-50.

169. Tomaszewska, B.; Tyszer, M. Assessment of the influence of temperature and pressure on the prediction of the precipitation of minerals during the desalination process. *Desalination* **2017**, 424, 102-109.

170. Mitrouli, S. T.; Kostoglou, M.; Karabelas, A.J. Calcium carbonate scaling of desalination membranes: Assessment of scaling parameters from dead-end filtration experiments. *Journal of Membrane Science* **2016**, 510, 293-305.

171. Zarga, Y.; Boubaker, H. B.; Ghaffour, N.; Elfil, H. Study of calcium carbonate and sulfate co-precipitation. *Chemical Engineering Science* **2013**, 96, 33-41.

172. Hamdona, S. K.; Al Hadad, O. A. Influence of additives on the precipitation of gypsum in sodium chloride solutions. *Desalination* **2008**, 228 (1-3), 277-286.

173. Greenberg, G.; Hasson, D.; Semiat, R. Limits of RO recovery imposed by calcium phosphate precipitation. *Desalination* **2005**, 183 (1-3), 273-288.

174. Malki, M.; Abbas, V. Relationship between phosphate scales and silica fouling in wastewater RO membrane systems. *IDA Journal of Desalination and Water Reuse* **2013**, 5 (1), 15-24.

175. Ning, R. Y.; Troyer, T. L. Colloidal fouling of RO membranes following MF/UF in the reclamation of municipal wastewater. *Desalination* **2007**, 208 (1-3), 232-237.

176. Jurenka, R. A.; Chapman-Wilbert, M. Maricopa Ground Water Treatment Study: Water Treatment Technology Program Report No. 15. US Department of the Interior, Bureau of Reclamation, Denver, CO. **1996**.

177. Visual MINTEQ ver. 3.1 (released 2014) J. P. Gustafsson

178. Benjamin, M. M. Water chemistry. Waveland Press **2014**.

179. Menten, L.; Michaelis, M. I. Die kinetik der invertinwirkung. *Biochem Z* **1913**, *49*, 333-369.

180. American Public Health Association, American Water Works Association, Water Pollution Control Federation and Water Environment Federation, *Standard methods for the examination of water and wastewater* **1915**. American Public Health Association.

181. Rahardianto, A.; McCool, B. C.; Cohen, Y. Reverse osmosis desalting of inland brackish water of high gypsum scaling propensity: kinetics and mitigation of membrane mineral scaling. *Environmental science & technology* **2008**, 42 (12), 4292-4297.

182. Zeiher, E. K.; Ho, B.; Williams, K. D. Novel antiscalant dosing control. *Desalination* **2003**, 157 (1-3), 209-216.

183. Klepetsanis, P. G.; Koutsoukos, P. G. Kinetics of calcium sulfate formation in aqueous media: effect of organophosphorus compounds. *Journal of crystal growth* **1998**, 193 (1-2), 156-163.

184. Oh, H. J.; Choung, Y. K.; Lee, S.; Choi, J. S.; Hwang, T. M.; Kim, J. H. Scale formation in reverse osmosis desalination: model development. *Desalination* **2009**, 238 (1-3), 333-346.

185. Li, F.; Zhang, B.; Wang, H.; Wu, Y. Ethylenediamine core, octamethylenephosphonic acid terminated, PAMAM dendrimer and its use as antiscalant. *U.S. Patent Application* **2014**, 13 (943), 672.

186. He, S.; Oddo, J. E.; Tomson, M. B. The nucleation kinetics of calcium sulfate dihydrate in NaCl solutions up to 6 m and 90 C. *Journal of Colloid and Interface Science* **1994**, 162 (2), 297-303.

187. Lancia, A.; Musmarra, D.; Prisciandaro, M. Measuring induction period for calcium sulfate dihydrate precipitation. *AIChE Journal* **1999**, 45 (2), 390-397.

188. Mahmoud, M. H. H.; Rashad, M. M.; Ibrahim, I. A.; Abdel-Aal, E. A. Crystal modification of calcium sulfate dihydrate in the presence of some surface-active agents. *Journal of colloid and interface science* **2004**, 270 (1), 99-105.

189. Christoffersen, J.; Christoffersen, M.R. Kinetics of spiral growth of calcite crystals and determination of the absolute rate constant. *Journal of crystal growth* **1990**, 100 (1-2), 203-211.

190. Wu, W.; Nancollas, G. H. Determination of interfacial tension from crystallization and dissolution data: a comparison with other methods. *Advances in colloid and interface science* **1999**, 79 (2-3), 229-279.

191. Boistelle, R.; Lopez-Valero, I. Growth units and nucleation: the case of calcium phosphates. *Journal of crystal growth* **1990**, 102 (3), 609-617.

192. Becker, R. V.; Döring, W. Kinetic treatment of the formation of nuclei in over-saturated steam. *Ann Phys* **1935**, 5 (24), 719-752.

193. Frenkel, J. A. A general theory of heterophase fluctuations and pretransition phenomena. *The Journal of Chemical Physics* **1939**, 7 (7), 538-547.

194. Markov, I.V. Crystal Growth for Beginners: Fundamentals of Nucleation, Crystal Growth and Epitaxy. **2003**: World Scientific.

195. Myerson, A. S.; Jacovs, J.; Jacovs, J. Handbook of industrial crystallization **1993**. *Massachusetts: Butterworth-Heinemann.*

196. Opalko, F. J.; Adair, J. H.; Khan, S. R. Heterogeneous nucleation of calcium oxalate trihydrate in artificial urine by constant composition. *Journal of crystal growth* **1997**, 181 (4), 410-417.

197 Chen, Y., 2017. Removing phosphonate antiscalants from membrane concentrate solutions using ferric hydroxide adsorbents.

198 Nowack, B., Environmental chemistry of phosphonates. *Water research*, **2003**, 37(11), 2533-2546.

199 Bond, R. and Veerapaneni, S., *Zero liquid discharge for inland desalination*. Awwa Research Foundation, **2007**.

200 Aghdam, M.A., Zraick, F., Simon, J., Farrell, J. and Snyder, S.A., A novel brine precipitation process for higher water recovery. *Desalination*, **2016**, 385, 69-74.

201 Wang, X.X., Wu, Y.H., Zhang, T.Y., Xu, X.Q., Dao, G.H. and Hu, H.Y., Simultaneous nitrogen, phosphorous, and hardness removal from reverse osmosis concentrate by microalgae cultivation. *Water research*, **2016**, 94, 215-224.

202 Shim, J.H., Jeong, J.Y. and Park, J.Y., SWRO brine reuse by diaphragm-type chlor-alkali electrolysis to produce alkali-activated slag. *Desalination*, **2017**, 413, 10-18.

203 Loganathan, P., Naidu, G. and Vigneswaran, S., Mining valuable minerals from seawater: a critical review. *Environmental Science: Water Research & Technology*, **2017**, 3(1), 37-53.

204 Naidu, G., Jeong, S., Choi, Y. and Vigneswaran, S., Membrane distillation for wastewater reverse osmosis concentrate treatment with water reuse potential. *Journal of Membrane Science*, **2017,** 524, 565-575.

205 Lin, L., Xu, X., Papelis, C. and Xu, P., Innovative use of drinking water treatment solids for heavy metals removal from desalination concentrate: Synergistic effect of salts and natural organic matter. *Chemical Engineering Research and Design*, **2017**, 120, 231-239.

206 Boels, L., Tervahauta, T. and Witkamp, G.J., Adsorptive removal of nitrilotris (methylenephosphonic acid) antiscalant from membrane concentrates by iron-coated waste filtration sand. *Journal of hazardous materials*, **2010**, 182, 855-862.

207 Chen, Y., Baygents, J.C. and Farrell, J., Removing phosphonate antiscalants from membrane concentrate solutions using granular ferric hydroxide. *Journal of Water Process Engineering*, **2017**,19, 18-25.

208 Li, W., Patton, S., Gleason, J.M., Mezyk, S.P., Ishida, K.P. and Liu, H., UV Photolysis of chloramine and persulfate for 1, 4-Dioxane removal in reverse-osmosis permeate for potable water reuse. *Environmental science & technology*, **2018**, 52(11), 6417-6425.

209 Jurenka, R. A.; Chapman-Wilbert, M. Maricopa Ground Water Treatment Study: Water Treatment Technology Program Report No. 15. US Department of the Interior, Bureau of Reclamation, Denver, CO. **1996**.

210 Benjamin, M. M. Water chemistry. Waveland Press **2014**.

211 Wegelin, M., Canonica, S., Mechsner, K., Fleischmann, T., Pesaro, F. and Metzler, A., Solar water disinfection: scope of the process and analysis of radiation experiments. Aqua, **1994**, 43(4), 154-169.

212 Wordofa, D.N., Walker, S.L. and Liu, H., Sulfate radical-induced disinfection of pathogenic Escherichia coli O157: H7 via iron-activated persulfate. Environmental Science & Technology Letters, **2017**,4(4), 154-160.

213 A.D. Eaton, L.S. Clesceri, E.W. Rice, A.E. Greenberg (Eds.), Standard Methods for the Examination of Water and Wastewater, American Public Health Association, American Water Works Association, Water Environment Federation, Washington, D.C (**2005**)

214 Wiesner, A.D., Katz, L.E. and Chen, C.C., The impact of ionic strength and background electrolyte on pH measurements in metal ion adsorption experiments. *Journal of colloid and interface science*, **2006**, 301(1), 329-332.

215 Baumann, E.W., Determination of pH in concentrated salt solutions. *Analytica Chimica Acta*, **1973**, 64(2), 284-288.

216 Jain, T.; Sanchez, E.; Owens-Bennett, E.; Trussell, R.; Walker, S. and Liu, H., Impacts of antiscalants on the formation of calcium solids: implication on scaling potential of desalination concentrate. *Environmental Science: Water Research & Technology* **2019**, 5, 1285-1294.

217. Visual MINTEQ ver. 3.1 (released **2014**) J. P. Gustafsson

218. Wang, F.; Davis, T. E.; Tarabara, V. V. Crystallization of calcium sulfate dihydrate in the presence of colloidal silica. *Industrial & Engineering Chemistry Research* **2010**, *49* (22), 11344-11350.

219. Söhnel, O.; Mullin, J.W. Interpretation of crystallization induction periods. *Journal of colloid and interface science* **1988**, 123 (1), 43-50.

220 Demadis, K.D. and Katarachia, S.D., Metal-phosphonate chemistry: Synthesis, crystal structure of calcium-amino tris-(methylene phosphonate) and inhibition of CaCO3 crystal growth. Phosphorus, Sulfur, and Silicon, **2004**, 179(3), 627-648.

221 Oshchepkov, M.S., Pervov, A.G., Golovesov, V.A., Rudakova, G.Y., Kamagurov, S.D., Tkachenko, S.V., Andrianov, A.P. and Popov, K.I., Use of a Fluorescent Antiscalant to Investigate Scaling of Reverse Osmosis Membranes. Membranes and Membrane Technologies, **2019**, 1(4), 254-266.

222. Rahardianto, A.; McCool, B. C.; Cohen, Y. Reverse osmosis desalting of inland brackish water of high gypsum scaling propensity: kinetics and mitigation of membrane mineral scaling. *Environmental science & technology* **2008**, 42 (12), 4292-4297.

223. Zeiher, E. K.; Ho, B.; Williams, K. D. Novel antiscalant dosing control. *Desalination* **2003**, 157 (1-3), 209-216.

224. Klepetsanis, P. G.; Koutsoukos, P. G. Kinetics of calcium sulfate formation in aqueous media: effect of organophosphorus compounds. *Journal of crystal growth* **1998**, 193 (1-2), 156-163.

225. Oh, H. J.; Choung, Y. K.; Lee, S.; Choi, J. S.; Hwang, T. M.; Kim, J. H. Scale formation in reverse osmosis desalination: model development. *Desalination* **2009**, 238 (1-3), 333-346.

226. Li, F.; Zhang, B.; Wang, H.; Wu, Y. Ethylenediamine core, octamethylenephosphonic acid terminated, PAMAM dendrimer and its use as antiscalant. *U.S. Patent Application* **2014**, 13 (943), 672.

227 Studnik, H., Liebsch, S., Forlani, G., Wieczorek, D., Kafarski, P. and Lipok, J., Amino polyphosphonates–chemical features and practical uses, environmental durability and biodegradation. New biotechnology, **2015**, 32(1), 1-6.

228 Wang, Z., Chen, G., Patton, S., Ren, C., Liu, J. and Liu, H., Degradation of nitrilotris-methylenephosphonic acid (NTMP) antiscalant via persulfate photolysis: Implications on desalination concentrate treatment. *Water research*, **2019**, 159, 30-37.

229 Andreozzi, R., Caprio, V., Insola, A. and Marotta, R., Advanced oxidation processes (AOP) for water purification and recovery. Catalysis today, **1999**, 53(1), 51-59.

230 Comninellis, C., Kapalka, A., Malato, S., Parsons, S.A., Poulios, I. and Mantzavinos, D., Advanced oxidation processes for water treatment: advances and trends for R&D. Journal of Chemical Technology & Biotechnology: International Research in Process, Environmental & Clean Technology, **2008**, 83(6), 769-776.

231 Ribeiro, A.R., Nunes, O.C., Pereira, M.F. and Silva, A.M., An overview on the advanced oxidation processes applied for the treatment of water pollutants defined in the recently launched Directive 2013/39/EU. Environment international, **2015**, 75, 33-51.

232 Appiani, E., Page, S.E. and McNeill, K., On the use of hydroxyl radical kinetics to assess the number-average molecular weight of dissolved organic matter. Environmental science & technology, **2014**, 48(20), 11794-11802.

233 Minisci, F., Citterio, A. and Giordano, C., Electron-transfer processes: peroxydisulfate, a useful and versatile reagent in organic chemistry. Accounts of Chemical Research, **1983**, 16(1), 27-32.

234 Neta, P., Madhavan, V., Zemel, H. and Fessenden, R.W., Rate constants and mechanism of reaction of sulfate radical anion with aromatic compounds. Journal of the American Chemical Society, **1977**, 99(1), 163-164.

235 Kanmani, S. and Gandhimathi, R., Investigation of physicochemical characteristics and heavy metal distribution profile in groundwater system around the open dump site. Applied Water Science, **2013**, 3(2), 387-399.

236 Ackah, M., O. Agyemang, A. K. Anim, J. Osei, N. O. Bentil, L. Kpattah, E. T. Gyamfi, and J. E. K. Hanson. "Assessment of groundwater quality for drinking and irrigation: the case study of Teiman-Oyarifa Community, Ga East Municipality, Ghana." Proceedings of the International Academy of Ecology and Environmental Sciences 1, no. 3-4 (**2011**): 186.

237 Prasanth, S.S., Magesh, N.S., Jitheshlal, K.V., Chandrasekar, N. and Gangadhar, K., Evaluation of groundwater quality and its suitability for drinking and agricultural use in the coastal stretch of Alappuzha District, Kerala, India. Applied Water Science, **2012**, 2(3), 165-175.

238 Behailu, T.W., Badessa, T.S. and Tewodros, B.A., Analysis of physical and chemical parameters in ground water used for drinking around Konso Area, Southwestern Ethiopia. J Anal Bioanal Techn, **2017**, 8(5), 379.

239 Peng, J., Wang, G., Zhang, D., Zhang, D. and Li, X., Photodegradation of nonylphenol in aqueous solution by simulated solar uv-irradiation: the comprehensive effect of nitrate, ferric ion and bicarbonate. Journal of Photochemistry and Photobiology A: Chemistry, **2016**, 326, 9-15.

240 Walse, S.S., Morgan, S.L., Kong, L. and Ferry, J.L., Role of dissolved organic matter, nitrate, and bicarbonate in the photolysis of aqueous fipronil. Environmental science & technology, **2004**, 38(14), 3908-3915.

241 Lu, X., Shao, Y., Gao, N., Chen, J., Deng, H., Chu, W., An, N. and Peng, F., Investigation of clofibric acid removal by UV/persulfate and UV/chlorine processes: Kinetics and formation of disinfection byproducts during subsequent chlor (am) ination. Chemical Engineering Journal, **2018**, 331, 364-371.

242 Lutze, H.V., Kerlin, N. and Schmidt, T.C., Sulfate radical-based water treatment in presence of chloride: formation of chlorate, inter-conversion of sulfate radicals into hydroxyl radicals and influence of bicarbonate. Water research, **2015**, 72, 349-360.

243 Jurenka, R. A.; Chapman-Wilbert, M. Maricopa Ground Water Treatment Study: Water Treatment Technology Program Report No. 15. US Department of the Interior, Bureau of Reclamation, Denver, CO. **1996**.

244 American Public Health Association , American Water Works Association , Water Pollution Control Federation and Water Environment Federation , Standard methods for the examination of water and wastewater , American Public Health Association, **1915**, vol. vol. 2

245 Deluchat, V., Bollinger, J.C., Serpaud, B. and Caullet, C., Divalent cations speciation with three phosphonate ligands in the pH-range of natural waters. Talanta, **1997**, 44(5), 897-907.

246 Lutze, H.V., Bircher, S., Rapp, I., Kerlin, N., Bakkour, R., Geisler, M., von Sonntag, C. and Schmidt, T.C., Degradation of chlorotriazine pesticides by sulfate radicals and the influence of organic matter. *Environmental science & technology*, *49*(3), **2015**, 1673-1680.

248 Comninellis, C., Kapalka, A., Malato, S., Parsons, S.A., Poulios, I. and Mantzavinos, D., Advanced oxidation processes for water treatment: advances and trends for R&D. Journal of Chemical Technology & Biotechnology: International Research in Process, Environmental & Clean Technology, **2008**, 83(6), 769-776.

249 Klavarioti, M., Mantzavinos, D. and Kassinos, D., Removal of residual pharmaceuticals from aqueous systems by advanced oxidation processes. Environment international, **2009**, 35(2), 402-417.

250. Deluchat, V.; Bollinger, J.C.; Serpaud, B.; Caullet, C. Divalent cations speciation with three phosphonate ligands in the pH-range of natural waters. *Talanta* **1997**, 44 (5), 897-907.

251. Popov, K.; Rönkkömäki, H.; Lajunen, L. H. Critical evaluation of stability constants of phosphonic acids (IUPAC technical report). *Pure and applied chemistry* **2001**, 73 (10), 1641-1677.

252. Gillard, R. D.; Newman, P. D.; Collins, J. D. Speciation in aqueous solutions of di-ethylenetriamine-N, N, N′, N ″, N ″-pentamethylenephosphonic acid and some metal complexes. *Polyhedron* **1989**, *8* (16), 2077-2086.

253. Powell, K. J.; Pettit, L. D. IUPAC stability constants database. *Academic Software* **1997**, Otley.

254. Tomson, M. B.; Kan, A. T.; Oddo, J. E. Acid/base and metal complex solution chemistry of the polyphosphonate DTPMP versus temperature and ionic strength. *Langmuir* **1994**, 10 (5), 1442-1449.

255 Li, W., Jain, T., Ishida, K. and Liu, H., A mechanistic understanding of the degradation of trace organic contaminants by UV/hydrogen peroxide, UV/persulfate and UV/free chlorine for water reuse. *Environmental Science: Water Research & Technology*, **2017**, 3(1), 128-138.

256 Liang, C. and Su, H.W., Identification of sulfate and hydroxyl radicals in thermally activated persulfate. Industrial & Engineering Chemistry Research, **2009**, 48(11), 5558-5562.